Max-Planck-Institut für Meteorologie
Max Planck Institute for Meteorology

The impact of african air pollution: A global chemistry climate model study

Adetutu Mary Aghedo


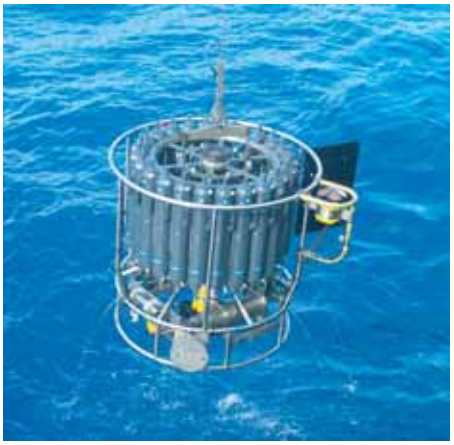


Berichte zur Erdsystemforschung 45/2007

Reports on Earth System Science

Hinweis

Die Berichte zur Erdsytemforschung werden vom Max-Planck-Institut für Meteorologie in Hamburg in unregelmäßiger Abfolge herausgegeben.

Sie enthalten wissenschaftliche und technische Beiträge, inklusive Dissertationen.

Die Beiträge geben nicht notwendigerweise die Auffassung des Instituts wieder.

Die "Berichte zur Erdsystemforschung" führen die vorherigen Reihen "Reports" und "Examensarbeiten" weiter.

Notice

The Reports on Earth System Science are published by the Max Planck Institute for Meteorology in Hamburg. They appear in irregular intervals.

They contain scientific and technical contributions, including Ph. D. theses.

The Reports do not necessarily reflect the opinion of the Institute.

The "Reports on Earth System Science" continue the former "Reports" and "Examensarbeiten" of the Max Planck Institute.

Anschrift / Address

Max-Planck-Institut für Meteorologie
Bundesstrasse 53
20146 Hamburg
Deutschland

Tel.: +49-(0)40-4 11 73-0
Fax: +49-(0)40-4 11 73-298
Web: www.mpimet.mpg.de

Layout:

Bettina Diallo, PR & Grafik

Titelfotos:
vorne:
Christian Klepp - Jochem Marotzke - Christian Klepp
hinten:
Clotilde Dubois - Christian Klepp - Katsumasa Tanaka

Berichte zur Erdsystemforschung 45/2007

The impact of african air pollution: A global chemistry climate model study

Dissertation zur Erlangung des Doktorgrades der Naturwissenschaften
im Departement Geowissenschaften der Universität Hamburg
vorgelegt von

Adetutu Mary Aghedo
aus Igbara-Oke, Nigeria

Hamburg 2007

Reports on Earth System Science 45/2007

ISSN 1614-1199

Adetutu Mary Aghedo
Max-Planck-Institut für Meteorologie
Bundesstrasse 53
20146 Hamburg
Germany

Als Dissertation angenommen
vom Departement Geowissenschaften der Universität Hamburg

auf Grund der Gutachten von
Prof. Dr. Hartmut Graßl
und
Dr. Martin G. Schultz

Hamburg, den 11. Mai 2007
Prof. Dr. Kay-Christian Emeis
Leiter des Departements für Geowissenschaften

ISSN 1614-1199

THE IMPACT OF AFRICAN AIR POLLUTION:
A global chemistry climate model study

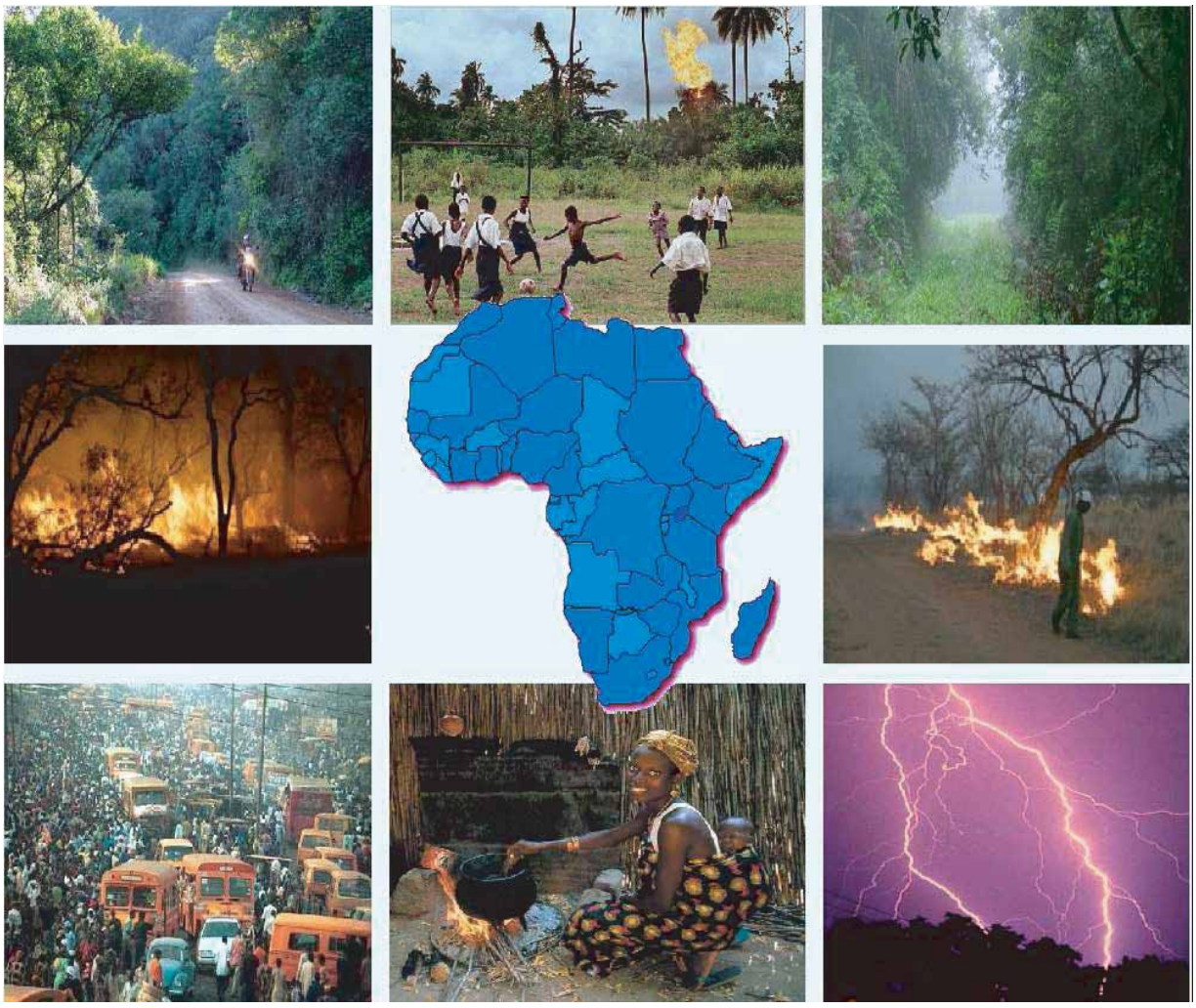

Adetutu Mary Aghedo

Hamburg 2007

Cover picture sources

Africa forest by Steve and Carole Eilertsen, available at
http://www.flamesonmytank.co.za/TourReports/limpopo2.htm

Photojournalist Chris Hondros, Pictures that tell story from around the world: **Nigeria, the price of oil**, available at:
http://www.chrishondrosphotography.com/.

Picture of fire: http://www.bushveld.co.za/pictures-of-south-africa-fire.htm

Oshodi, Lagos traffic: source uncertain, but picture available at:
http://www.swedetrack.com/lagosbus.jpg

Picture of African lightning and an African woman cooking: websites are no longer accessible.

Contents

List of Figures

List of Tables

Dedication

In memory of my late mother, Mrs Comfort Bolanle Bamiwo (nee Shadare).
I will forever appreciate your foresight and making your children education
the most fundamental passion of your life.

This thesis is dedicated to my “love” and “prince”
Olutope Bolanle Aghedo and Muyibolanle N. Salvatore Aghedo.
A million thanks for your undaunting love and support.

Acknowledgement

My immense gratitude goes to the ZEIT Foundation "(ZEIT-Stiftung Ebelin und Gerd Bucerius)", who provided the fellowship through the International Max Planck Research School on Earth System Modelling (IMPRS-ESM), Hamburg for this doctorate study.

The study no doubt benefited from the critical and sound judgment, continual support and encouragement, unwavering dedication and availability of my immediate supervisor, Dr. Martin G. Schultz and co-advisor Dr. Sebastian Rast. I have really enjoyed working with you. I appreciate the support, encouragement and geniality of my professor, who also served as the Chairman of my advisory panel meeting throughout the three-year period of this thesis, in person of Prof. Dr. Hartmut Graßl. Thank you so much for providing the general guidance and for channelling the course of this thesis, and above all for making me feel comfortable and very welcomed at knocking on your door at anytime without appointment.

I acknowledge the MOZAIC programme, who provided the data used in the evaluation of our model, made possible by the support of the European Commission, Airbus, CNRS-France, FZJ-Germany and the airlines (Lufthansa, Air France, Austrian and former Sabena, who carry the MOZAIC instrumentation free of charge since the commencement of the campaign in 1994). SHADOZ ozonesonde and surface CO concentrations data provided by NASA Goddard Space Flight Centre and NOAA Earth System Research Laboratory-Global Monitoring Division, respectively are duly acknowledged. We appreciate the lightning flashes from the Lightning Imaging Sensor and Optical Transient Detector (LIS/OTD) made available free of charge by the NASA Global Hydrology and Climate Center, and the MEGAN model, made available by the Biosphere-Atmosphere Interaction research group, Atmospheric Chemistry Division, National Center for Atmospheric Research.

This study stands on the shoulders of two giant computing facilities made possible by the German Climate Computing Centre ("Deutsches Klimarechenzentrum" (DKRZ)), and the Max-Planck Society (i.e. the NEC SX-6 computer and the Sun Computing system, YANG). This study would not have been possible without such super facilities. Immense gratitude goes to the entire staff of the Central Information technology Services (CIS), DKRZ, and Model and Data, for their support.

I am grateful for the technical assistance provided by Sebastian Rast, Luis Kornblueh, Monika Esch, Uwe Schulzweida and Hui Wan at various stages of this study. I equally appreciate the scientific discussions with Alex Guenther, Christine Wiedinmyer, Johann Feichter, Melissa Anne Pfeffer, Hui Wan, Guy Brasseur, Valerie Thouret, Mark Lawrence, Bastien Sauvage, Adewale M. Adio, and all members of the IMPRS-ESM, and Aerosols, Chemistry and Climate (now Aerosols, Clouds and Climate) group in Hamburg.

I appreciate the entire board of directors, the library and administrative staff of the Max Planck Institute for Meteorology, Hamburg, for providing me with a conducive atmosphere, office, computer, stationery and above all a good kitchen

(fully equipped with microwave, refrigerator and boiling jug), all of which have contributed to the smooth progress of this thesis. Specifically, I thank Prof. Dr. Guy Brasseur, Prof. Dr. Jochem Marotzke, Prof. Dr. Martin Claussen, and Dr. Daniela Jacob for their continued support, smiles, encouraging words and gestures. Antje Weitz and Cornelia Kampmann have been like sisters to me, thank you very much and God bless you. Appreciation also goes to Frau Birgit Paulsen, Bettina Diallo and Evelyn Wolters.

Special appreciation goes to the Vice Chancellor, the Registrar, the Dean, Faculty of Science, the Head of Department and the entire staff of the Department of Physics, Obafemi Awolowo University, Ile-Ife, Nigeria, for their support, emails and encouragement.

I appreciate the support of my mother-in-law Chief (Mrs) F. I. Olamosu, my family: Omolade, Adebanke, Adebayo, Adediti, Adeola, Aderonke, Oluwakorede and their respective families, and my special friends: Mrs Ilse Adam, Prof. Dr. Pastor Bamidele Ajayi, Pastor (Mrs) Bola Ajayi, Dr. Imoh B. Obioh, Prof. Dr. O. O. Jegede, Pastor Moses Osikoya, Pastor Mayowa Makinde, Pastor Francis Ofori, Pastor Craig Rees, Thomas and Soo Schwillo, Kethlyn and Heleno Ivo, and Brad Boelkins. I also appreciate Revd. Father Stefan Seibert and Revd. Father Andreas Kohlbrecher, the "ex-Kollegsleiter" and "KollegsLeiter", Franziskus Kolleg, Hamburg. Gratitude goes to Alexandra, Britta Jensen, Hendrikje Dieckmann, and all members of staff of the "Kita Karo Kids" for their care, understanding and love for Muyi.

Special thanks goes to Okechukwu Anopuo, Peter Owotoki, Ibiyemi Ilesanmi and all Nigerian students in Hamburg, for the jokes, laughter, food and time spent together to remember home and cool-off tension. You are all appreciated. My profound gratitude also to Dorothea Banse for her help with translations, cake for my birthday and the "nuggarts", time share together and for her general friendliness. The love of all my friends in the International Baptist Church of Hamburg, and worldwide are duly appreciated.

And to all those who have contributed, either directly or indirectly, to the successful completion of this thesis, I say God bless you all. Finally, I thank God for life, excellent health, peace and sound mind.

Abstract

The problem of air pollution has a long history, which probably dated back to the beginning of human existence. In addition to its local and regional impact, such as its effect on human health, and damage to vegetation including agricultural crops, infrastructure and other historical artefacts, and its reduction of visibility, air pollution is also a global problem because pollutants can be transported far away from their source region, and the ability of photochemical pollutants to influence the radiative balance of the earth, thereby causing climate change.

Air pollution emitted in Africa is from biomass burning, emissions from vegetation and soil, lightning, and anthropogenic emissions. The atmospheric trace species emitted from these sources include NO_x, CO, methane (CH_4) and non-methane organic compounds (VOCs). Emissions of these trace species significantly affect tropospheric chemistry and lead to the formation of tropospheric ozone, which is a greenhouse gas with atmospheric radiative forcing of 0.35 (0.25–0.65) W/m^2 (IPCC AR4, 2007). Africa intricate meteorological patterns and high concentrations of OH radical, makes the continent a region of intense mixing, transport and photochemistry. This thesis therefore investigates the global and regional impact of each of the Africa emission categories, by quantifying the magnitude, the seasonality, the inter-annual variability and assessing the dynamics of transport of primary and secondary air pollutants due to African emissions.

This study employs the 3-D global chemistry climate model ECHAM5-MOZ, which provides a consistent link of the chemistry calculation (MOZART2 tropospheric chemistry) to the parameterisation of the dynamics and the physics of the ECHAM5 model. This thesis presents the first evaluation of the ECHAM5-MOZ model, and it shows that the ECHAM5-MOZ model is both able to simulate the magnitude and the seasonality of ozone and surface CO concentrations worldwide, with a general bias of less than 30 ppbv for ozone. As a contribution of this work to the ECHAM5-MOZ development, the MEGAN biogenic emissions was implemented into the ECHAM5-MOZ model. The global annual emissions estimated by MEGAN are about 488 Tg(C)/yr for isoprene, 172 Tg(C)/yr for terpenes, 41 Tg(C)/yr for CO and 175 Tg(C)/yr for other non-terpene VOCs.

The transport of idealized tracers in the ECHAM5 model is rather similar across various model resolutions (T21L19, T42L19, T42L31, T63L31 and T106L31), except that large differences occur when there is a change in the vertical resolution or lifetime of the artificial tracers, or when the model is forced towards ERA40 meteorology. The T42L31 resolution gives very similar results to the other finer horizontal resolutions with the same vertical levels, although the ECHAM5 model climate simulations give better results at higher spatial resolutions (Roeckner et al., 2006). The use of ERA40 data only slightly affect the meridional and vertical transport of tracers at the surface and the tropopause, whereas it increases the inter-hemispheric and vertical transport of tracers in the stratosphere by about 10% – 150% and a factor of 2.5, respectively.

The model studies indicate that the surface ozone concentration may rise by up to 50 ppbv in the burning region of Africa during the biomass burning seasons. Biogenic emissions yield between 5 ppbv and 30 ppbv increase in the near surface ozone concentration over tropical Africa. The impact of lightning on surface ozone is negligible, while anthropogenic emissions yield a maximum of 7 ppbv increase in the annual-mean surface ozone concentration over Nigeria, South Africa and Egypt. The results show that biogenic emissions are the most important African emission source affecting total tropospheric ozone worldwide, due to the combined effect of intense convection on biogenic isoprene and methanol emissions, and their reaction products, which increases the upper troposphere ozone concentrations. The influence of each of the African emissions on the global tropospheric ozone burden (TOB) of 384Tg yields about 9.5 Tg, 19.6 Tg, 9.0 Tg and 4.7 Tg for biomass burning, biogenic, lightning and anthropogenic emissions emitted in Africa respectively. The impact of each of these emission categories on African TOB of 33 Tg is 2.5 Tg, 4.1 Tg, 1.75 Tg and 0.89 Tg respectively, which together represents about 28% of the total TOB calculated over Africa, indicating that more than 70% of the tropospheric ozone produced by each of the African emissions is found outside the continent, thus exerting a noticeable influence on a large part of the tropical troposphere. Apart from the Atlantic and Indian Ocean, Latin America experiences the largest impact of African emissions, followed by Oceania, the Middle East, Southeast and south-central Asia, northern North America (i.e. the United States and Canada), Europe and north-central Asia, for all the emission categories.

Chapter 1

Introduction

1.1 What is air pollution?

Air pollution is a broad term, and the following definitions describe its utilisation in this thesis:

- Air pollution is the contamination of the atmosphere by the discharge of emissions of undesirable substances and gases, or the formation of these gases from the emissions by chemical reactions in the atmosphere. This definition can be found in the glossary of the department of Environment and Conservation, Environmental Protection Authority, New South Wales, available at http://www.epa.nsw.gov.au/soe/95/28.htm.

- Air pollution is the presence of substances in the atmosphere, particularly those that do not occur naturally. These substances are generally contaminants that substantially alter or degrade the quality of the atmosphere. The term is often used to identify undesirable substances produced by human activity, that is, anthropogenic air pollution. Air pollution usually designates the collection of substances that adversely affects human health, animals, and plants; deteriorates structures; interferes with commerce; or interferes with the enjoyment of life. This definition is from the glossary of the American Meteorological Society, available at http://amsglossary.allenpress.com/glossary/.

The first definition identifies primary and secondary pollutants. The primary pollutants are emitted directly into the atmosphere, while the secondary pollutants are formed by the chemical reactions involving the primary pollutants. Examples of primary pollutants include nitrogen oxides (i.e. $NO_x = NO + NO_2$), volatile organic compounds (VOCs) and carbon monoxide (CO). Tropospheric ozone (O_3) and peroxy acetyl nitrate (PAN) are good examples of photochemically produced secondary air pollutants (Seinfeld and Pandis, 1998).

In the second definition, the impact of air pollution is clearly elucidated. It also links air pollution with human activity. Energy is consumed by various human activities, and as long as this energy is derived by fossil-fuel combustion, rise in air

pollution will remain the natural consequence of increasing energy use. However, the adoption of clean energy technology, such as hydrogen fuel, solar and wind energy, can abate this consequence.

1.2 Historical perspective on Air pollution

The history of air pollution probably dated back to the beginning of human existence. During the stone age, the cavemen invented fires in their poorly ventilated cave, causing indoor air pollution. For example, Mummies from Egypt and other places have been found with signs of anthracosis[1] and other respiratory disorders (e.g. Bernard Shaw, 1938; Brothwell et al., 1969; Walker et al., 1986; Pabst and Hofer, 1998), which may be related to exposure to open fires.

In the thirteenth century, shortly after the introduction of imported coal in London, the problem of air pollution caused public reaction (Brimblecombe, 1975). Despite this initial dispute, coal shortly afterwards became an alternative source of fuel, in place of firewood and charcoal, due to rise in the prices of firewood. This change to coal for domestic and industrial purposes engendered air pollution on an urban scale. By the end of seventeenth century, London air quality had greatly deteriorated (Brimblecombe, 1976) and anti-air-pollution sentiments became popular (Brimblecombe, 1978a, and references therein). The industrial revolution that began in England and later spread throughout part of Europe in the eighteenth and nineteenth century also resulted in urbanisation. Former rural dwellers moved to urban centres in search of factory work. These industrial advancement and urbanisation gave rise to an increase in environmental pollution (Brimblecombe, 1976, 1978b, 1992).

A particularly bad smog (mixture of smoke and fog) episode, termed as "London smog" in 1952, caused by sulphur and soot emissions from bituminous coal burning for heating and industrial purposes led to about 4000 deaths in approximately one week (Wilkins, 1954; Bell et al., 2004). Also in the 1960s, another type of smog, caused by high concentrations of secondary air pollutants (ozone, organic nitrates and aldehydes) was observed in the Los Angeles area. This was dubbed "summer smog" or "Los Angeles smog" and resulted in respiratory illnesses and significant decrease in crop yields (Haagen-Smith, 1964). This "summer smog" later became a serious problem all over Europe.

Although the governments and local authorities of the developed countries, especially Europe, have responded to the problem of air pollution by regulating pollutant concentrations or emission levels, as demonstrated by the successful reduction of SO_2 and surface sulphate concentrations in Europe (Mylona, 1996; Boucher et al., 2002) and the decreasing trends in NO_x, CO, benzene concentrations and particulates in urban areas due to catalyst-equipped vehicles and anti-lead fuels, the problems of air

[1] also known as black lung, **anthracosis** is defined as the accumulation of carbon in the lungs from inhaled smoke or coal dust by The American Heritage Stedman's Medical Dictionary, 2nd Edition 2004 by Houghton Mifflin Company.

pollution still persists (e.g. Solberg et al., 2005). For example, most densely populated urban regions of the world still exceed the U.S. National Ambient Air Quality Standard (NAAQS) and European ozone exposure limit (Benton et al., 1995; Lin et al., 2001; De Leeew and De Paus , 2001; Chan et al., 2003). Moreover several developing countries, such as China and India, are currently experiencing rapid economy growth, which results in rising energy consumption, high coal dependency, growing traffic of vehicles and increasing urbanisation, all of which increases pollutant emissions (International Energy Outlook, 2006) and subsequent formation of secondary air pollutants. The recent developments in Africa have also led to severe air pollution problems in parts of the continent. The specific nature of African air pollution and its historical perspective will be discussed in Section 1.4.

In addition to its local and regional impact, such as its effect on human health, its corrosive effect on building and other historical artefacts, damage to plants and agricultural crops, and its reduction of visibility, air pollution is also a global problem due to their inter-hemispheric and long-range transport by the wind (e.g. Li et al., 2002; Hudman et al., 2004), and the ability of secondary photochemical pollutants to influence the radiative balance of the earth (Chalita et al., 1996; Naik et al., 2005; Dentener et al., 2005), which results in climate change (Wang et al., 1980; Hansen et al., 2002).

1.3 The global nature of air pollution

1.3.1 Global distribution of sources

The major classification of pollutants is based on their sources, and their two broad categories include anthropogenic and natural sources. Anthropogenic emissions occur as a result of day-to-day human activities connected with industry, transportation, mining, construction, and domestic life in the household (such as cooking and heating). Natural sources include volcanic, lightning, and all biogenic emissions from living vegetation, soil, termites, and the digestive tracts of animals. Biomass burning is a special category of sources, categorised as savanna, forest and agricultural waste burning. It consists of both human-made and natural fires.

The estimate of global emissions of CO, NO_x, CH_4 and non-methane volatile organic compounds is about 664 Tg(C)/yr, 52 Tg(N)/yr, 598 Tg(C)/yr and 571 Tg(C)/yr, respectively according to IPCC TAR (2001).

1.3.2 Air pollution and tropospheric chemistry

The lowest 6–15 km of the earth atmosphere, known as the troposphere, is like a chemical reactor in which trace species emitted into the atmosphere from various sources are transported by winds and turbulence, chemically processed and converted into products. Many tropospheric reactions are induced by solar ultraviolet (UV) radiation reaching the troposphere. The complex reactions involving VOCs, CO, NO_x and other emitted trace species, are initiated through the oxidation by

the hydroxyl (OH) radical (Levy II, 1972; Thompson, 1992; Kley, 1997). OH radicals are formed through the photodissociation of tropospheric ozone by solar UV radiation, aided by water vapour (H_2O), according to Reactions (R1) and (R2).

$$O_3 + h\nu \rightarrow O(^1D) + O_2 \quad \text{(R1)}$$
$$O(^1D) + H_2O \rightarrow 2\,OH \quad \text{(R2)}$$

where $h\nu$ is a photon of wavelength, $\lambda \lesssim 320\,\text{nm}$.

OH does not react with the major constituents of the atmosphere, such as N_2, O_2, CO_2 and H_2O. However, it is the major tropospheric sink for many trace species. Therefore, the resident times and spatial distribution of tropospheric trace species are largely determined by their reactivity with OH and by the OH spatio-temporal distribution. Besides the primary source of OH in the troposphere through photolysis of tropospheric ozone (Reaction R1 and R2), OH is also recycled and regenerated in the polluted atmosphere.

$$(CO, CH_4, \text{VOCs}) + OH \rightarrow \cdots + HO_2 \quad \text{(R3)}$$
$$HO_2 + NO \rightarrow NO_2 + OH \quad \text{(R4)}$$

where Reaction (R3) represents a generalised description of the oxidation of carbon monoxide, methane and other non-methane VOCs.

Tropospheric ozone is central to the chemistry of the troposphere, due to its role as OH precursor and its influence on the oxidation capacity of the atmosphere. It is also a greenhouse gas (Wang et al., 1980; Chalita et al., 1996; Hansen et al., 2002) with atmospheric radiative forcing of 0.35 (0.25–0.65) W/m^2 (IPCC AR4, 2007), due to its ability to absorb solar and infrared radiation. Close to the boundary layer, high ozone concentrations in the air also affect human health (e.g. Peden, 2001; Desqueyroux et al., 2002; Mortimer et al., 2002) and damage vegetation, including agricultural crops (e.g. Mauzerall and Wang, 2001; Oksanen and Holopainen, 2001).

Transport from the stratosphere was long thought to be the dominant source of ozone in the troposphere (e.g. Junge, 1962; Danielsen, 1968). However, in the early 1970s, Crutzen (1973) and Chameides and Walker (1973) suggested that the dominant source of tropospheric ozone is by photochemical oxidation of CO and hydrocarbons (HC), catalysed by NO_x and HO_x (i.e. OH + HO_2). Since then, several studies using global budget analysis (e.g. Fishman, 1985), scaling of precursor emissions (Liu et al., 1987), aircraft observations (Jacob et al., 1996) and models (Fishman and Crutzen, 1978; Crutzen, 1994; Müller and Brasseur, 1995; Roelofs and Lelieveld, 1995; Wang et al., 1998a) all agree that a substantial amount of tropospheric ozone concentration is due to photochemical production in the troposphere. Using separate tracers for ozone produced in the stratosphere and different regions of

the troposphere, Wang et al. (1998b) show in a model study that the contribution of transport of ozone from the stratosphere to ozone concentrations in the troposphere is about 30% at mid-latitudes in winter, 10% in summer, and 5% in the tropics.

Photochemical production of ozone is linked to the presence of NO_x emitted from various sources, through the reactions:

$$NO_2 + h\nu \rightarrow NO + O(^3P) \quad \text{(R5)}$$

$$O(^3P) + O_2 + M \rightarrow O_3 \quad \text{(R6)}$$

where $h\nu$ is a photon of wavelength, $\lambda \lesssim 420$ nm and M is any atmospheric molecule to which the excess energy produced is transferred. Through Reactions (R4)–(R6), a fast photochemical cycle is established between NO and NO_2. The efficiency of ozone formation depends critically on the NO/NO_2 ratio. Tropospheric chemistry becomes much more complex when CO, methane and VOCs reactions are included (Finlayson-Pitts and Pitts, 1997; Kley, 1997; Seinfeld and Pandis, 1998; Brasseur et al., 1999) due to the possibility for several reaction pathways, depending on the concentrations of reactants and the condition of the atmosphere (especially, the amount of radiation and humidity).

The increase in NO_x, VOCs and CO emissions has led to a worldwide increase in tropospheric ozone concentrations. This increase has been observed globally over the past century (Fishman and Crutzen, 1978; Logan, 1985; Bojkov, 1986; Volz and Kley, 1988; Anfossi et al., 1991; Crutzen, 1995). Specifically, the reconstructed data of ozone concentrations show more than two-fold increase in ozone concentrations over the entire troposphere of Europe (Anfossi et al., 1991; Staehelin et al., 1994). Presently, mean surface ozone concentrations measured in the remote areas of the world (about 30 – 40 ppbv) are between two to three times higher than those measured in the pre-industrial times (about 10 – 15 ppbv) (Volz and Kley, 1988). Perhaps even more meaningful is the fact that peak ozone concentration at Montsouris never exceeded 40 ppbv, while concentrations well above 200 ppbv were frequently measured in Los Angeles and Mexico city in the 1970s and 1990s respectively.

1.3.3 Transport of air pollution

Most tropospheric trace species are not homogeneously distributed. This is because they have spatially inhomogeneous sources. Also, they have different atmospheric resident times, which is determined by how fast they are oxidized by OH, O_3 or NO_3. The atmosphere also transports and mixes trace gas constituents at various time scales. Transport times in the troposphere are governed by wind speeds, small and large scale turbulence, planetary wave action and slow residual circulations (Mahlman, 1997).

Inter-hemispheric exchange is achieved in about 1 to 2 years, meridional transport across latitude belts takes months, and zonal transport in bands of constant latitudes is achieved in about 2 weeks. Vertical mixing can occur in as long time as 1 month, or in as short time as 1 hour, when deep convection is active, and boundary layer air is

lifted to the upper troposphere. Pollutants are also affected by advective transport, which leads to export and import of species emitted far away (e.g. see Schultz and Bey, 2004). Hence the impact of the species can be felt farther from their region of emissions or formation, thereby making air pollution a global problem.

The similarity of oxidation and transport time scales leads to the connection between transport and chemistry (Kley, 1997). Due to this connection and the complexity of tropospheric chemistry, chemistry transport models are needed to simulate the inter-dependency of trace gas emissions, concentrations and their chemical reactions. Models also represent the only way to assess how perturbations in emissions or from climate change might affect the atmospheric chemical composition and air pollution. However, models need to be evaluated in order to test their ability to correctly predict the distributions of atmospheric trace species. The global nature of air pollution and summary of this section is represented in the schematic diagram in Fig. 1.1.

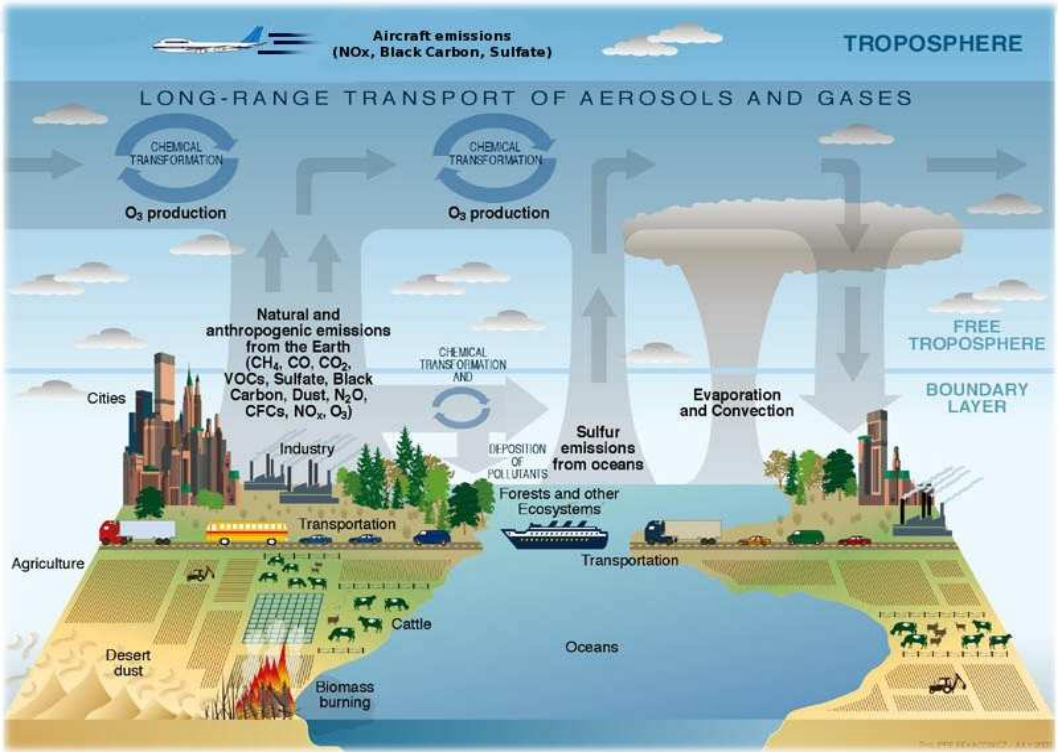

Figure 1.1— Schematic of air pollution, chemical transformation and transport processes related to atmospheric trace species. These processes link the atmosphere with other components of the Earth system, including the oceans, land, and terrestrial and marine plants and animals. Picture is taken from the US Climate Change Science Programme website http://www.climatescience.gov/.

1.4 Air pollution in Africa

1.4.1 Air pollution history and future changes in Africa

Economic and industrial development in Africa is much slower than in other parts of the world (UNIDO Industrial development report, 2004, 2005). The World Bank World Development Indicators (2006) indicate that about 44% of African population live on less than 1 USD per day in 2003. Agriculture is the principal source of employment and income for most poor people in Africa, therefore emissions of atmospheric trace species in Africa are mostly from natural and agriculture-related sources.

Despite the slow economy, rapid urbanisation occurred in some regions of Africa, for example Nigeria, caused by rural–urban migration due to a combination of factors serving as incentives to migrants, which include social amenities, industry, schools and health-care facilities (Afolayan, 1985). Lagos, Nigeria population has increased from 1.7 million in 1975 to about 10.9 million in 2005, and it is projected to become the first and the eleventh most populous city in Africa and the world, respectively by 2015 (UN World Urbanization Prospects, 2005) with about 16 million inhabitants. This high population density resulted in high emissions (e.g. Baumbach et al., 1995).

Farmers clear agricultural land in preparation for planting season (i.e. the onset of wet season). These include clearing forest and brush land, conversion of forests to agricultural and pastoral lands, and removal of bush and litter. The residues are typically burnt in open fires or used as firewood. In its most general form, biomass burning is the burning of living and dead vegetation. It includes human-initiated burning of vegetation for land clearing and land-use change as well as natural and lightning-induced vegetation burning.

Repeated burning modifies the nutrient balance of soils, especially through the process of pyrodenitrification (Crutzen and Andreae, 1990). Over longer time periods, fires may also result in partial or complete destruction of vegetation, through landscape disturbance and impact on soil nutrients. Biomass burning, agriculture, land-use change, deforestation and population dynamics are therefore closely linked in a complex and non-linear interaction (Ojima et al., 1994; Hugh and Lambin, 2000; Hunter, 2000). For example, fires affect vegetation cover, and land-use changes driven by human need for agricultural extension and other human activities result in deforestation (Houghton, 1994), but deforestation directly influences available biomass for burning. Deforestation also influences the spontaneous propagation of fires, due to landscape fragmentation (Hugh and Lambin, 2000). Therefore quantifying the spatio-temporal distribution of the amount of trace gases and aerosols emitted during biomass burning is difficult and complex (Hao and Liu, 1994). The UNDP reported that the African continent lost more than $53\,000\,\mathrm{km}^2$ of its virgin forest in the 1990s, apart from the regular savanna burning.

Studies on air pollution over Africa did not become popular until after the discovery of the influence of African biomass burning emissions on tropospheric ozone in the 1970s (e.g. Crutzen et al., 1979). Long before then, research on fire in Africa

focused on the ecological and management aspects, with little or no thought given to the regional and global atmospheric implications of emitted trace species from fires (e.g. see Charter and Keay, 1960; Hopkins, 1963, 1965). The large-scale impact of African fires first became clear from the satellite data obtained from the Total Ozone Mapping Spectrometer (TOMS) and the Stratospheric Aerosol and Gas Experiment (SAGE) between 1979 and 1989 (Fishman and Larsen, 1987), when the tropospheric data show a well-defined maximum of ozone of more than 45 DU over large part of central Africa during September and October (Fishman et al., 1990). Since then, many field experiments and campaigns have been carried out in Africa in order to quantify the enormous amount of trace species emitted by African biomass burning and to understand their transport and impact on tropospheric chemistry. The major international field experiments on the African continent are listed in Table 1.1.

Although, African anthropogenic emissions are currently much lower than those in other parts of the world, this may change in the future, due to industrial advancement, transfer of old technologies from western world and continued increase urbanisation. On the other hand, biomass-burning emissions may be reduced as a result of firmer legislation on bush burning and improvement in the dissemination of information regarding health and climate implications of bush burning.

1.4.2 Main sources of air pollution in Africa

Biomass burning and natural sources dominate emissions in Africa, while the emissions of industrialised countries are mainly anthropogenic in origin. This is due to higher energy consumption and industrial activities in industrialised countries than in Africa. For example the total energy consumed by the OECD countries[2] in the year 2003 is about 56% of the total energy consumed by the world, despite that these countries are just 18% of the world population (International Energy Outlook, 2006). Natural emissions in Africa are mainly from vegetation and soil, lightning NO_x emissions. Africa contributes a significant amount to the global emissions from these three sources, while emissions from fossil fuel combustion are important only on the regional scale.

Biomass burning is a leading source of air pollution in the tropics (Crutzen and Andreae, 1990; Hao and Liu, 1994). Presently, Africa is responsible for about 40% of biomass burning activities occurring globally (Crutzen et al., 1979; Andreae, 1991; Hao and Liu, 1994; Helas et al., 1995a; Schultz et al., in review). Human activities are the primary source of African biomass burning emissions and they include savanna, forest and agricultural waste burning (Crutzen and Andreae, 1990). The large variation observed in biomass burning emissions is driven by the "slash and burn" agricultural practices that take place during the dry seasons – late Novem-

[2]Organisation for Economic Cooperation and Development (OECD) countries include United States, Canada, and Mexico, Austria, Belgium, Czech Republic, Denmark, Finland, France, Germany, Greece, Hungary, Iceland, Ireland, Italy, Luxembourg, the Netherlands, Norway, Poland, Portugal, Slovakia, Spain, Sweden, Switzerland, Turkey, and the United Kingdom, Japan, South Korea, Australia, and New Zealand.

Table 1.1— Major African campaigns and experiments conducted to understand the complex interaction of emissions (biomass burning, biogenic and aerosols) and tropospheric chemistry

Acronym	Place and Duration	References
TROPOZ[a] I	West Africa (WA), Dec. 11–22, 1987	Jonquieres et al. (1998)
TROPOZ II	WA, Jan. 9–Feb. 1, 1991	
DECAFE	Congo, Central Africa, Feb. 1988	Fontan et al. (1992)
FOS/DECAFE[b]	Cote d' Ivoire, WA, 1991	Lacaux et al. (1995)
SAFARI-92[c]	South Africa (SA), Sept.–Oct., 1992	Lindesay et al. (1996)
TRACE-A[d]		Fishman et al. (1996)
SA'ARI-94[e]	SA, May 1994	Helas et al. (1995b)
EXPRESSO[f]	Central Africa, Nov.–Dec., 1996	Delmas et al. (1999)
Aerosols99	Cruise from Norfolk, Virginia (USA) to Cape Town (SA) Jan.–Feb., 1999	Bates et al. (2001)
SAFARI-2000	Lusaka, Zambia, Aug.–Sept(1999,2000)	Swap et al. (2002, 2003)
SHADOZ[g]	Kenya, SA and Benin, 1998 (ongoing)	Thompson et al. (2003a,b)
MOZAIC[h]	Major African cities, 1997 – 2004	Marenco et al. (1998)

[a]TROPOZ: TROpospheric OZone experiment.
[b]FOS/DECAFE: Fire of Savannas/Dynamique et Chimie Atmosphérique en Forêt Equatoriale.
[c]SAFARI: Southern Africa Fire-Atmosphere Research initiative.
[d]TRACE-A: Transport and chemistry near the Equator-Atlantic.
[e]SA'ARI: Southern African Atmosphere Research Initiative.
[f]EXPRESSO: EXPeriment for Regional Sources and Sinks of Oxidants.
[g]SHADOZ: Southern Hemisphere ADditional OZonesondes.
[h]MOZAIC: Measurement of OZone and water vapour by Airbus In-service airCraft.

ber to early March in the northern hemisphere (NH), and July to October in the southern hemispheric (SH) part of Africa (Marenco et al., 1990).

African biomass burning exerts large influence on tropospheric chemistry (Crutzen and Andreae, 1990; Andreae, 1993; Helas et al., 1992, 1995a; Marufu et al., 2000). For example tropospheric ozone data obtained from ozone sondes, launched over a 2-year period at Brazzaville, Congo show a maximum of 45 DU between July and September during the fire season in southern Africa (Cros et al., 1992; Nganga et al., 1996). The climatological analysis of MOZAIC data over equatorial Africa also shows elevated ozone throughout the whole troposphere (Sauvage et al., 2005).

Transport of African biomass burning emissions has been observed to influence tropospheric ozone concentrations over the southern Atlantic Ocean (Roelofs et al., 1997),and over the tropical South Pacific (Schultz et al., 1999; Staudt et al., 2002). The latter found that southern Africa and South America make comparable contributions to the long-range transport of biomass burning pollution to the southern Pacific Ocean, from a global chemical model interpretation of Pacific Exploratory Mission-Tropics A (PEM-Tropics A, Hoell et al., 1999) observations. Chatfield et al. (1998, 2002) show the role of African biomass burning emissions in causing el-

evated CO concentrations over the tropical southern Atlantic and Pacific ocean; a feature they referred to as "great African plume" and "subtropical global plume". The spatial scale of the transport of biomass burning plumes observed extends over approximately 10 000 km, making it a planetary-scale phenomenon.

The tropical region has maximum lightning activity. Africa is located in the tropical region, therefore substantial amount of global lightning activity occurs over Africa. Lightning produces NO_x, mostly in the middle to upper troposphere (Ridley et al., 1996; Pickering et al., 1996; Lamarque et al., 1996; Pickering et al., 1998; DeCaria et al., 2000), where it has longer lifetime and greater ozone production potential than in the lower troposphere (Liu et al., 1987; Pickering et al., 1990). However, the uncertainty of tropical lightning NO_x is particularly large, because tropical thunderstorms are the least well characterized.

Vegetation emits a wide range of VOCs (Kesselmeier and Staudt, 1999), including isoprene and terpenes, which are the two most important (Fehsenfeld et al., 1992; Guenther et al., 1995, e.g.). Biogenic VOCs can have a significant impact on tropospheric chemistry as soon as they are released into the air, because of their high reactivity. They lead to the production (or destruction) of ozone in high (or low) NO_x conditions (Wang and Shallcross, 2000; Tie et al., 2003). African rainforest and savannas occupy an area of about 2 million and 10 million km^2, respectively (Achard et al., 2002). Although, the rate of deforestation of virgin rainforest in Africa is about 0.43% per year (this represents 8500 km^2/yr), the results of global biogenic VOCs emissions from vegetation calculated by Guenther et al. (1995) shows that Africa remains one of the main source regions of biogenic emissions. This is because tropical plants have high biomass and are strong emitters of biogenic VOCs.

Anthropogenic emissions occurring in Africa are driven by emissions from transportation in the large cities (e.g. Lagos, (Nigeria) and Cairo (Egypt)), industrial activities in the few industrial regions of the continent (e.g. the Highveld region of South Africa, and the Niger-Delta in Nigeria), and gas-flaring (e.g. flares from Libya and the ever-burning flares across the entire Niger Delta region of Nigeria). The aggregate of these three classes of anthropogenic emissions in almost the same region of the continent makes their regional impact substantial.

1.4.3 Factors influencing the export of air pollution from Africa

The tropical region is a photochemically active region of the atmosphere, due to the combination of high concentrations of water vapour and solar radiation, which lead to the highest OH concentrations worldwide. In combination with this, Africa intricate meteorological patterns, also make the continent an interesting region for intense mixing, transport, and chemistry.

The known dynamical processes at play in Africa include deep convection, advection, monsoon flow, Africa easterly jet (AEJ), tropical easterly jet (TEJ) and anti-cyclones. These processes control the distribution, formation and deposition of atmospheric trace species in Africa. Deep convection is very intense in Africa (Figure 1.2). It causes trace species emitted at the surface to be transported into

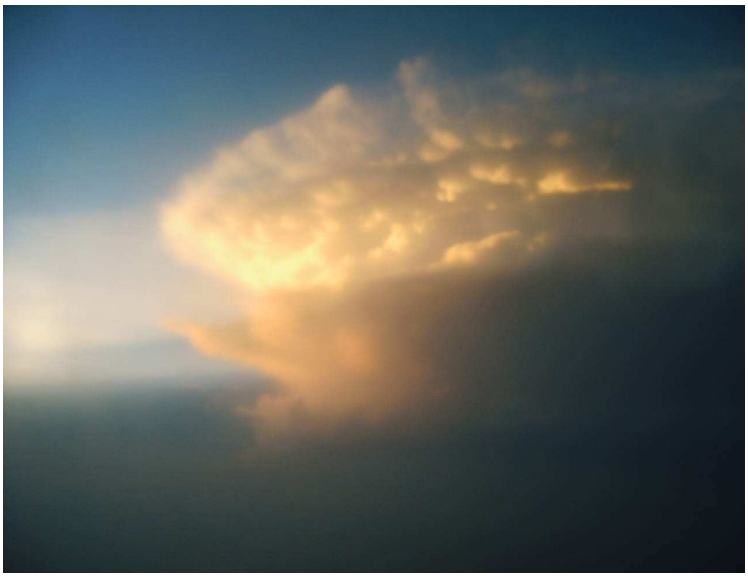

Figure 1.2— Convective cloud over west African region on December 3, 2005. Picture taken by A. M. Aghedo.

the upper troposphere and the stratosphere.

Monsoons are macroscale phenomena, occurring as a result of the differential heating of the land and the ocean, latent heat release into the atmosphere, planetary rotation, and land surface characteristics of the continents (Webster, 1987). Xue et al. (2004) show that exchange of water and energy between vegetation and atmosphere is also one of the important mechanisms governing the development of monsoon, especially the West African and east Asian monsoon. The West African monsoon is a synoptic flow from the south to the west in May through October (e.g. Adefolalu, 1983), extending from the surface to pressure levels around 700 hPa.

The African easterly jet (AEJ, also known as the West African jet) is a westward propagating, synoptic-scale disturbance over West Africa from June to early October, with a period of 3–5 days, a wavelength of about 2000–4000 km (Piersig, 1936; Regula, 1936; Hubert, 1939; Carlson, 1969; Burpee, 1972). The wave is located between 700 – 600 hPa, with a maximum at around 600 hPa (Burpee, 1972; Reed et al., 1977; Cook, 1999). These waves propagate across the tropical North Atlantic Ocean often reaching the Caribbean and even the eastern Pacific. These waves have been recognized to contribute to the initiation of tropical storms and hurricanes not only in the Atlantic and the Caribbean (e.g. Riehl, 1954; Frank, 1970; Landsea, 1993) but also in the eastern Pacific basin (Avila and Pasch, 1992).

The Tropical Easterly Jet (TEJ) is located higher up in the troposphere at around 100 – 200 hPa. It covers 5–20°N, and extends from South China across Southern Asia to Northern Africa, in June through September (Koteswaram, 1958; Flohn, 1964). The TEJ is much stronger than the AEJ, with a maximum speed of about 40 m/s

over India, which decreases to about 10 m/s over Africa (Krishnamurti, 1971a,b). It has been linked to the meridional thermal gradient, which settles over the Tibetan highlands and the Indian Ocean during the southwest Asian monsoon circulation. It exhibits high inter-annual variability (e.g. Kobayashi , 1974; Tanaka, 1982). Recent studies show a decreasing trend in the strength of TEJ (e.g. see Rao et al., 2004; Sathiyamoorthy, 2005). A good review on the description, formation and influence of TEJ on Sahel rainfall is provided in (Hulme and Tosdevin, 1989). The arrival of TEJ is coincident with the onset of the monsoon over Africa and Asia.

During the north-African dry seasons (October – April), north Africa is under the influence of the northeasterly winds referred to as Harmattan, which carries the Saharan dust over to the western Africa, the tropical Atlantic and the gulf of Guinea. The Harmattan wind is met by the southwesterly trade winds at the Inter-tropical convergence zone (ITCZ). The ITCZ shifts from its equatorial position during the dry season to around 10–12°N during the wet season.

The southern Africa region located between the Atlantic and Indian Oceans, is influenced by the large-scale subsidence occurring between the Hadley and Ferret cells of the southern hemisphere general circulation (Newell et al., 1972). Apart from this, the region is also being affected by large-scale recirculation of air, occurring over southern Africa south of 10°S (e.g. see trajectory analysis by Pickering et al., 1994) due to anticyclones. This circulation of air may also occur locally over individual countries, e.g. South Africa (Annegarn et al., 1993; Held et al., 1994). Specifically, Garstang et al. (1996) show that during the NH summer, five anticyclonic modes can be used to describe the horizontal transport out of southern Africa, while three major levels of stable discontinuities persist vertically at around 3, 5 and 8 km respectively. These vertical stability layers limit vertical mixing and transport. The 3 km stable layer often experiences breakage by passage of westerly waves, hence it occurs on and off, whereas the 5 km layer is the most persistent of all the stable layers. The horizontal anticyclones spatial scales vary from few hundreds to thousands of kilometres. On exit from the anticyclones, atmospheric species previously trapped within the cyclone can be transported over the Atlantic ocean by a semi-stationary easterly wave, or by the westerlies to the east into the Indian Ocean. Diab et al. (1996) show the influence of this circulation on the distribution of ozone data collected during SAFARI-92.

In contrast to western and southern Africa, the eastern Africa circulation is slightly different due to the influence of topography and the proximity of the Indian ocean. The Arabian and Mascarene anticyclones, with East African low-level Jet (EAJ, popularly known as Somali Jet) (Findlater, 1969, 1972, 1974) prevail over eastern Africa. The Eastern Africa and Malagasy mountains have been shown to constitute an important factor in the evolution of EAJ (Krishnamurti et al., 1976). The EAJ originates from South Indian Ocean in form of southeast trades, crossing the tips of Malagasy mountain in Madagascar. Their typical speed is 5–10 m/s.

1.5 Scope and contents of this thesis

This thesis aims at investigating the global impact of air pollution emitted in Africa. It quantifies the magnitude and characterises the seasonality, the inter-annual variability and the dynamics of transport of primary and secondary air pollutants due to African emissions. Due to the global nature of pollution impact, this work is carried out with a global three-dimensional (3D) model, which encompasses a detailed general circulation model of the atmosphere and a chemistry transport model. The thesis is structured in the following way:

Chapter 2 provides the description of the global 3D general chemistry climate model (ECHAM5-MOZ) employed in this study.

Chapter 3 presents the contribution of this PhD work to model development by the implementation of the model of biogenic VOCs emissions (MEGAN) into ECHAM5-MOZ. The results of a study on the influence of climate on biogenic VOCs emissions are also presented in this chapter.

Chapter 4 offers a detailed evaluation of ECHAM5-MOZ by comparing the simulated tropospheric ozone and CO to measurement data.

Chapter 5 gives the results of the sensitivity analysis of the transport patterns in ECHAM5. The sensitivity study presents the results involving nine global tracers "emitted" at various latitudinal and vertical levels of the atmosphere. Sensitivity of transport of tracers to variation in model resolution, driving meteorology and lifetime of tracers is tested.

Chapter 6 presents an investigation into the influence of African air pollution. The regional and global impacts of biomass burning, biogenic, lightning and anthropogenic emissions were simulated in series of model simulations, and are discussed here together with some estimates of uncertainty.

Chapter 7: This chapter contains the summary and conclusions. The main findings of the thesis are highlighted.

The work presented in Chapter 5 is being prepared for submission to a peer-review journal, while the study described in Chapter 6 has been published in Atmospheric Chemistry and Physics.

Chapter 2

The global chemistry climate model ECHAM5-MOZ

The 3-D global chemistry climate model ECHAM5-MOZ is part of the Max Planck Institute, Hamburg Earth System Model (ESM) and consists of the 3-D global general circulation model (GCM) ECHAM5 (Roeckner et al., 2003) into which the tropospheric chemistry of the chemical transport model (CTM), MOZART2 (Horowitz et al., 2003) has been implemented. The surface ultraviolet (UV) albedo was adapted from Laepple et al. (2005). The ECHAM5-MOZ model also includes a dry and wet deposition scheme, and interactive calculation of lightning NO_x and biogenic VOC emissions. This chapter presents a brief description of the ECHAM5-MOZ model, the full description of the model and its sensitivity to different emission inventories and driving meteorology can be found in Rast et al. (in prep.)[1]. Figure 2.1 shows the schematics of the ECHAM5-MOZ model. In addition to this gas-phase chemistry module MOZ, a multi-model aerosol scheme HAM has also been developed by Stier et al. (2005) as part of the Hamburg ESM. Recently, HAM and MOZ were coupled together to form the HAMMOZ model (Pozzoli, 2007).

2.1 Model description

2.1.1 Atmospheric dynamics

The dynamical core of ECHAM5 solves prognostic equations for vorticity, divergence, logarithm of surface pressure and temperature expressed in spectral coefficients. The vertical axis uses a hybrid terrain-following sigma-pressure coordinate system (Simmons and Burridge, 1981). The model uses a semi-implicit leapfrog time integration scheme (Robert et al., 1972; Robert, 1981, 1982) with a special time filter (Asselin, 1972). Details of the physical parameterisations including radiation,

[1]Rast, S., Schultz, M. G., Aghedo, A. M., Diehl, T., Rhodin, A., Schmidt, H., Stier, P., Ganzeveld, L. and Walters, S.: Sensitivity of a chemistry climate model to changes in emissions and the driving meteorology, in preparation.

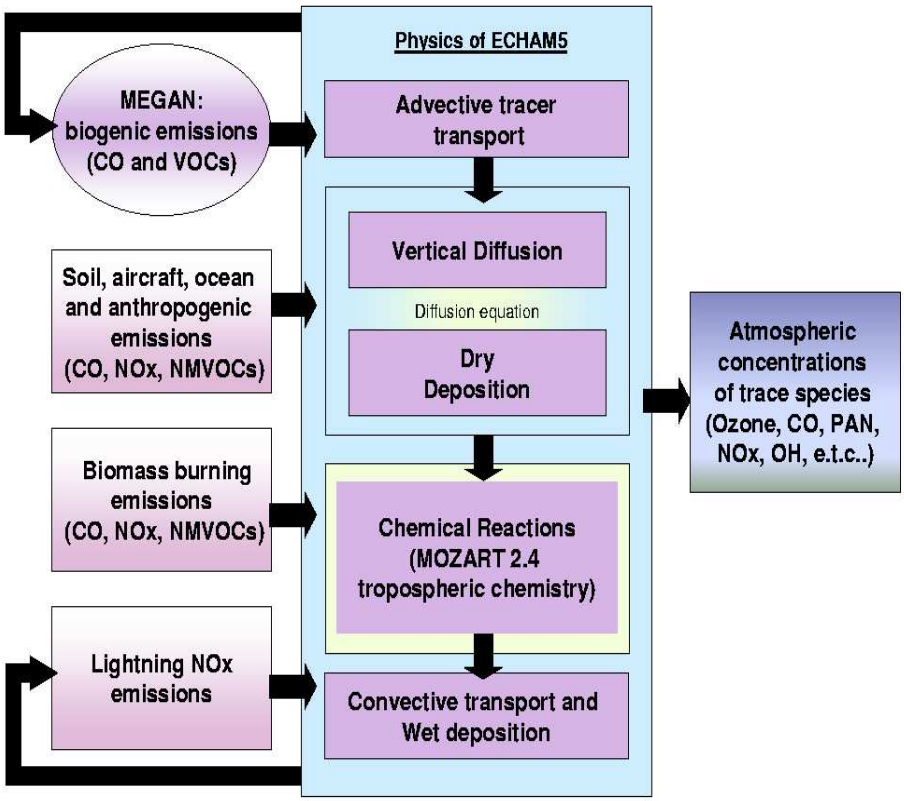

Figure 2.1— Schematics of the ECHAM5-MOZ model. ECHAM5 transports the trace species and calculates meteorological variables such as temperature and humidity. The MOZART2.4 tropospheric chemistry accepts emissions as inputs and calculates the concentration of trace species. Deposition, lightning NO_x and all emissions are as shown.

surface processes such as heat and water budget, gravity wave drag, cumulus convection, stratiform cloud formation, orbit variations, and subgrid scale orography can be found in Roeckner et al. (2003).

ECHAM5-MOZ (just as ECHAM5) can be run as a coupled ocean-atmosphere model or in an atmosphere-only mode. It can also be run in various horizontal resolutions such as T42 ($\sim 2.8^\circ \times 2.8^\circ$), T63 ($\sim 1.9^\circ \times 1.9^\circ$) and T106 ($\sim 1^\circ \times 1^\circ$) using 19 or 31 σ-hybrid vertical levels and standard ECHAM5 time steps. The time step depends on both horizontal and vertical resolutions; for L19, it is 30, 20 and 10 minutes while for L31, it is 20, 12 and 6 minutes for T42, T63 and T106 respectively. The effect of varying model resolutions on simulated climate in ECHAM5 is described in Roeckner et al. (2006). The sensitivity of transport of tracers in ECHAM5 to model resolution and forcing meteorology is discussed in Chapter 5.

2.1.2 Chemistry scheme

The ECHAM5-MOZ model uses the MOZART2 tropospheric chemistry scheme, consisting of 63 transported species and 168 chemical reactions. The details of the chemical species, reactions, kinetic equations and the chemistry solver are described in Horowitz et al. (2003). As in the original MOZART model, the ECHAM5-MOZ chemical reaction scheme is flexible due to the MOZART2 pre-processor that produces machine dependent optimised (e.g. vectorized and parallelized) code for a specific set of user-defined reactions. An implicit Euler method is applied for the integration of the kinetic non-linear differential equations for most of the species. The ECHAM5-MOZ model employs a consistent link of the chemistry calculation with the parameterisation of the dynamics and the physics of the ECHAM5 model.

2.1.3 Tracer transport and deposition

Tracers in ECHAM5-MOZ undergo advective and convective transport, vertical diffusion, dry and wet deposition, and chemical reactions in the atmosphere. The advection of tracers is based on a mass conserving flux-form semi Lagrangian transport scheme (Lin and Rood, 1996) on a Gaussian grid (Arakawa C-grid, Mesinger and Arakawa (1976)). Convective transport is parameterised according to the mass-flux algorithm of Tiedtke (1989) with modifications proposed by Nordeng (1994). ECHAM5-MOZ extends the vertical diffusion equations of ECHAM5 to include the net flux of tracers at the earth's surface (e.g emission and dry deposition). The dry deposition is according to the scheme of Ganzeveld (2001). The wet deposition is based on the wet deposition scheme of Stier et al. (2005), with modifications for below-cloud scavenging for species like HNO_3 using the model described in Seinfeld and Pandis (1998), page 1003. This dynamical wet deposition scheme takes into consideration the solubility of the tracers and the possibility of the release of trace gases into the atmosphere by re-evaporation of precipitation.

2.2 Emissions

The ECHAM5-MOZ model needs gridded emission data for NO_x, CO and non-methane VOCs. Emissions are either calculated interactively within the model (as in the case of lightning and biogenic VOC emissions) or supplied as globally-gridded files.

2.2.1 Biogenic emissions

The ECHAM5-MOZ model contains an interactive online calculation of species emitted from vegetation according to the Model of Emissions of Gases and Aerosols from Nature (MEGAN) (Guenther et al., 2006). The species calculated by MEGAN include isoprene, terpenes, carbon monoxide, methanol, formaldehyde, acetaldehyde, acetone, propene, ethane and ethene.

The description of the MEGAN module, its implementation and the estimated emissions flux in the present-day, past and future climate is provided in Chapter 3. Other biogenic emissions from soil and termites, which are not calculated by MEGAN are prescribed as gridded fields.

2.2.2 Lightning emissions

ECHAM5-MOZ includes interactive lightning NO_x emissions according to the parameterisation of Grewe et al. (2001). The lightning frequency is calculated as a function of the mean updraught velocity in a convective column. The mean updraught velocity is resolution dependent, because it depends on the size of the grid boxes. Therefore, the parameterisation contains one freely adjustable global factor that accounts for the grid-box dependency. The NO_x emissions are proportional to the calculated flash frequency and are distributed vertically in the atmosphere using C-shaped profiles for tropical and extra-tropical continental and marine clouds as described in Pickering et al. (1998). This parameterisation yields global lightning emissions of about 2.7 Tg (N)/yr in ECHAM5-MOZ. Over Africa, total lightning emissions are about 0.7 Tg (N)/yr.

The lightning NO_x emissions is directly proportional to the lightning flash frequency. Figure 2.2 shows the comparison of total lightning flashes (i.e. cloud-to-ground (CG) and intra-cloud (IC) flashes) calculated by the ECHAM5-MOZ model with Lightning Imaging Sensor (LIS) and Optical Transient Detector (OTD) data (Boccippio, 2002; Christian et al., 2003), available for free at http://thunder.nsstc.nasa.gov/. Figure 2.2 compares the seasonal climatology of the flash frequency calculated by the ECHAM5-MOZ model in 1991–2000 to LIS/OTD data in 1995–2005. Figure 2.2 shows that the seasonal distribution of the lightning flashes is well captured by the ECHAM5-MOZ model. The model slightly overestimates the magnitude of the lightning flash frequency over the tropical Pacific and Indian Ocean, and over the western Sahel region.

2.2.3 Other emissions

Other emissions besides lightning and biogenic emissions are not calculated interactively within ECHAM5-MOZ. These emissions are therefore prescribed as globally gridded files. Usually the ECHAM5-MOZ model reads emission files once per month. However, the frequency at which the files are read depends on the time resolution of the emission files. ECHAM5-MOZ also provides the possibility of switching off all interactive emissions, and using prescribed emissions only. Aircraft and fire emissions are injected into ECHAM5-MOZ at various model heights, while surface emissions are introduced as a flux boundary condition in the vertical diffusion routine of ECHAM5.

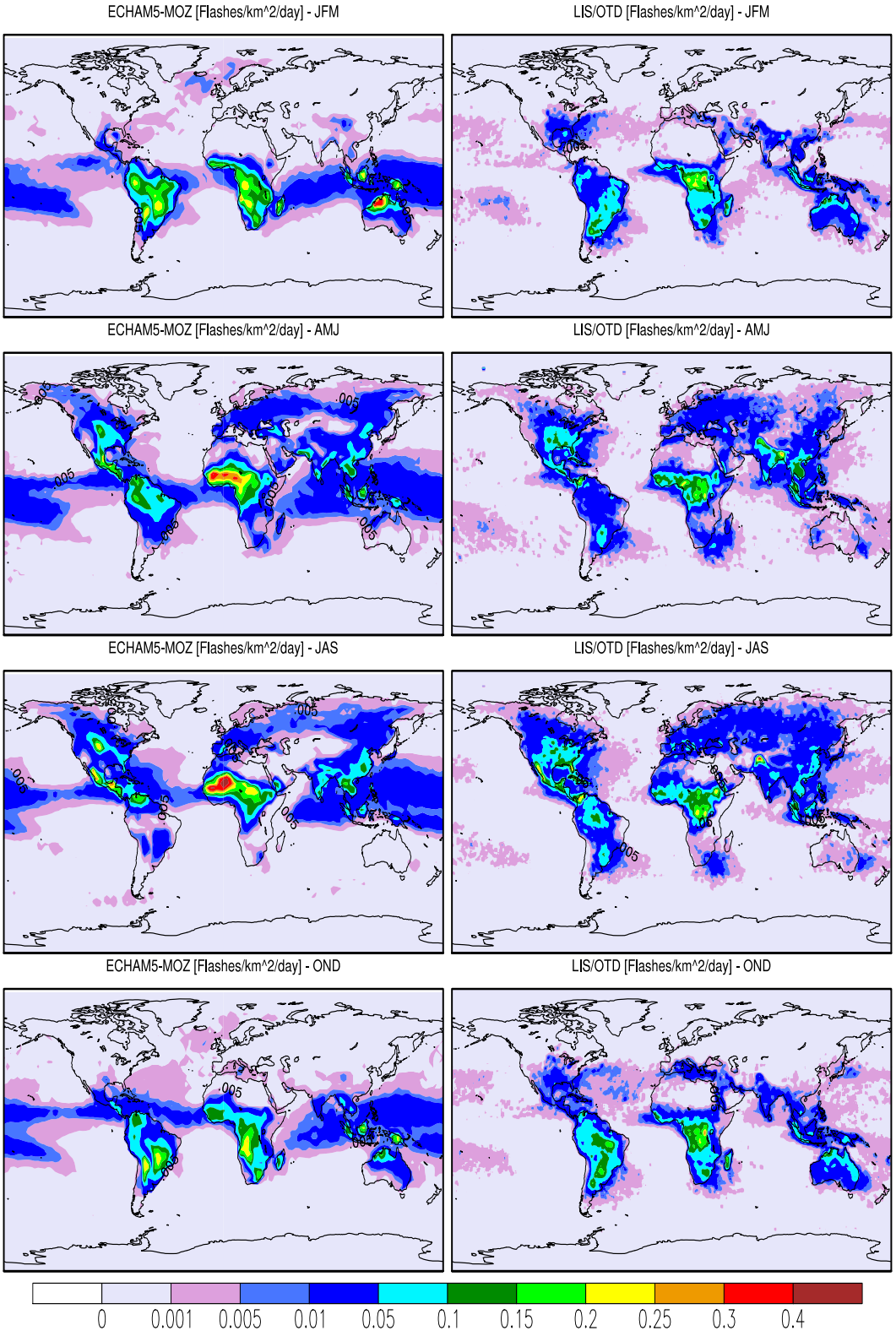

Figure 2.2— The comparison of the seasonal climatology of the total lightning flashes (IC+CG) calculated in ECHAM5-MOZ (left) in 1991 – 2000 with LIS/OTD data (right) of 1995–2005.

2.3 Conclusion

The ECHAM5-MOZ model has been briefly described in this chapter. Based on its combination of the full dynamics of the ECHAM5 GCM and the tropospheric chemistry of MOZART2, ECHAM5-MOZ provides a good model architecture for studying and assessing the global impact of emissions occurring at any given location, and it is one of the few existing models to allow for the assessment of climate-chemistry interactions.

Chapter 3

MEGAN: Biogenic emissions from vegetation in ECHAM5-MOZ

3.1 Introduction

The Model of Emissions of Gases and Aerosols from Nature (MEGAN) was developed at the Biosphere-Atmosphere Interaction research group of the Atmospheric Chemistry Division, National Center for Atmospheric Research (NCAR) by Guenther and co-workers (see http://bai.acd.ucar.edu/) . MEGAN replaces the global volatile organic compounds (VOCs) model released in 1995 (Guenther et al., 1995). The MEGAN model is designed for simple implementation into regional and global models.

The version 1.0 of MEGAN can calculate emissions of 52 atmospheric trace species from vegetation. These species consist of isoprene, 27 terpenes (which are lumped together), 23 non-terpene VOCs, and carbon monoxide (CO). Isoprene, terpenes, CO and 7 non-terpene VOCs, which include acetaldehyde (CH_3CHO), acetone (CH_3COCH_3), ethane (C_2H_6), ethene (C_2H_4), formaldehyde (CH_2O), propene (C_3H_6), and methanol (CH_3OH), are currently implemented in the MEGAN module of ECHAM5-MOZ. The remaining 16 non-terpene VOCs that are not included in the MEGAN implementation altogether represents about 10% of the global biogenic VOCs emissions. The global isoprene emissions calculated by MEGAN and their sensitivity to various driving variables are presented in Guenther et al. (2006).

The emissions of isoprene, terpenes, CO and other VOCs from the terrestrial vegetation are of great significance for the chemistry of the troposphere, in particular in the tropical region. This chapter presents the present-day emission flux estimated by MEGAN in ECHAM5-MOZ. As these emissions are temperature and radiation dependent, one may expect significant impacts from global warming. We therefore investigate the changes in emissions under the climate conditions of the past and the future.

The current version of MEGAN does not account for changes in the vegetation types and their distribution due to the influence of climate change. This feedback is nevertheless important and some of the results presented here may change if this feedback is considered. For example Sanderson et al. (2003) shows that the increase recorded in isoprene emissions from 1990s to 2090s reduces by about 39 Tg/yr (from 736 Tg/yr to 697 Tg/yr) when vegetation change is taken into account. However, Constable et al. (1999) modelled the independent and combined influence of simulated changes in temperature, CO_2 concentration and vegetation distribution due to climate change (caused by doubling CO_2 concentration) on biogenic VOC emissions over the United States. They show that the increase recorded in biogenic VOC emissions due to increase in CO_2 concentration is balanced by the decrease in biogenic VOC emissions due to the decline in area covered by vegetation classes which emit VOCs at higher rates. In their conclusion, they state that "the total annual U.S. VOC emission in the future climate scenario differs little from that predicted by temperature alone". Lathière et al. (2006) show in a model study that land use change (depicted by an artificial scenario of tropical deforestation) could result in about 29% decrease in global isoprene emissions and about 22% increase in global methanol emissions.

The implementation of MEGAN in ECHAM5-MOZ is presented in Section 3.2, while the model simulation set-up is described in Section 3.3. The present-climate emission rate estimated by MEGAN is discussed in Sections 3.4, estimations of past and future emissions are presented in Section 3.5. Section 3.6 discusses the influence of meteorology on biogenic emissions. The conclusion is given in Section 3.7.

3.2 MEGAN implementation in ECHAM5-MOZ

The description in this section follows the MEGAN documentation. MEGAN calculates the emission rate, E of a trace species, s from a terrestrial ecosystem to the atmosphere at a specific location and time as:

$$E_s = \varepsilon_s \cdot \gamma_s \cdot \rho_s \tag{3.1}$$

where ε (in $\mu g\,(C)\,m^{-2}h^{-1}$) is the emission factor at standard atmospheric conditions. The standard atmospheric conditions include leaf area index (LAI) of 5, and a canopy with 80% mature, 10% growing and 10% old foliage; environmental conditions include air temperature of 303 K, photosynthetic photon flux density (PPFD) of 1500 $\mu mol\,m^{-2}s^{-1}$ at the top of the canopy, humidity of 14 g/kg, wind speed of 3 m/s and soil moisture of 0.3 m^3/m^3. All vegetation types at the location and time are classified into six plant functional types (PFTs) in MEGAN. These PFTs are broadleaf trees, fineleaf evergreen trees, fineleaf deciduous trees, shrubs, crops and grass. Grass includes other ground cover such as forbs, serges and mosses. The emission factor, ε therefore represents the weighted average emission factor of the six PFTs at a certain location (i.e. grid-box). The activity factors, γ and ρ account

for changes in emissions due to deviation from the standard atmospheric conditions. The activity factor, γ accounts for changes in vegetation canopy (i.e. LAI and leaf age), while ρ accounts for the influence of changes in temperature and solar radiation on the emission flux of the species.

There are two types of γ. Type 1 (γ_1) is for isoprene, while type 2 (γ_2) is for other species. γ_1 is defined as:

$$\gamma_1 = \left(\frac{0.49\,\lambda}{\sqrt{1 + 0.2\,\lambda^2}} \right) \cdot (0.01\,\psi_n + 0.5\,\psi_g + \psi_m + 0.33\,\psi_o) \tag{3.2}$$

Where λ is the LAI, and ψ are dimensionless factors, which depend on the canopy leaf age. The subscripts n, g, m and o represent new, growing, mature and old leaves respectively. The canopy is divided into age groups depending on the differences between the LAI of the current month (λ_c) and the previous month (λ_p). If $\lambda_\mathrm{c} = \lambda_\mathrm{p}$, then $\psi_m = 1$ and $\psi_n = \psi_g = \psi_o = 0$. If $\lambda_\mathrm{c} < \lambda_\mathrm{p}$, then $\psi_n = \psi_g = 0$, $\psi_o =$ (λ_p - λ_c)/ λ_p and $\psi_m = 1 - \psi_o$. In the final case where $\lambda_\mathrm{c} > \lambda_\mathrm{p}$, $\psi_o = 1$, and ψ_n, ψ_g, and ψ_m is determined based on the number of days after bud-break required to induce isoprene emissions, t_i and the number of days after bud-break required to reach peak isoprene emission rates, t_m as:

$$\psi_n = \begin{cases} 1 - \lambda_p/\lambda_c & \text{if } t \leqslant t_i \\ \left(\frac{t_i}{t}\right)\left(1 - \frac{\lambda_p}{\lambda_c}\right) & \text{if } t > t_i \end{cases}$$

$$\psi_g = \begin{cases} 0 & \text{if } t \leqslant t_i \\ \left(\frac{t_g - t_i}{t}\right)\left(1 - \frac{\lambda_p}{\lambda_c}\right) & \text{if } t > t_i \end{cases}$$

$$\psi_m = \begin{cases} \lambda_p/\lambda_c & \text{if } t \leqslant t_m \\ \frac{\lambda_p}{\lambda_c} + \left(\frac{t - t_m}{t}\right)\left(1 - \frac{\lambda_p}{\lambda_c}\right) & \text{if } t > t_m \end{cases}$$

where

$$t_g = \begin{cases} t & \text{if } t \leqslant t_m \\ t_m & \text{if } t > t_m \end{cases}$$

γ_2 is calculated from:

$$\gamma_2 = \frac{\lambda}{5} \tag{3.3}$$

There are also two types of ρ, based on the assumption that emissions of some trace species such as isoprene are controlled by temperature and radiation, while all the others (e.g. terpenes) are primarily influenced by temperature. Type 1 (ρ_1) is used for isoprene, while type 2 (ρ_2) is used for all other species. ρ_1 is defined as:

$$\rho_1 = \left(\frac{452 \cdot e^{70x}}{200 - 70(1 - e^{200x})} \right) \cdot \left(\frac{1.21\,\alpha\,\beta}{\sqrt{1 + \alpha^2\,\beta^2}} \right) \tag{3.4}$$

where β (in μmol m^{-2}s^{-1}) is the PPFD (also called the photosynthetically active radiation, PAR), $\alpha = 0.001$, and x in Equation (3.4) is calculated from:

$$x = \frac{1}{R}\left(\frac{1}{T_m} - \frac{1}{T}\right)$$

where $R = 0.00831$ kJ/(mol K) is the universal gas constant, $T_m = 317$ K and T (in K) is the air temperature directly above the canopy. The PPFD, β is the total photon flux in the 400 to 700 nm wavelength band. It is approximated from the incoming short wavelength solar radiation (GSW), ω (in W/m^2) by assuming that half of GSW is in the 400 to 700 nm wavelength band, and a conversion factor of 4.766 (μmol m^{-2}s^{-1} per W/m^2), that is:

$$\beta = \omega \times 4.766 \times 0.5$$

ρ_2 is given by:

$$\rho_2 = \exp[\kappa(T - 303.15)] \tag{3.5}$$

where $\kappa = 0.09\,\mathrm{K}^{-1}$. Note that for standard atmospheric conditions, γ and ρ are equal to 1.0.

The quantity ε is provided as global annual-average gridded data within MEGAN. There are three such files for isoprene (ε_i), terpenes (ε_t) and other non-terpene VOCs (ε_n) respectively. The emission activity, γ is supplied as global monthly-average gridded data. These global gridded data are supplied in 1° by 1° resolution. The air temperature above the canopy, T needed in MEGAN is assumed to correspond to the temperature at the lowest model level in ECHAM5-MOZ. The incoming short wavelength solar radiation is calculated in the ECHAM5 radiation module as:

$$\omega = \omega_t - \omega_r \tag{3.6}$$

where ω_t is the net solar radiation (code 176 in ECHAM5), and ω_r is the reflected solar radiation (code 204 in ECHAM5). Note that ω_r is negative in sign, therefore, Equation (3.6) depicts an addition.

The emission flux of each compound calculated by MEGAN within ECHAM5-MOZ is therefore:

Isoprene:	$E_i = \varepsilon_i \times \gamma_1 \times \rho_1$
Terpenes:	$E_t = \varepsilon_t \times \gamma_2 \times \rho_2$
Other non-terpene compounds	
Methanol:	$E = 30.7 \times \varepsilon_n \times \gamma_2 \times \rho_2$
Formaldehyde:	$E = 4.1 \times \varepsilon_n \times \gamma_2 \times \rho_2$
Acetaldehyde:	$E = 3.1 \times \varepsilon_n \times \gamma_2 \times \rho_2$
Acetone:	$E = 1.9 \times \varepsilon_n \times \gamma_2 \times \rho_2$
Propene:	$E = 1.36 \times \varepsilon_n \times \gamma_2 \times \rho_2$
Ethane:	$E = 0.5 \times \varepsilon_n \times \gamma_2 \times \rho_2$
Ethene:	$E = 0.5 \times \varepsilon_n \times \gamma_2 \times \rho_2$
Carbon monoxide:	$E = 12.5 \times \varepsilon_n \times \gamma_2 \times \rho_2$

where the emission flux, E of the non-terpene VOCs includes a factor (the first numbers on the right-hand side of equations above), which relate the lumped emission factor, ε_n (in μg(C) m^{-2}h^{-1}) to emission flux, E (in millimoles of compound km^{-2}h^{-1}). The emission flux, E_i and E_t for isoprene and terpenes is in μg(C) m^{-2}h^{-1} respectively.

MEGAN in ECHAM5-MOZ therefore calculates hourly, daily, seasonal and annual variation in emissions of biogenic trace species from living vegetation. The formula for calculating the emission flux, E for the remaining 16 non-terpene VOCs, which are not implemented in the MEGAN module are provided in Appendix A. The appendix also includes MEGAN input files (i.e. ε_i, ε_t, ε_n, γ_1 and γ_2).

3.3 Model set-up and simulations

In order to investigate the potential changes in biogenic VOC emissions under different climate conditions, we performed one experiment for the past (1891 – 1900), one experiment for the present-climate (1991 – 2000) and two experiments for the future climate (2091 – 2100). All experiments were run in the resolution T31L19 (approximately 3.75°by 3.75°, which is about 400km by 400km) with a spin-up period of 6 years. The two future simulations are based on two different scenarios, which are the most optimistic (B1) and the most pessimistic (A2) IPCC SRES scenarios. These scenarios respectively correspond to the S11 and the S16 experiments in the ECHAM5-MPIOM IPCC simulations, which were performed at the Max Planck Institute for Meteorology, Hamburg. All experiments were driven with sea surface temperatures (SST), sea ice cover (SIC) and greenhouse gases (GHG) from these coupled ocean-atmosphere simulations with ECHAM5-MPIOM.

The results of the present-climate conditions are reported in Section 3.4. The difference between the past and the present-climate simulations is discussed in Section 3.5.1, while the difference of the future and the present-climate experiments is presented in Section 3.5.2. Table 3.1 gives the summary of the experiment set-up.

Table 3.1— Simulations performed to calculate biogenic emission rates by MEGAN in the ECHAM5-MOZ model in the past, present-day, and the future climate.

Experiments	Duration	Driving meteorology
Present-climate	1991 – 2000	ECHAM5-MPIOM IPCC SST, SIC and greenhouse gases
Present-day[a]	1991 – 2000	ERA-40 SST, temperature, surface pressure, vorticity and divergence
Past-climate	1891 – 1900	ECHAM5-MPIOM IPCC SST, SIC and greenhouse gases
Future 1	2091 – 2100	ECHAM5-MPIOM IPCC scenario B1 SST, SIC and greenhouse gases
Future 2	2091 – 2100	ECHAM5-MPIOM IPCC scenario A2 SST, SIC and greenhouse gases

[a] This experiment is described in Section 3.6.

3.4 Present-climate biogenic emissions

3.4.1 Emission distribution and seasonal variability

Figures 3.1 shows the spatial distribution of the emission flux of isoprene, terpenes and CO and other non-terpene VOCs as calculated in the present-climate experiment. The isoprene emission distribution shown in Figures 3.1 (top panel) reveals high emissions over the Australian desert in January, and over western USA in July due to high emission factor, ε_i over both regions (see Section 3.6 for the correction of this overestimation and simulation using ERA-40 meteorology). The global annual emissions flux estimated by MEGAN is 587 Tg(C)/yr for isoprene, 172 Tg(C)/yr for terpenes, 41 Tg(C)/yr for CO and 175 Tg(C)/yr for other non-terpene VOCs (see Table 3.5 for the individual non-terpene VOCs global annual emissions).

The contribution from various geographical land regions to global annual emissions of isoprene, terpenes and CO and other non-terpene VOCs is shown in Tables 3.2, 3.3 and 3.4, respectively. The second column of Tables 3.2 to 3.4 shows that Latin America, Africa, Southeast and South-central Asia together account for about 61%, 67% and 69% of global isoprene, terpenes, and non-terpene VOCs emissions respectively.

The seasonal variation of isoprene, terpenes and other non-terpene VOCs emissions are as shown in Fig. 3.2. The seasonality shows that emissions occur throughout the whole year in the tropical region, whereas emissions start in late-spring and continue until early-autumn in the extra-tropical regions.

3.4.2 Comparison of present-climate emissions with other models

Table 3.5 presents the comparison of our global emission estimate to estimates from other global studies. The table shows that our global isoprene emissions are within the range of global values (440 – 660 Tg(C)/yr) calculated by other models that use MEGAN (Guenther et al., 2006). Our global isoprene estimate also lies within the values reported in other literature as shown in Table 3.5.

The global terpene emission estimate reported in Levis et al. (2003) and Naik et al. (2004) are lower than our estimate (172 Tg(C)/yr) by about a factor of 2.5 and 5, respectively. This is because Levis et al. (2003) uses lower emission rates for some plant functional types, and different land cover and LAI. Also Naik et al. (2004) terpene emissions from tropical forests and temperate evergreen conifer forests are particularly low.

Our estimate of global methanol emissions (102 Tg (C)/yr) is within the range of those reported in earlier studies, except the estimate of Galbally and Kirstine (2002) (37.5 Tg(C)/yr), which is significantly lower. This is because the Galbally and Kirstine (2002) model is based on an entirely different approach, which estimates methane emissions based on flowering plant biosynthesis and metabolic properties. These plant properties were then extrapolated by the net primary production of terrestrial ecosystems to calculate their global methanol emissions. Their result-

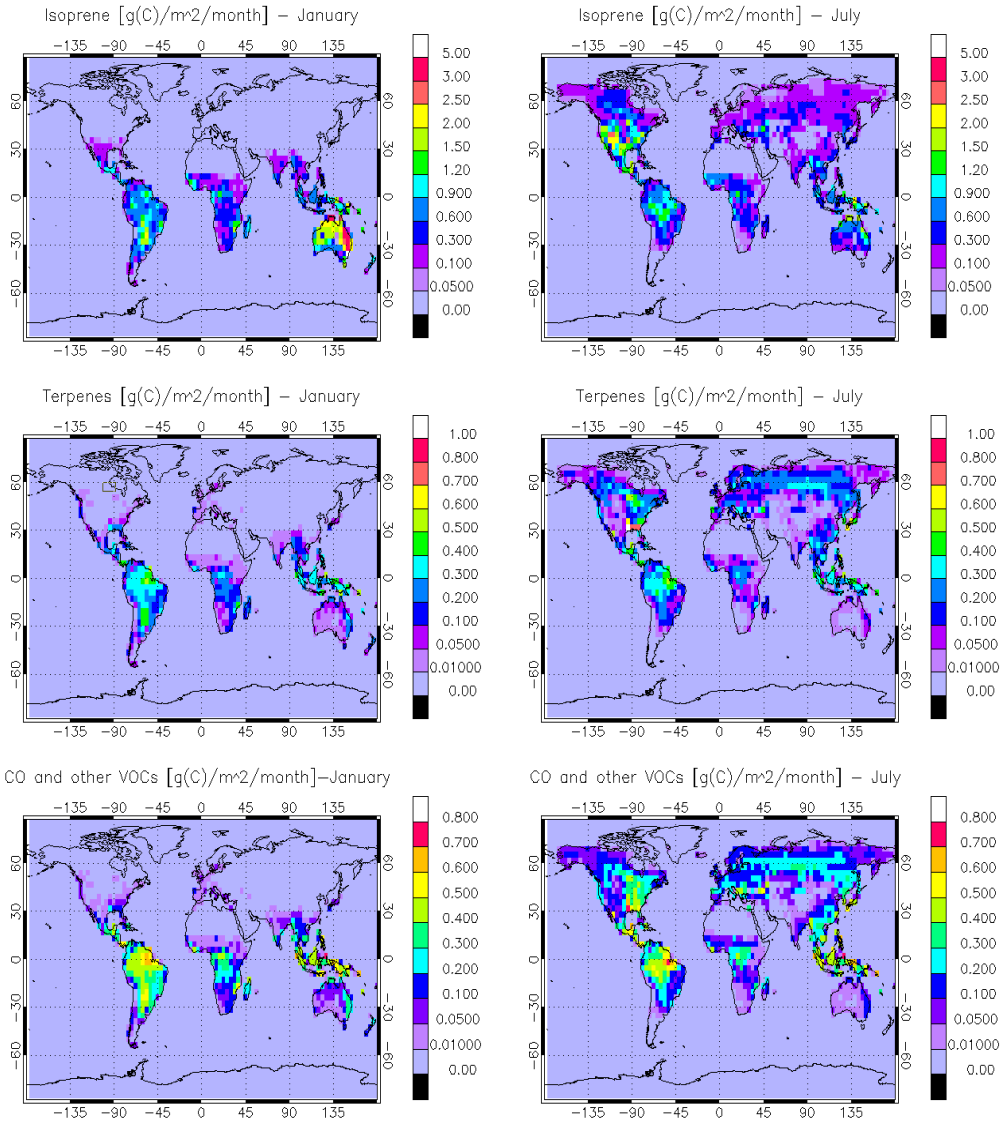

Figure 3.1— The 1991–2000 monthly average emission flux of isoprene (top), terpenes (middle) and CO and other non-terpene VOCs (bottom) from vegetation in January and July calculated with MEGAN in ECHAM5-MOZ in the present-climate experiment. Note high isoprene emissions over Australia in January and western USA in July.

ing methanol emissions are so low, probably because they do not account for the temperature dependency.

Our global acetaldehyde and formaldehyde emission estimate is about 40% higher than those reported in Lathière et al. (2006), while our acetone emissions of 19 Tg(C)/yr is about a factor of 2 lower. However, these estimates are within the

Table 3.2— Global and regional annual-average emissions (in $\mathrm{Tg(C)/yr}$) of isoprene estimated by MEGAN in the ECHAM5-MOZ model, as calculated in the present-climate, past and the future-climate scenario experiments. The contributions of various world regions are also included.

Regions	Present climate	ERA-40[a] (present)	Past	Future (B1)	Future (A2)
Global	586.51	487.69	557.18	718.40	832.39
Regional contribution					
Latin America[b]	172.10	185.85	164.21	215.90	252.60
Africa	105.71	119.58	101.12	122.27	148.86
Southeast and South-central Asia[c]	81.76	90.26	77.93	95.40	110.69
USA and Canada	51.28	36.16	48.04	68.40	75.99
North-central and East Asia[d]	17.52	23.67	16.40	23.60	26.07
Oceania[e]	126.73	27.52	119.83	154.79	175.81
Europe	9.53	9.67	8.75	12.35	13.35
Middle East[f]	8.48	6.59	7.98	10.92	11.88

[a]This experiment uses the modified isoprene emission factor, ε_i, see discussion in Section 3.6.

[b]Latin America includes Mexico, all countries in South America and the Caribbean Islands.

[c]South-central and Southeast Asia countries are India, Pakistan, Bangladesh, Sri-Lanka, Nepal, Maldives, Kashmir, Bhutan, eastern Afghanistan, Brunei, Cambodia, East Timor, Laos, Vietnam, French Indo-China, Indonesia, Malaysia, Myanmar, Papua New Guinea, Philippines, Singapore, Thailand.

[d]North-central and East Asia countries are Russia Federation, Mongolia, China, Hong Kong, Japan, Democratic peoples Republic of Korea, Republic of Korea, Macau and Taiwan.

[e]Australia, New Zealand, Fijis, French Polynesia, Guam, New Caledonia, Niue, Samoa and Vanuatu.

[f]The Middle East includes western part of Afghanistan, Bahrain, Cyprus, Gaza strip, Iran, Iraq, Israel, Jordan, Kazakhstan, Kuwait, Kyrgyzstan, Lebanon, Oman, Pakistan, Qatar, Saudi Arabia, Syrian Arab republic, Turkey, Turkmenistan, United Arab Emirates, Uzbekistan, West Bank and Yemen.

range of those reported in Wiedinmyer et al. (2004). A review of biogenic emissions estimated before 1995 is provided in Kesselmeier and Staudt (1999).

Although all the studies listed in Table 3.5 are based on the model of Guenther et al. (1995), except Galbally and Kirstine (2002), their global estimates differ from those of the Guenther et al. (1995) estimate. This clearly elucidates the influence of employing different meteorology, vegetation type and distribution or different emission rate on the emission fluxes.

Table 3.3— Global and regional annual-average emissions (in $\mathrm{Tg(C)/yr}$) of terpenes estimated by MEGAN in the ECHAM5-MOZ model, as calculated in the present-climate, past and the future-climate scenario experiments.

Regions	Present Climate	ERA-40 (present)	Past	Future (B1)	Future (A2)
Global	171.81	174.96	162.64	214.27	249.80
Regional contribution					
Latin America	58.00	61.03	54.95	74.40	89.11
Africa	27.09	29.62	25.66	32.23	38.71
South-central and southeast Asia	29.66	34.21	28.18	35.26	40.95
USA and Canada	17.00	18.49	15.90	22.08	24.76
North-central and East Asia	14.34	17.60	13.60	18.65	20.42
Oceania	6.64	6.56	6.32	8.17	9.55
Europe	9.46	10.60	8.84	12.02	13.22
Middle East	1.37	1.33	1.28	1.85	2.06

Table 3.4— The global and regional annual-average emissions (in $\mathrm{Tg(C)/yr}$) of CO and other non-terpene VOCs estimated by MEGAN in the ECHAM5-MOZ model, as calculated in the present-climate, past and the future-climate scenario experiments.

Regions	Present Climate	ERA-40 (present)	Past	Future (B1)	Future (A2)
Global	216.04	218.77	204.51	269.14	314.42
Regional contribution					
Latin America	74.65	79.09	70.73	95.70	114.57
Africa	35.40	38.52	33.54	42.15	50.64
South-central and southeast Asia	38.99	44.94	37.03	46.35	53.83
USA and Canada	18.05	19.15	16.84	23.58	26.55
North-central and East Asia	15.52	19.26	14.72	20.16	22.11
Oceania	8.98	8.84	8.54	11.08	12.95
Europe	11.07	12.48	10.33	14.15	15.52
Middle East	2.17	2.01	2.02	2.92	3.26

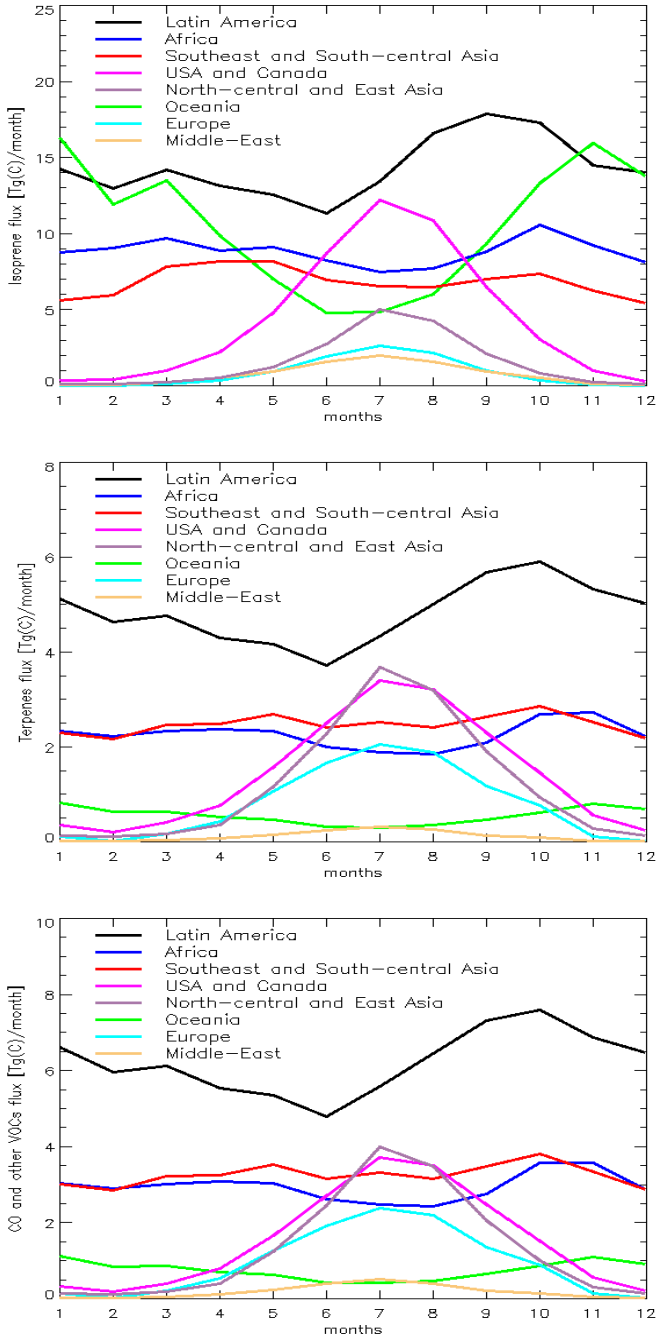

Figure 3.2— Seasonal variation in isoprene (top) and terpenes (middle) and other non-terpene VOCs and CO (bottom) emissions in the present-climate (1991–2000) experiment.

Table 3.5— Comparison of MEGAN present-climate emission estimates (in $\mathrm{Tg\,(C)/yr}$) with recent estimates from other global models for all species.

Species	Isoprene	Terpenes	Methanol	CO	Acetaldehyde	Formaldehyde	Acetone	Propene	Ethane	Ethene
This study (present-climate)	586.5	171.81	101.6	41.4	20.5	13.6	18.9	13.5	3.31	3.31
This study (ERA-40)[¶]	487.69[†]	174.96	102.88	41.89	20.77	13.7	19.1	13.67	3.35	3.35
Guenther et al. (2006)	440 – 660[a]									
Lathière et al. (2006)[b]	460	117	106		15	10	42			
Tao and Jain (2005) [c]	601	103		73						
Naik et al. (2004)[d]	454	72								
Wiedinmyer et al. (2004)[e]			50 – 250		10 – 50	2–10	10 – 50			
Levis et al. (2003)[f]	507	33								
Sanderson et al. (2003)[g]	484									
Galbally and Kirstine (2002)[h]			37.5							
Adams et al. (2001)[i]	561	116								
Potter et al. (2001)[j]	559									
Wang and Shallcross (2000)[k]	530									
Guenther et al. (1995)[§]	503	127								

[¶]This study is discussed in Section 3.6.
[†]This study uses the modified isoprene emission factor. See Section 3.6 for detailed explanation.
[a]The range of global isoprene emission estimate in other studies using MEGAN.
[b]Lathière et al. (2006) is based on Guenther et al. (1995) model (henceforth referred to as G95) implemented in ORCHIDEE (ORganizing Carbon and Hydrology in Dynamic EcosystEms) for years 1983 – 1995. They also account for the dependence of isoprene and methanol emissions on leaf age.
[c]Tao and Jain (2005) employ the G95 model modified according to Guenther et al. (1999, 2000) implemented in ISAM terrestrial ecosystem model. Their ISAM model uses prescribed meteorology (i.e. temperature, radiation and precipitation).
[d]Naik et al. (2004) calculates isoprene and terpene emissions based on the implementation of G95 within the Integrated Biospheric Simulator version 2.5 (Foley et al., 1996; Kucharik et al., 2000) for 1961 – 1990.
[e]Wiedinmyer et al. (2004) presents the review of biogenic VOCs emissions from vegetation up to year 2001.
[f]Levis et al. (2003) is also based on G95 model implemented in the Community Land Model version 2.0 (Bonan et al., 2002).
[g]Sanderson et al. (2003) is also based on G95 model implemented in the Hadley Centre Climate Model (HadCM3, Gordon et al. (2000)) coupled with Land surface processes model, MOSES2 (Essery et al., 2001) and TRIFFID Dynamic Global Vegetation Model (Cox , 2001).
[h]Galbally and Kirstine (2002) estimate global methanol emissions based on biosynthesis of methanol from flowering plants.
[i]Adams et al. (2001) is based on the G95 model.
[j]Potter et al. (2001) employed biogenic emission model similar to the G95 model in the biosphere model, NASA-CASA. The model NASA-CASA is driven by satellite-derived ecosystem classification and vegetation index.
[k]Wang and Shallcross (2000) uses G95 with a more detailed net primary production and cloud cover implemented in Land Surface Model version 1 (Bonan, 1996).
[§]Model G95.

3.5 Impact of climate change on biogenic emissions

3.5.1 Past biogenic emissions

The past simulation reveal a slightly cooler climate in the 1890s compared to the 1990s, except over the entire Europe in January, where temperature had been warmer by 2–3 K. Figure 3.3 shows the relative difference in isoprene and terpene emissions in 1991 – 2000 with respect to 1891 – 1900 (in percentage). The figure shows a general increase in isoprene and terpene emissions in January and July. The decrease calculated in the northern hemisphere in January is not significant because it represents a decrease in a small value. The percentage change in CO and other non-terpene VOCs emissions are similar to the changes calculated for terpene emissions, because they also depend on only temperature, just like terpenes.

As can be calculated from Tables 3.2, 3.3 and 3.4, the global annual emissions of the present-climate are about 5%, 5.6% and 5.6% higher than those of the past for isoprene, terpenes and CO and other non-terpene VOCs respectively. Although the regional decrease recorded in past climate with respect to the present-climate differs across the geographical land regions for all species, they all lie within -4.5% – -8.9%.

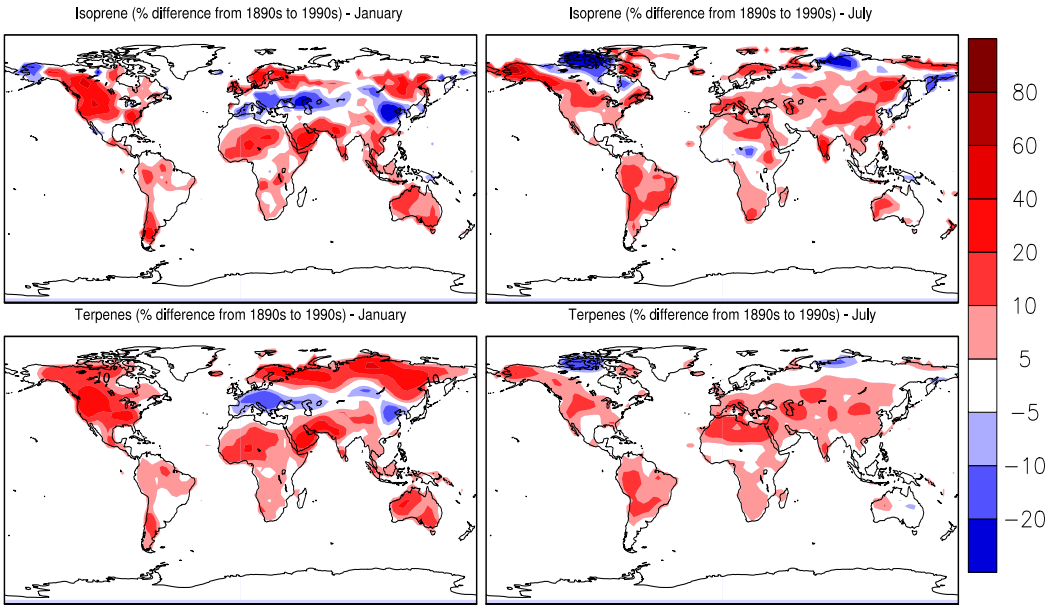

Figure 3.3— Percentage difference in isoprene and terpene emissions in 1991–2000 relative to 1891–1900.

3.5.2 Future biogenic emissions

Figures 3.4 and 3.5 show the percentage difference in isoprene and terpene emissions due to climate change as predicted by the ECHAM5-IPCC scenarios B1 and A2, respectively. The figures show the influence of changes in temperature and radiation in the case of isoprene, and changes in temperature in the case of terpenes.

In the B1 experiment, the global average temperature increases by about 2 K. This led to the increase of about 22.5% and 24.7% in the global isoprene and terpenes emission flux, respectively. Whereas, in the A2 experiment, an increase of about 42% and 45% is estimated in the isoprene and terpene emissions flux, due to a 3 K rise in global-mean temperature. This increase occurs in isoprene despite the decrease in global short wavelength radiation by 3 W/m^2 and 4 W/m^2 in the B1 and A2 experiments, respectively. The global annual emissions of isoprene, terpenes, CO and other non-terpenes VOCs calculated over the various geographical land regions in the future scenarios are included in the fifth and the sixth column of Tables 3.2, 3.3 and 3.4, respectively.

Figure 3.4 and Figure 3.5 show that the increase in isoprene and terpene emissions differs from location to location. For example, in the B1 future-climate scenario, Fig. 3.4 shows a slight decrease in terpene emissions over south-eastern USA and the UK, and an increase of about 80 – 100% over parts of south-central Russia and Mongolia in January. The maximum increase of 60–80% is found in July over eastern Europe and north-central Brazil. Changes in isoprene emissions in the B1 scenario show similar patterns as in the terpenes in January. However, due to changes in radiation, a decrease is measured over Scandinavia and parts of eastern and central Africa, and an increase of more than 100% over China and Mongolia. The decrease in isoprene emissions over Scandinavia persists in July, while most of Africa shows less than 20% increase. Over Eastern Europe, eastern Canada and northern Siberia in July, isoprene emissions increase by more than 60%.

The increase in isoprene and terpene emissions in the A2 scenario (Fig. 3.5) shows similar patterns as the B1 scenario, but with higher percentage increase. The percentage change in CO and other non-terpene VOCs emissions are similar to the changes calculated for terpene emissions, because they depend on only temperature, just like terpenes. The changes in isoprene and terpene emissions recorded in January over the northern hemisphere represent a change (decrease or increase) by a small amount, therefore, they may not be important for tropospheric chemistry.

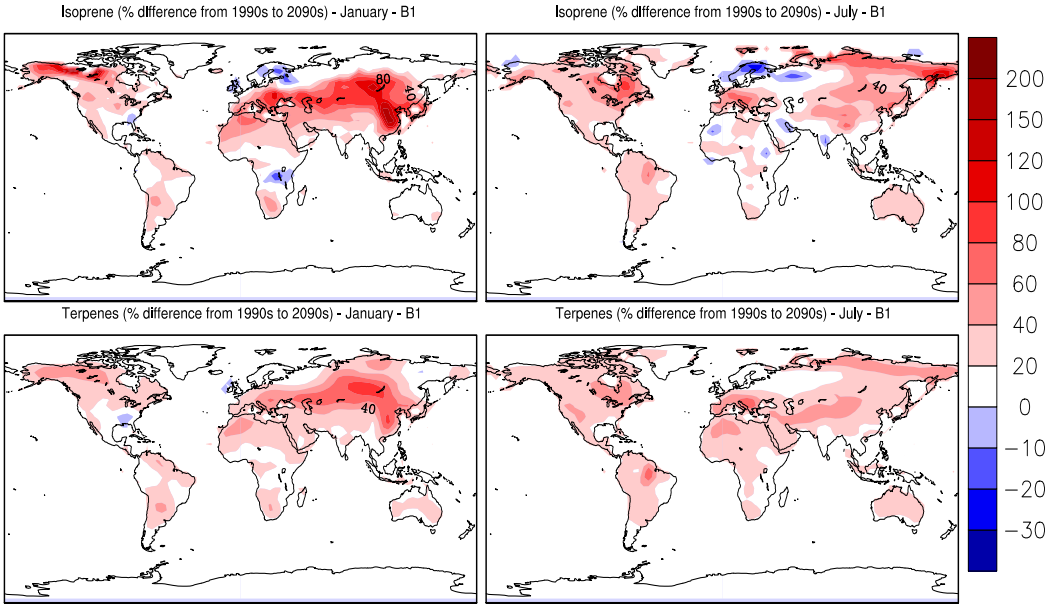

Figure 3.4— Percentage difference in isoprene and terpene emissions in 2091–2100 relative to 1991–2000, as predicted in the future climate change scenario B1.

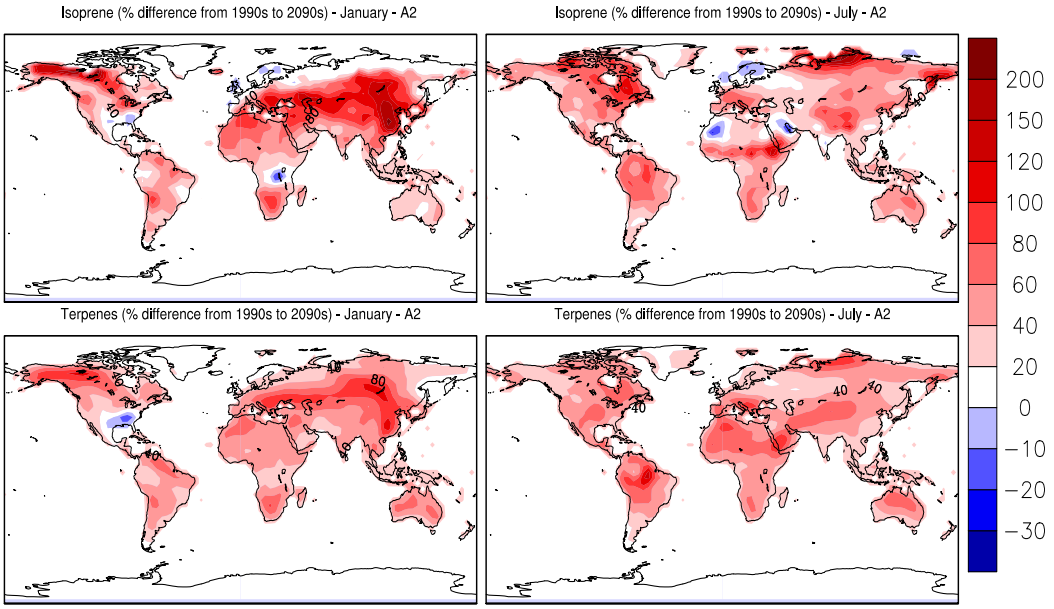

Figure 3.5— Percentage difference in isoprene and terpene emissions in 2091–2100 relative to 1991–2000, as predicted in the future climate change scenario A2.

3.6 Present-day simulation using ERA-40 meteorology

3.6.1 Modified isoprene emission factor and experiment set-up

Due to an overestimation of isoprene emissions over Australia and western USA, the emission factor, E_i of isoprene were modified. Figure 3.6 shows the comparison of the original and the modified versions of ε_i over both regions. The isoprene emission factor, ε_i over other regions remains unaltered (see Figure A.1 in Appendix A).

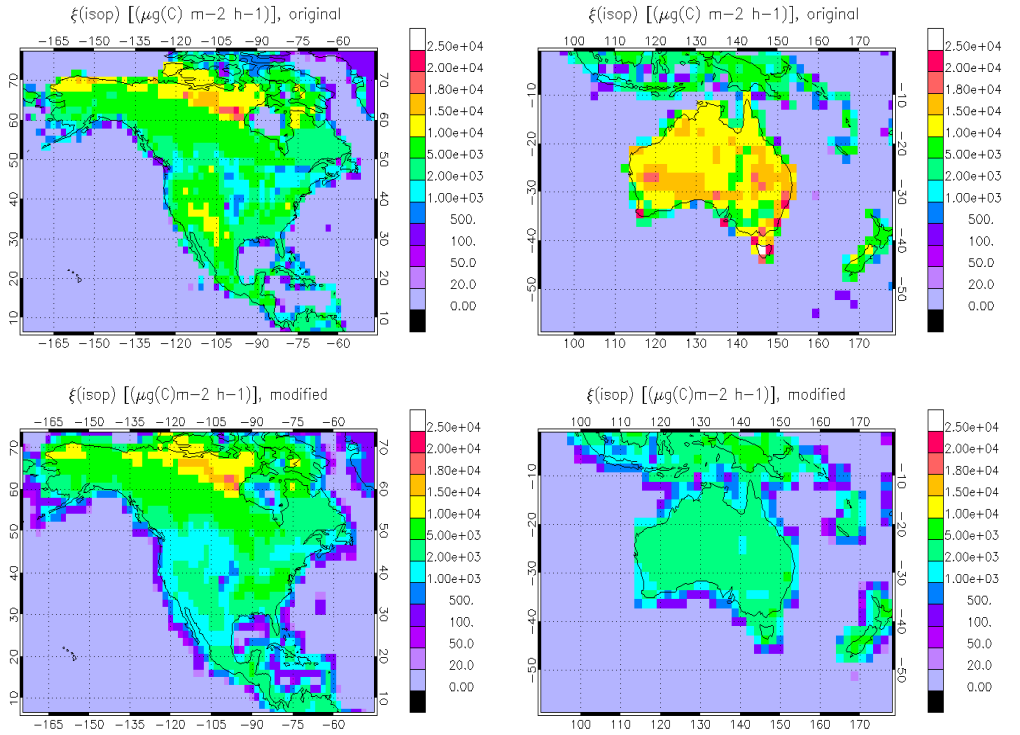

Figure 3.6— Modified emission factors of isoprene (ε_i) from the MEGAN input data for the year 2000. Figures show the comparison of the original (top) and the modified (bottom) versions over north-America (left) and Australia (right). Note the high values over the Australia desert and western USA in the original files. The emission factors over other regions are not altered.

In order to investigate the influence of meteorology on biogenic emissions, we performed one present-day experiment constrained to ERA-40 meteorology (temperature, surface pressure, divergence and vorticity) using the modified emission factor for isoprene. The emission factors of other compounds are not altered.

3.6.2 Influence of meteorology on biogenic emissions

The global annual emissions calculated for isoprene in the ERA-40 experiment are shown in the third column of Table 3.2. The modified isoprene emission factor, ε_i, resulted in the reduction of isoprene emissions by 98.82 Tg(C)/yr (about 17%) compared to the present-day simulation, as shown in Table 3.2.

The global annual emissions calculated for terpenes, and CO and other non-terpene VOCs in the ERA-40 experiment are shown in the third column of Tables 3.3 and 3.4, respectively. The differences between the present-climate (second column in the tables) and ERA-40 experiment reveal the influence of meteorology on biogenic emissions. Table 3.3 shows about 1.8% increase in global terpene emissions due to ERA-40 meteorology, while global CO and other non-terpene VOCs also increase by 1.3% (Table 3.4). However, the changes due to ERA-40 meteorology are very diverse across the geographical land regions. Most regions show an increase except Oceania and the Middle East, where reductions are recorded. The largest percentage increase is recorded over Asia (22.7% increase in terpenes and 24% increase in CO and other non-terpene VOCs over North-Central and East Asia, and 15% increase for both category of compounds over Southeast and South-central Asia), followed by Europe (about 12% and 12.7% increase in terpenes and CO and other non-terpene VOCs respectively) and Africa (about 8.8% and 9.0% increase in terpenes and CO and other non-terpene VOCs respectively).

In contrast to present-climate experiment, the third column of Tables 3.2, 3.3 and 3.4 shows that Latin America, Africa, Southeast and South-central Asia contribute about 81%, 71% and 74% to isoprene, terpenes, and CO and other non-terpene VOCs emissions respectively. The spatial distribution of isoprene, terpenes, and CO and other non-terpene VOCs emissions is shown in Figure 3.7.

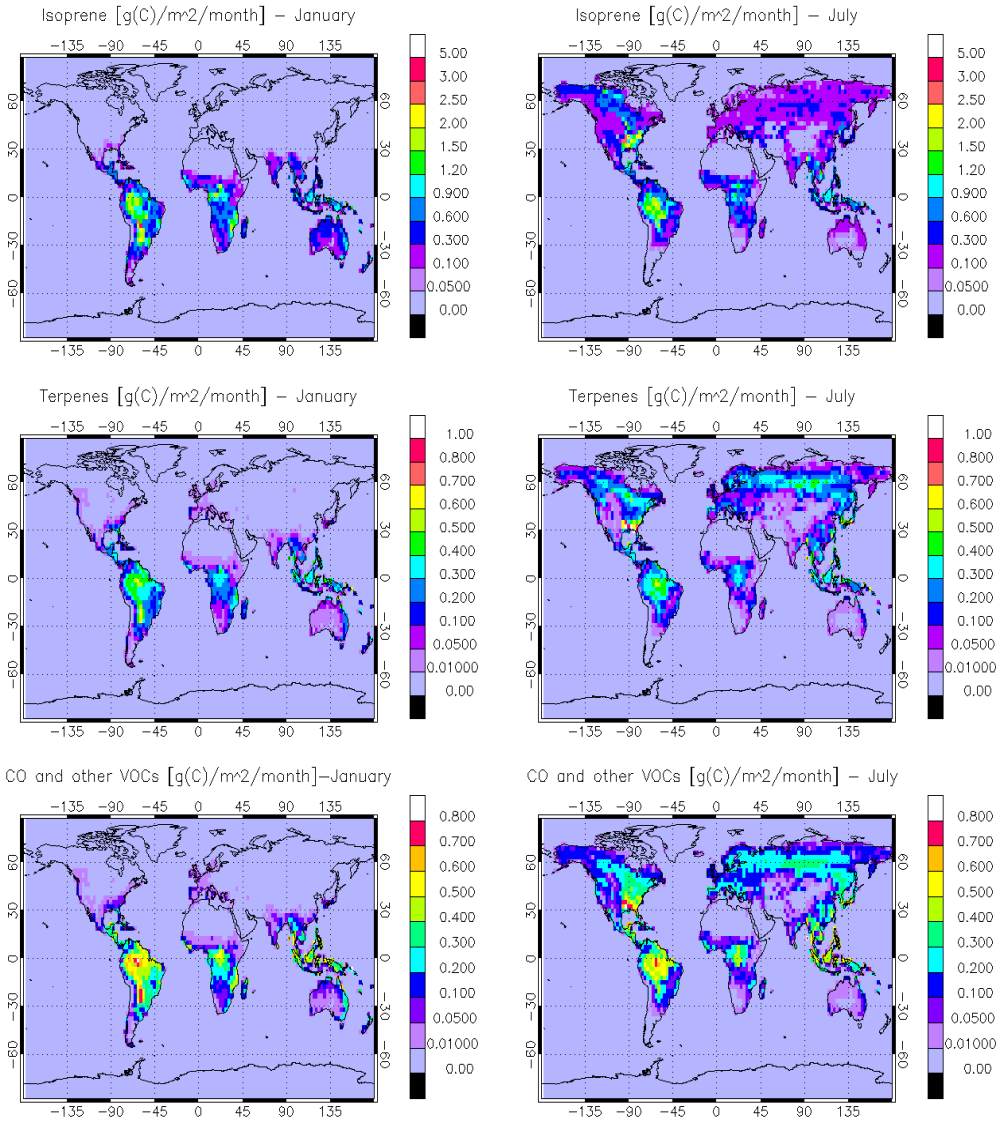

Figure 3.7— The 1991–2000 monthly average emission flux of isoprene (top), terpenes (middle) and CO and other non-terpene VOCs (bottom) from vegetation in January and July calculated with MEGAN in ECHAM5-MOZ constrained to ERA-40 meteorology.

3.6.3 Inter-annual variability

The inter-annual variability of isoprene and terpenes is shown in Fig. 3.8. The figure reveals about 11% and 8% higher than average global isoprene and terpene emissions respectively in the year 1998, coinciding with the 1997/98 El-Nino event. It also shows less than an average emissions over all regions in 1993.

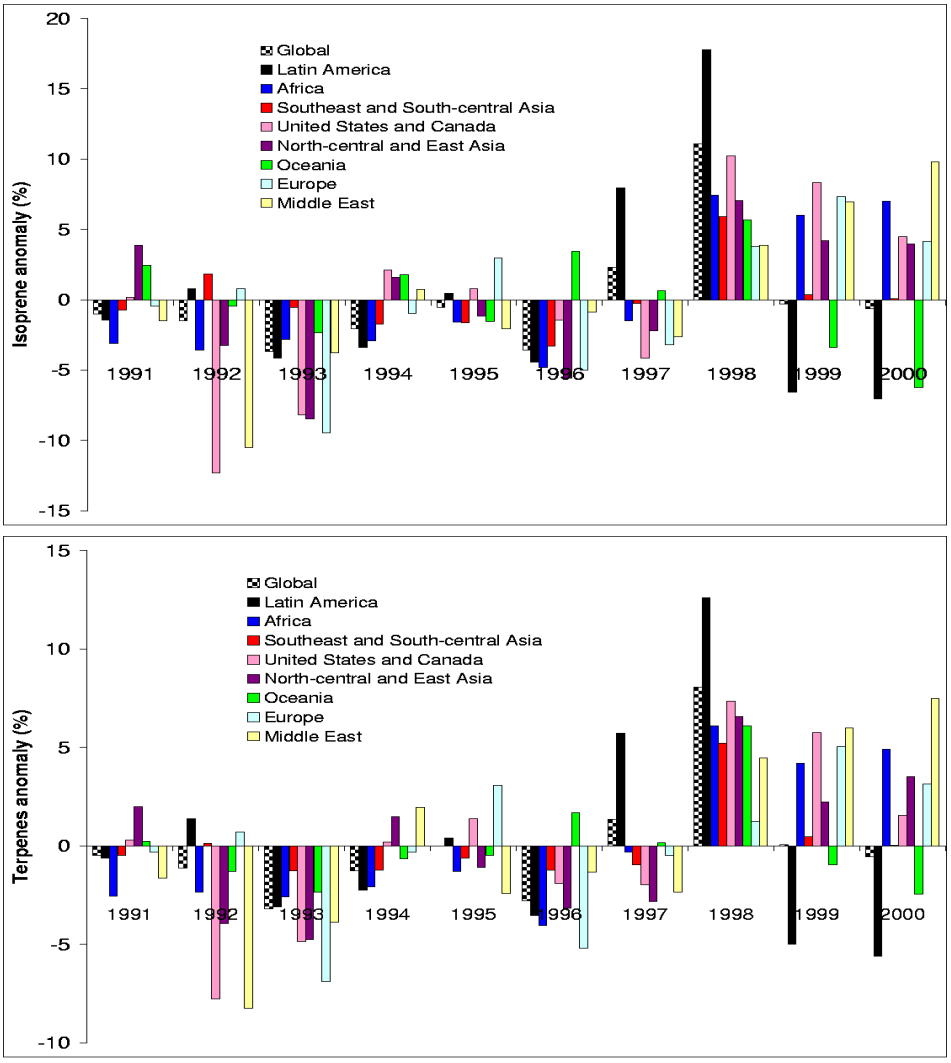

Figure 3.8— Inter-annual variability in isoprene (top) and terpenes (bottom) emissions in the ERA-40 (1991 – 2000) experiment.

3.7 Conclusions

This chapter presents the implementation of biogenic emission model, MEGAN in ECHAM5-MOZ. The current implementation calculates the emission flux of isoprene, terpenes, methanol, carbon monoxide, acetaldehyde, formaldehyde, acetone, propene, ethane and ethene from vegetation. The impact of changes in temperature and radiation caused by climate change, on the emissions flux of each of the species is also discussed.

MEGAN estimates in the present-day climate yield a global emissions of 587 Tg(C)/yr for isoprene, 172 Tg(C)/yr for terpenes, 41 Tg(C)/yr for CO, 102 Tg(C)/yr for methanol, 20.5 Tg(C)/yr for acetaldehyde, 13.6 Tg(C)/yr for formaldehyde, 18.9 Tg(C)/yr for acetone, 13.5 Tg(C)/yr for propene, 3.3 Tg(C)/yr for ethane and 3.3 Tg(C)/yr for ethene. The global emissions of isoprene probably have a bias due to overestimates in the emission factor over Australia and North America. The modification to isoprene emission factor, ε_i, over Australia and western USA resulted in the reduction of isoprene emission flux by 98.82 Tg(C)/yr (about 17%) compared to the present-day simulation.

The past climate (1890s) is about 2 – 3 K cooler than the present (1990s), and this results in a decrease of 29.33 Tg(C)/yr in isoprene, 9.17 Tg(C)/yr in terpenes, and 11.53 Tg(C)/yr in CO and other non-terpene VOCs emissions respectively. In the 2090s, the global-mean temperature is likely to increase by about 2 K or 3 K as predicted in the B1 (optimistic) or the A2 (pessimistic) scenario of the future trends in greenhouse gas emissions. This temperature rise increases isoprene emissions by 131.89 Tg(C)/yr and 245.88 Tg(C)/yr in the B1 and A2 scenario respectively. These increases form a lower and upper boundary for the increase of 165 Tg(C)/yr in isoprene emissions calculated by (Sanderson et al., 2003) in a fixed vegetation experiment, which employs the IS92a scenario of future-climate. The global terpene emissions increase by 42.46 Tg(C)/yr and 77.99 Tg(C)/yr in the B1 and A2 future scenarios respectively, and the emissions of CO and other non-terpene VOCs increase by 53.10 Tg(C)/yr and 98.38 Tg(C)/yr in both scenarios respectively.

The modifications made to isoprene emission factor should not affect the relative changes in the global isoprene emissions in the past and the future climate experiments presented in this study, therefore our conclusions remain valid. However, these results may overestimate the climate-related biogenic emission changes of all the compounds, because the experiments do not account for the impact of climate change on vegetation types, their geographical distribution and density.

The results of the future simulations show an increase in global isoprene emissions despite the decrease in the global short wavelength radiation by about 3 W/m^2 and 4 W/m^2 in the B1 and A2 scenarios respectively.

Chapter 4

ECHAM5-MOZ model evaluation

4.1 Introduction

The evaluation of a global model constitutes a major challenge in two specific ways: (1) It requires that measurement data be available on a global scale (2) It also requires that model-calculated concentrations of species be compared to measurement data in a consistent way. This is because model calculations are performed on model grid boxes, while data are collected in a particular location and at a particular vertical level.

The first challenge is becoming abated due to continuing availability of systematic global-coverage of in-situ measurement data of some tropospheric trace species, e.g. ozone and CO. Some of the programmes providing measurement data with some sort of global coverage include the MOZAIC programme (the Measurement of OZone and water vapour by Airbus In-service airCraft) and SHADOZ (Southern Hemisphere ADditional OZonesondes data) both of which provides ozone data. Also NOAA Earth Systems Research Laboratory Global Monitoring Division (NOAA/ESRL-GMD) provides measurement of global surface CO concentrations.

MOZAIC (Marenco et al., 1998; Thouret et al., 1998a, 2006; Zbinden et al., 2006) was initiated in 1993 by the European Scientist, aircraft manufacturers and airlines. It came into full commencement in August 1994. MOZAIC was designed for collecting ozone and water vapour data by using automated equipment. These equipments were carried free of charge by 5 long-range Airbus A340 aircraft flying regularly around the world. Since its commencement, about 25 000 flights have been performed during the first 3 phases of MOZAIC which ended in February 2004. MOZAIC measurement accuracy was estimated to be about $\pm$2ppbv + 2% and has been shown to have good agreement with ozonesonde data (Thouret et al., 1998b). Moreover, MOZAIC data provides the first ozone climatology data covering major African cities, which were analysed by Sauvage et al. (2005).

SHADOZ project (Thompson et al., 2003a,b) aim to coordinate and augment

balloon-borne ozonesonde launches from tropical and subtropical operational sites, and to provide a central data archive location. The project was initiated in 1998 by NASA/Goddard Space Flight Center with other US and international co-investigators. There are currently 14 stations in the SHADOZ network, 2 of which commenced in 2005 (i.e. Cotonou, Benin and Heredia, Costa Rica). These two stations and Malindi, Kenya are not included in this analysis. Although measurement at Malindi station started in 1999, few measurements are conducted per year. The collective datasets (which is available online at http://croc.gsfc.nasa.gov/shadoz/) provides the climatological profile of ozone in the equatorial region.

NOAA/ESRL-GMD has collected CO data since 1990s (Novelli et al., 1992, 1994, 1998b, 2003). The CO data collected has been used to provide a better understanding of CO global distribution (Novelli et al., 1992, 1998b), CO budget and trends (Novelli et al., 1994, 1998a, 2003; Granier et al., 1996, 1999; Holloway et al., 2000), and also to validate measurements of CO made from space (Novelli et al., 1998a; Reichle et al., 1999).

Although global data of ozone and CO concentration are now available, other tropospheric trace species, such as NO_x, still lacks ample measurement data, moreover on a global and climatological basis. In this chapter, ECHAM5-MOZ calculated ozone and CO concentrations are evaluated by comparing them with data from these observations. Specifically, the model calculated ozone was compared to MOZAIC and SHADOZ data at various locations in the tropical and extra-tropical regions. ECHAM5-MOZ surface CO concentrations were also compared with the NOAA/ESRL-GMD CO data. The exact location for these comparison is as shown in Figure 4.1. The model set-up is explained in Section 4.2. The method employed to regrid the measurement data, in order to ensure a consistent comparison with ECHAM5-MOZ model is presented in Sect. 4.3. The evaluation of the ozone concentrations calculated by the model is discussed in Sections 4.4 and 4.5. The surface CO concentrations are compared with measurement data in Section 4.6.

4.2 Model set-up

The ECHAM5-MOZ model, described in Chapter 2 was run for 5 years (1997–2001) after a spin-up of 6 months. The simulation was performed in the T42L31 resolution (this represents a spatial grid of approximately 250 km and non-uniform 31 σ-hybrid vertical levels up to 10 hPa). The climate conditions (sea surface temperatures and sea ice fields) were taken from six consecutive years of coupled ocean-atmosphere simulations performed at the Max Planck Institute for Meteorology, Hamburg. Present-day constant concentrations of 1760 ppbv, 367 ppm and 316 ppbv were maintained for CH_4, CO_2 and N_2O respectively.

Lightning emissions are calculated within the ECHAM5-MOZ model as discussed in Section 2.2.2. Anthropogenic, biogenic, biomass burning, soil, ocean and aircraft emissions are identical to those used in the IPCC-ACCENT experiment (Stevenson et al., 2006). These data sets are a combination of emission inventories of the

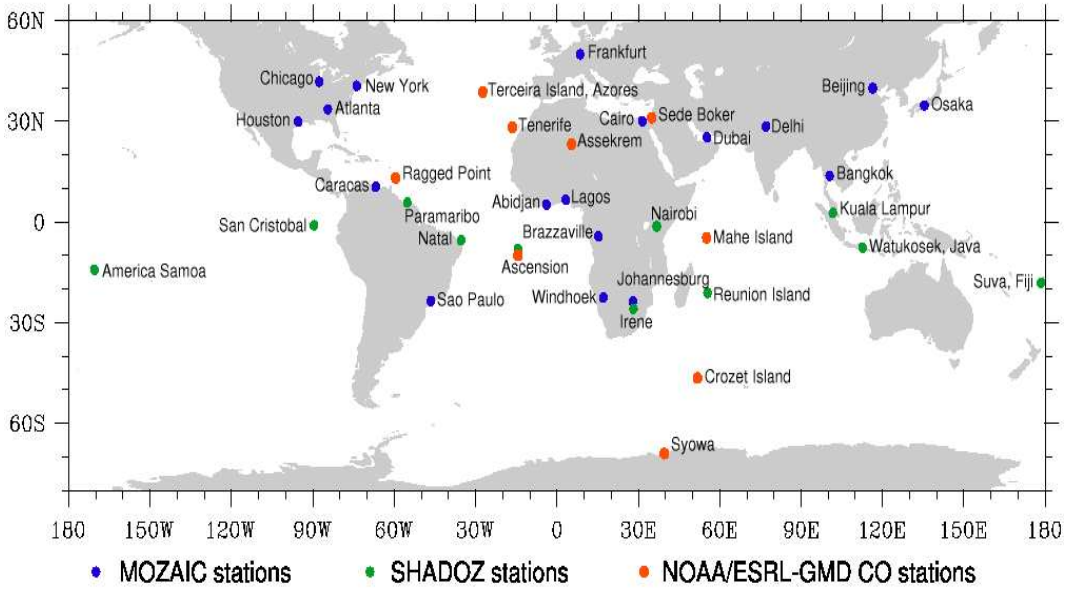

Figure 4.1— Plots showing MOZAIC airports, SHADOZ sondes stations and NOAA/ERSL-GMD stations.

Institute for Applied System Analysis (IIASA), the Global Emissions Inventory Activity (GEIA), the Global Fire Emissions Database (GFED) version 1 (Randerson et al., 2005) and the Emission Database for Global Atmospheric Research (EDGAR) version 3.2 (Olivier et al., 1999). The emissions are described in detail in Chapter 6.

4.3 Regridding of measurement data

MOZAIC aircraft measurement records ozone data at every 150 m during the ascend or descend at any given station. SHADOZ also provides ozone data at a finer vertical resolution of between 1 m and 50 m depending on the location. The comparison presented in this chapter uses MOZAIC climatological data of 1997 – 2002 and SHADOZ data of 1998 – 2004 for locations shown in Fig. 4.1. The total number of MOZAIC and SHADOZ measurements taken in any given month during these years are presented in Tables 4.1 and 4.2 respectively.

Due to model coarseness, the measurement data are averaged vertically at every location by using:

$$x_i = \frac{\sum_j y_j \, \chi_i(j)}{\sum_j \chi_i(j)}, \text{ for all } i = 1, \ldots, N \tag{4.1}$$

where

$$\chi_i(j) = \begin{cases} 1 & \text{if } i - 1/2 \leqslant j < i + 1/2 \\ 0 & \text{otherwise} \end{cases}$$

x_i: extracted measurement data at model level i
y_j: measurement raw data at measurement level j
N: model highest level, i.e. 10 hPa
$i + 1/2$ or $i - 1/2$: is the model level interface

Extraction of measurements data using Equation (4.1) regrids the measurement data at every location, so as to correspond with model grids at the same location. Using Equation (4.1) therefore ensures consistency between model and measurement data.

Table 4.1— The total number of measurement recorded at any given month in 1997 – 2002 by MOZAIC aircraft.

Stations	January	February	March	April	May	June	July	August	September	October	November	December
Africa												
Cairo	4	12	8	8	2	4	15	25	11	38	16	20
Abidjan	32	12	12	18	6	12	16	14	8	28	18	6
Lagos	14	28	20	54	12	2	18	16	6	27	20	14
Brazzaville	7	16	6	9	9	10	20	11	14	11	0	0
Windhoek	8	8	8	12	16	10	18	10	8	12	18	12
Johannesburg	40	33	47	11	44	24	24	23	38	24	38	49
North and Latin America												
Chicago	32	50	50	42	97	103	117	126	91	66	38	52
New York	152	108	137	148	137	152	173	161	180	218	148	147
Atlanta	73	96	59	67	51	52	47	60	42	72	86	73
Houston	55	50	49	44	39	34	62	54	75	47	35	42
Caracas	14	18	22	25	17	20	18	14	12	27	19	14
Sao Paulo	80	52	69	50	59	40	33	50	45	26	36	22
Europe, the Middle East and Asia												
Frankfurt	400	315	371	409	385	360	462	466	438	385	339	385
Dubai	74	30	21	47	18	36	68	48	41	52	31	21
New Delhi	22	10	28	37	30	48	44	32	50	49	16	25
Beijing	57	60	30	37	53	63	28	54	8	35	43	52
Osaka	74	57	85	74	59	58	90	94	85	97	73	65
Bangkok	43	41	54	8	8	12	12	12	6	2	2	12

Table 4.2— The total number of sondes recorded in 1998 – 2004 by SHADOZ network.

Stations	January	February	March	April	May	June	July	August	September	October	November	December
Africa and its surrounding												
Ascension	29	23	29	21	28	28	26	26	26	24	30	15
Irene	10	8	15	14	15	13	13	14	15	16	17	13
La Reunion	19	19	19	17	17	15	18	9	12	16	18	16
Nairobi	27	20	20	21	30	24	26	25	30	33	32	29
South America												
San Cristobal	19	19	36	15	14	15	26	23	33	26	20	28
Paramaribo	17	16	19	17	15	18	21	21	26	23	17	16
Natal	25	22	25	20	20	22	17	19	21	27	24	21
Asia and Pacific Ocean												
Kuala	13	12	17	14	15	13	13	13	14	14	15	12
Java	20	15	19	19	17	17	20	25	24	20	18	16
Fiji	21	19	27	25	12	17	21	20	17	19	19	12
Samoa	21	26	28	24	22	22	19	23	19	20	21	18

4.4 ECHAM5-MOZ ozone concentration comparison with MOZAIC aircraft data

In the ACCENT-IPCC scenario studies, ECHAM5-MOZ showed a high bias of about 20% in the global tropospheric ozone production and loss compared to the mean of all participating models (Stevenson et al., 2006). In terms of global dry deposition, it has a low bias of about 5%. Methane and CH_3CCl_3 tropospheric lifetimes are at the lower end of the currently accepted estimations (Prinn et al., 1995; Ehhalt et al., 2001). The surface ozone concentration is known to have a high bias in heavily polluted areas, such as industrial centres and large city agglomerations but also in the Mediterranean basin.

4.4.1 Africa

Figures 4.2 shows the comparison of ECHAM5-MOZ (open circles) to MOZAIC (filled squares) ozone vertical profiles for Cairo (Egypt), Abidjan (Cote d'Ivoire), Lagos (Nigeria), Brazzaville (Congo), Windhoek (Namibia) and Johannesburg (South Africa) in December – February (DJF), March – May (MAM), June – August (JJA), and September – November (SON). MOZAIC data were averaged over the years 1997–2002. The ECHAM5-MOZ model results do not reflect specific years but can be regarded as a 5-year climatology over the late 1990s. There are no measurements at Brazzaville airport in November and December of years 1997 – 2002 as shown in Table 4.1.

The ECHAM5-MOZ model shows a reasonable level of agreement with the measurements in the free troposphere (750 hPa – 350 hPa) at these six stations in all seasons. The model bias is about 20 ppbv, except over Cairo in July – November, and over Windhoek and Johannesburg in JJA, where the bias is up to 30 ppbv. During the dry season, i.e. DJF in Lagos and Abidjan, and JJA in Brazzaville, both model and measurements exhibit high ozone enhancement below-650 hPa over Lagos, Abidjan and Brazzaville. This is connected with an increase in local emissions of ozone precursors due to an increase in biomass burning activities in the vicinity of these stations. The reason why the ozone enhancement is limited to below-650 hPa is due to the high stability created by a combination of the Harmattan and the Saharan anticyclone, which prevents effective vertical mixing (Sauvage et al., 2005).

However, while the dry season maximum ozone enhancement in the MOZAIC data occurs at 850 – 650 hPa, it is confined within the surface – 800 hPa in the ECHAM5-MOZ model. This causes ECHAM5-MOZ lower tropospheric (surface–800 hPa) ozone concentrations to be highly biased during the dry season. For example, the surface ozone concentration is overestimated in ECHAM5-MOZ by about 35 – 50 ppbv and 50 – 100 ppbv over Lagos and Abidjan respectively in DJF, with the maximum bias occurring in December at both stations. Over Brazzaville, the bias in surface ozone varies between 35 ppbv and 60 ppbv in JJA, with a maximum

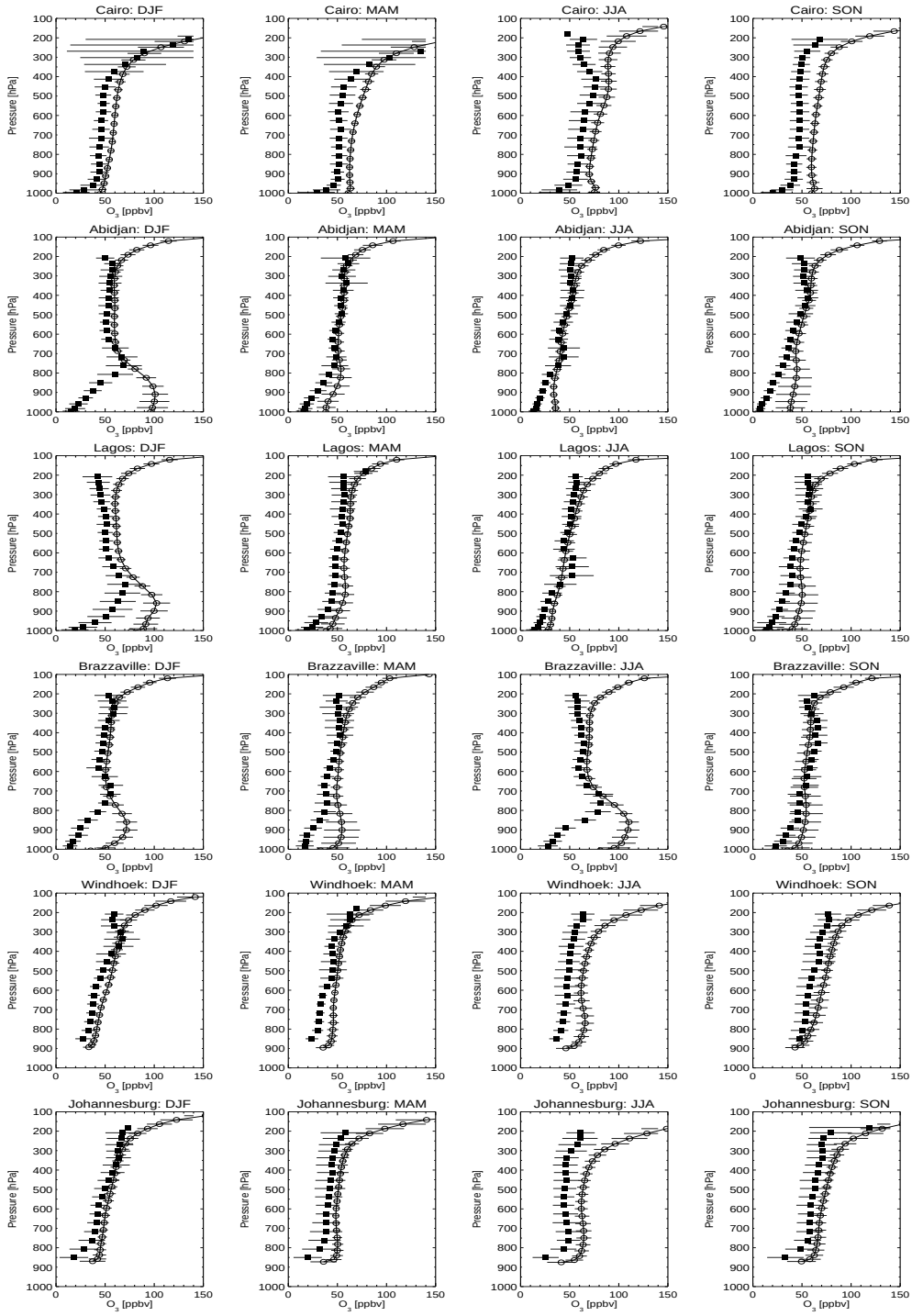

Figure 4.2— The comparison of 5-year average (1991–2000) model simulated (open circles with line) with 1997–2000 mean MOZAIC (filled-squares) ozone vertical profiles for Cairo (Egypt), Abidjan (Cote d'Ivoire), Lagos (Nigeria), Brazzaville (Congo), Windhoek (Namibia) and Johannesburg (South Africa) in December–February (DJF), March–May (MAM), June–August (JJA) and September–November (SON). The horizontal lines indicate $\pm 1\,\sigma$ standard deviation.

overestimation in July.

There are four potential reasons for this dry season bias: (a) ECHAM5-MOZ underestimates dry deposition during the dry seasons. As already stated above, the global dry deposition in ECHAM5-MOZ is about 5% lower than the multi-model-average dry deposition (Stevenson et al., 2006). (b) The lack of aerosols (especially mineral dust) in ECHAM5-MOZ may also contribute to this bias. (c) The particular choice of the reaction constants and their temperature dependence in ECHAM5-MOZ is known to favour high ozone concentrations in the troposphere (G.A. Folberth, personal communication (2006)). (d) Biomass burning emissions from the Global Fire Emissions Database (GFED) version 1 (Randerson et al., 2005) are particularly high over Africa.

4.4.2 North and Latin America

Figures 4.3 shows the comparison of ECHAM5-MOZ (open circles) to MOZAIC (filled squares) ozone vertical profiles for four cities in the United States of America (Chicago, New York, Atlanta and Houston), and two cities in South America (Caracas, Venezuela and Sao Paulo in Brazil).

The figure shows that the ECHAM5-MOZ model is in good agreement with the MOZAIC data throughout the troposphere of the four USA stations. The model slight bias is generally lower than 20 ppbv except over the boundary layer of New York in JJA, and over the whole troposphere of Atlanta in SON, where the model shows a bias of 37 ppbv and about 22–26 ppbv respectively. At the two stations considered in South America, the model shows a consistent bias of 20–30 ppbv, except at 200 hPa level over Sao Paulo in JJA, where the model bias is up to 42 ppbv.

4.4.3 Europe, the Middle East, Asia and the Pacific Ocean

Figures 4.4 shows the comparison of ECHAM5-MOZ (open circles) to MOZAIC (filled squares) ozone vertical profiles for six stations: one in Europe (Frankfurt, Germany), one in the Middle East (Dubai, United Arab Emirates), and four in Asia (Delhi, India; Beijing, China; Osaka, Japan; and Bangkok, Thailand) in DJF, MAM, JJA, and SON.

The ozone vertical profiles over Frankfurt, Beijing and Osaka calculated in the ECHAM5-MOZ model show very good agreement with MOZAIC data in all seasons, and the slight bias recorded by the model over these stations, lies within the standard deviation of the MOZAIC data.

Over Dubai, the model bias is below 20 ppbv in the free troposphere, whereas at the surface, the bias ranges from 18 ppbv in JJA to 26 ppbv in SON. Over Delhi, the model is consistently higher than the measurement data by about 30 ppbv in the free troposphere, while the at the surface, the model bias is between 40–55 ppbv in March through November. The model also shows a bias of below 20 ppbv throughout the troposphere over Bangkok, except in DJF and SON, when the bias is within 20–38 ppbv.

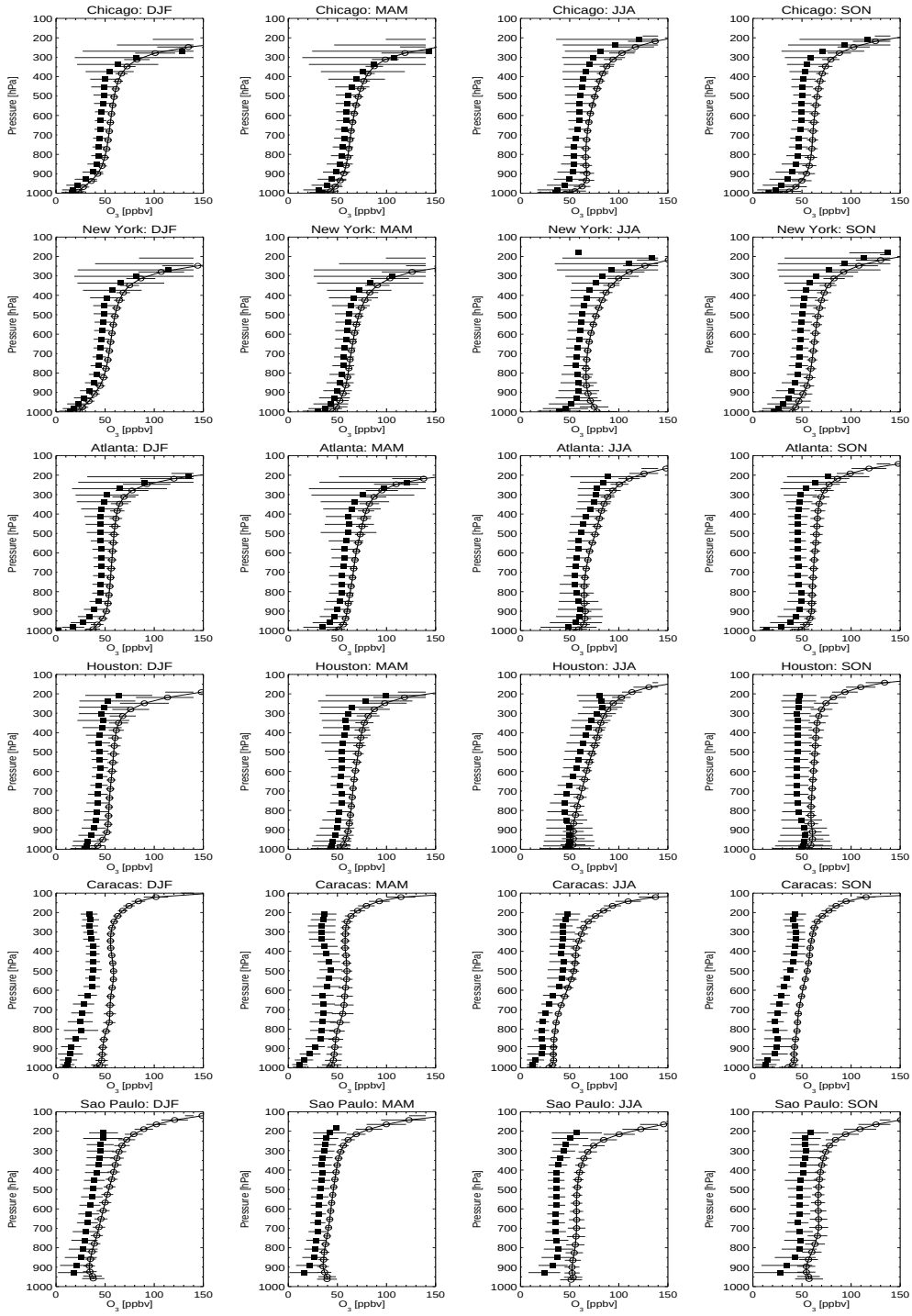

Figure 4.3— The comparison of 5-year average (1991–2000) model simulated (open circles with line) with 1997–2000 mean MOZAIC (filled-squares) ozone vertical profiles for four cities in the United States of America (Chicago, New York, Atlanta and Houston) and two cities in South America (Caracas, Venezuela ands Sao Paulo, Brazil) in December–February (DJF), March–May (MAM), June–August (JJA) and September–November (SON). The horizontal lines indicate $\pm 1\,\sigma$ standard deviation.

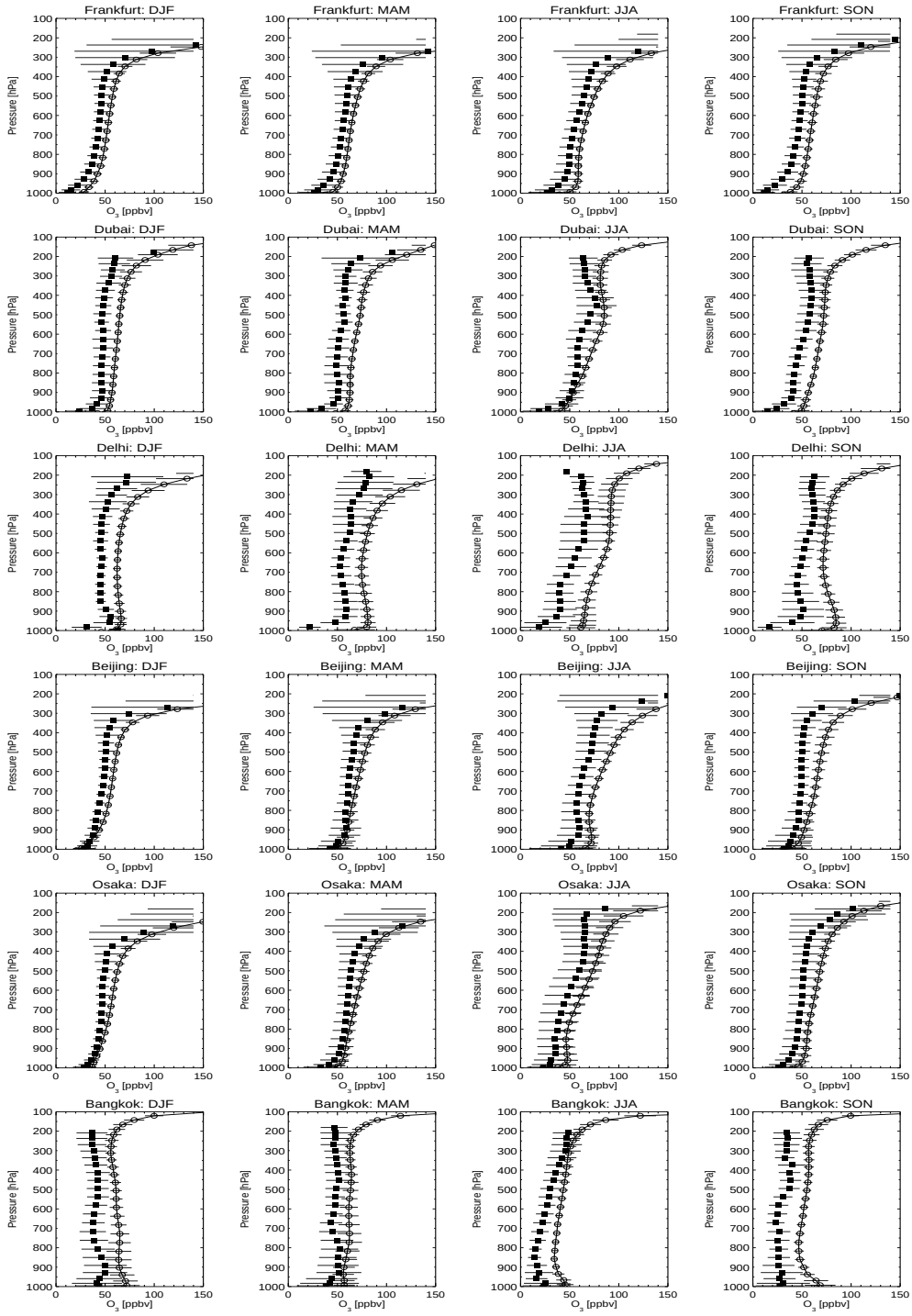

Figure 4.4— The comparison of 5-year average (1991–2000) model simulated (open circles with line) with 1997–2000 mean MOZAIC (filled-squares) ozone vertical profiles for Frankfurt (Germany), Dubai (United Arab Emirates), Delhi (India), Beijing (China), Osaka (Japan), and Bangkok (Thailand) in December–February (DJF), March–May (MAM), June–August (JJA) and September–November (SON). The horizontal lines indicate $\pm 1\,\sigma$ standard deviation.

4.5 ECHAM5-MOZ ozone concentration comparison with SHADOZ ozonesonde data

The comparison of the seasonal vertical profiles of the ozone concentrations calculated by the ECHAM5-MOZ model with SHADOZ ozonesonde data is shown in Appendix B. This section compares the monthly-mean climatology time series of the mode with SHADOZ data at three levels in the troposphere, i.e. at 300 hPa, 500 hPa and 800 hPa. The ozone bias (i.e. the difference of ECHAM5-MOZ and SHADOZ) throughout the troposphere up to 200 hPa over all the SHADOZ stations (see Figure 4.1) is also shown. The SHADOZ ozonesonde data are a climatology over years 1998 – 2004, and for the model, the ozone concentrations are the 5-year climatology, which represent the year 1990s.

4.5.1 Africa and Atlantic Ocean

We compare the monthly-mean time series of ozone concentrations calculated in ECHAM5-MOZ with SHADOZ data. Figure 4.5 shows this comparison over Ascension Island, Irene, Reunion and Nairobi at 300 hPa, 500 hPa and 800 hPa.

The agreement with the SHADOZ measurements is generally good at all stations and vertical levels. The simulated values show a smaller variability (i.e. standard deviation) over the 5-year period than the measurements which represent mean values over 7 years. The seasonal cycle is well captured at most stations and vertical levels, both in amplitude and phase. Nevertheless, there are some deviations of the model from the measurements in the lower troposphere, as shown by the plots at 800 hPa level. Specifically, Fig. 4.5 (bottom panel) shows an overestimation of the ozone concentration of about 15 ppbv at Reunion in June and July. At Irene and Nairobi, this overestimation reaches 20 ppbv in some months. On the other hand, the model underestimates the ozone concentration over Ascension throughout the year.

In Fig. 4.6, we show the seasonal (JFM, AMJ, JAS, OND) bias of the ECHAM5-MOZ model when compared with SHADOZ data at Ascension Island, Irene, Reunion and Nairobi. The bias is generally lower than 20 ppbv, except at Irene in AMJ and JAS and Nairobi in JAS. Interestingly, these months represent the dry seasons at Irene and Nairobi, thereby confirming that the ECHAM5-MOZ model has a bias higher than 20 ppbv during the dry season, which may be linked to the reasons stated earlier.

4.5.2 Latin America

Figure 4.7 shows the comparison of the ECHAM5-MOZ model ozone concentration with SHADOZ data at 300 hPa , 500 hPa and 800 hPa over San Cristobal (Ecuador), Paramaribo (Suriname) and Natal (Brazil). The figure shows that the model is good at capturing the seasonal variation of the ozone concentrations at these stations. Figure 4.8 shows that the model consistently overestimates the ozone concentrations

over San Cristobal by about 7–26 ppbv throughout the troposphere in all seasons. Over Paramaribo, the model shows a negative bias in the upper troposphere in July through December, and at the surface in all seasons, except JFM, otherwise, the model bias is lies within 0–20 ppbv. Over Natal, the model shows a very good comparison, and the bias is generally lies within the -4 – 10 ppbv, except in October – March at the surface – 850 hPa and in April– September at the upper troposphere above 300 hPa.

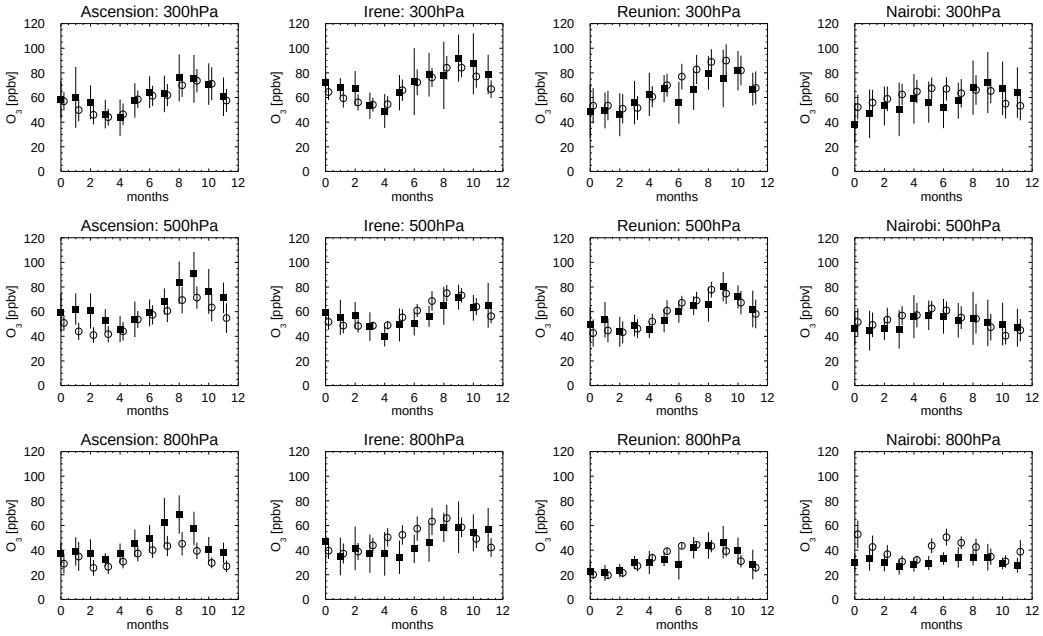

Figure 4.5— The comparison of 5-year average (1991–2000) ECHAM5-MOZ model (open circles) with 1998–2004 mean SHADOZ data (filled-squares) of ozone concentration (in ppbv) over Ascension Island, Irene (South Africa), Reunion Island, and Nairobi (Kenya) at 300 hPa (top), 500 hPa (middle), and 800 hPa (bottom). The horizontal lines indicate $\pm\,1\,\sigma$ standard deviation.

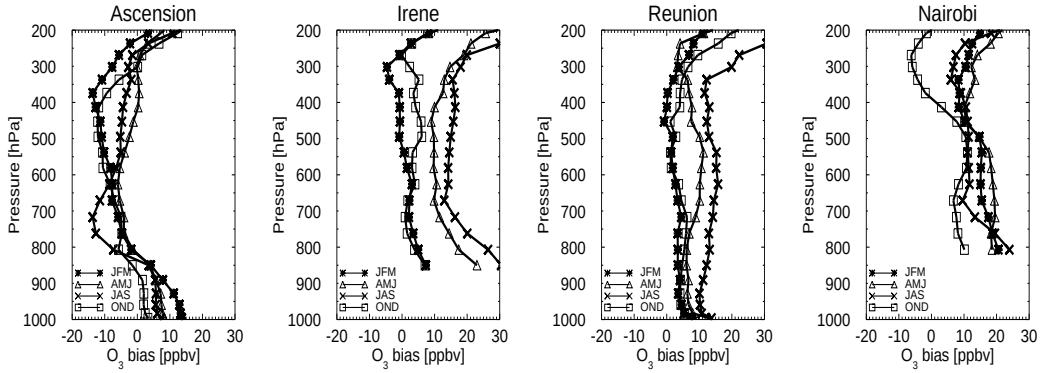

Figure 4.6— The vertical profile of the seasonal mean model bias (i.e. the difference of ECHAM5-MOZ and SHADOZ) over Ascension Island, Irene, Reunion and Nairobi.

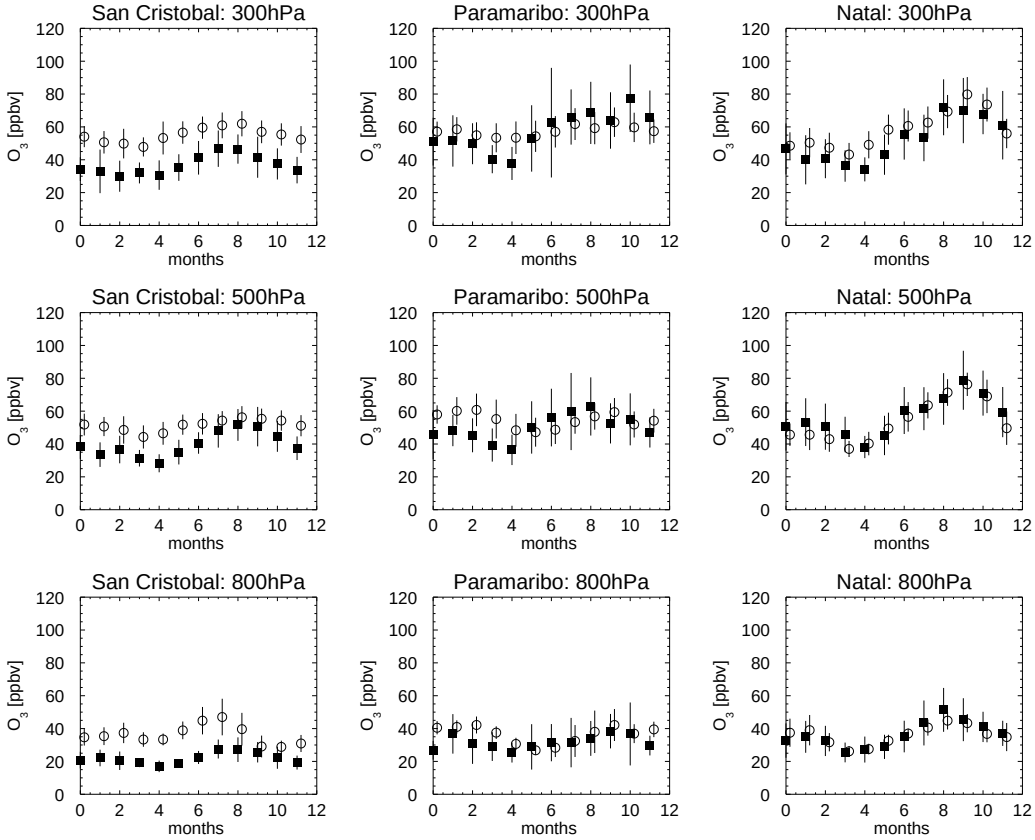

Figure 4.7— The comparison of 5-year average (1991–2000) ECHAM5-MOZ model (open circles) with 1998–2004 mean SHADOZ data (filled-squares) of ozone concentration (in ppbv) over San Cristobal (Ecuador), Paramaribo (Suriname), and Natal (Brazil) at 300 hPa (top), 500 hPa (middle), and 800 hPa (bottom). The horizontal lines indicate $\pm 1\,\sigma$ standard deviation.

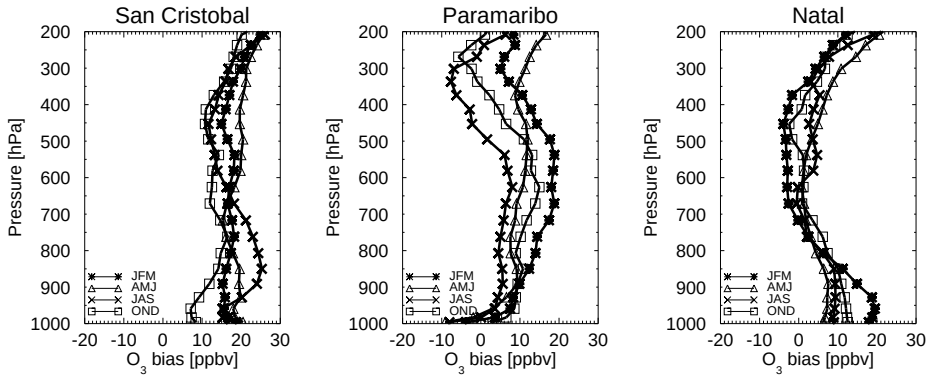

Figure 4.8— The vertical profile of the seasonal mean model bias (i.e. the difference of ECHAM5-MOZ and SHADOZ) over San Cristobal, Paramaribo and Natal.

4.5.3 Asia and the Pacific Ocean

The comparison of the monthly-mean time series of ozone concentrations calculated in ECHAM5-MOZ with SHADOZ data at 300 hPa, 500 hPa and 800 hPa over Kuala Lumpur (Malaysia), Watukosek (Java, Indonesia), Suva (Fiji), and America Samoa is shown in Figure 4.9. Again, the ECHAM5-MOZ model consistently overestimates the ozone concentrations at these three levels by about 10–25 ppbv over all the stations, except at 800 hPa over Suva and America Samoa, where the bias is less than 10 ppbv. The bias plots are as shown in Figure 4.10.

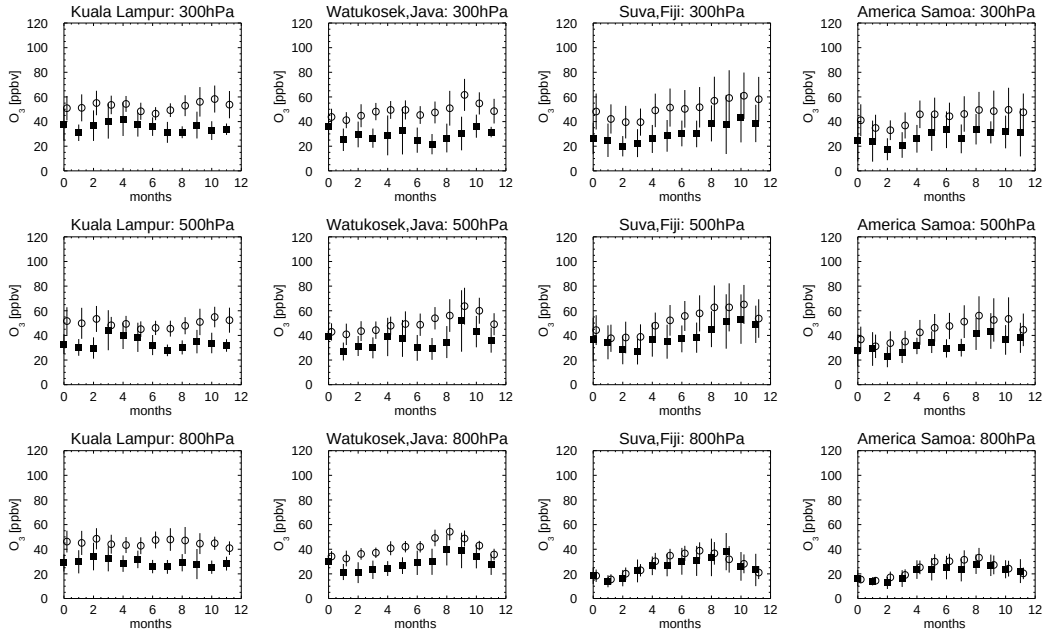

Figure 4.9— The comparison of 5-year average (1991–2000) ECHAM5-MOZ model (open circles) with 1998–2004 mean SHADOZ data (filled-squares) of ozone concentration (in ppbv) over Kuala Lumpur (Malaysia), Watukosek (Java, Indonesia), Suva (Fiji), and America Samoa at 300 hPa (top), 500 hPa (middle), and 800 hPa (bottom). The horizontal lines indicate $\pm 1\,\sigma$ standard deviation.

4.6 ECHAM5-MOZ comparison with NOAA/ESRL-GMD surface CO concentrations data

We compare CO surface concentrations calculated in ECHAM5-MOZ with 9 stations from the NOAA/ESRL-GMD CO data. These stations include 1 continental African station (Assekrem), 1 maritime African station (Mahe Island) and 7 stations downwind of Africa (see Figures 4.11 and 4.12 for the station names and coordinates).

At the stations north of the equator (i.e. Ragged Point, Terceira Island, Tenerife, Assekrem and Sede Boker), ECHAM5-MOZ underestimates the surface CO concen-

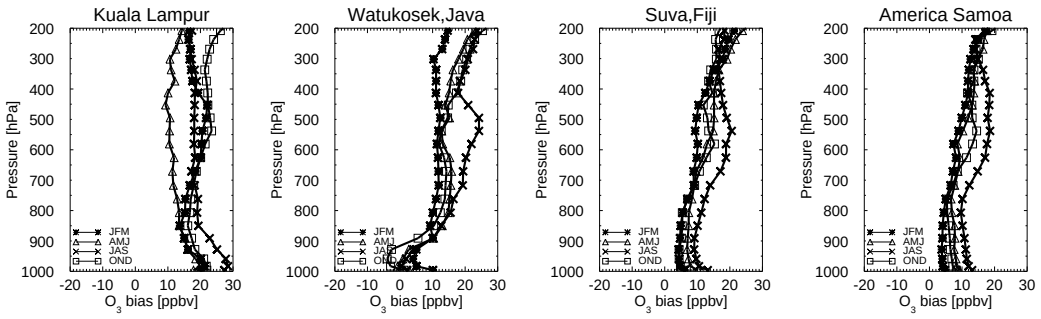

Figure 4.10— The vertical profile of the seasonal mean model bias (i.e. the difference of ECHAM5-MOZ and SHADOZ) over San Cristobal, Paramaribo and Natal.

tration, especially in January – May (Figure 4.11), whereas the seasonal variation and the magnitude of the surface CO concentration at the stations in the southern hemisphere (i.e. Ascension Island, Mahe Island, Crozet Island and Syowa) are well captured by the model as shown in Figure 4.12.

The inter-annual variability of the simulated surface CO concentration (error bars in Figures 4.11 and 4.12 is generally lower than that of the measurements. This may be related to inter-annual variations in emissions, which are not included in the model since the same monthly-mean emissions are prescribed in each of the simulation years.

4.7 Conclusions

The model calculated ozone and surface CO concentrations have been evaluated with the MOZAIC and SHADOZ ozone data, and NOAA/ESRL-GMD CO data, respectively at various locations in the tropical and extra-tropical regions. The measurement data recorded in all stations were regridded to model vertical resolution in order to ensure a consistent comparison.

Generally the ECHAM5-MOZ model captures the vertical profile and the seasonal variation of the tropospheric ozone in all months and over all the locations considered. The magnitude of the ozone concentrations calculated by the model also show good comparison with MOZAIC and SHADOZ data, and the model bias is generally less than 30 ppbv everywhere in the troposphere up to 300 hPa over all the stations considered. The only exceptions occur over Africa during the dry seasons, where the model shows some high biases of more than 30 ppbv. Other exceptions are recorded at the surface to around 900 hPa over Delhi, India in March through November and over New York in June through August. During these months, the model bias ranges between 35 ppbv and 55 ppbv. ECHAM5-MOZ is also able to simulate the seasonal variation and magnitude of the surface CO concentration at all the stations discussed.

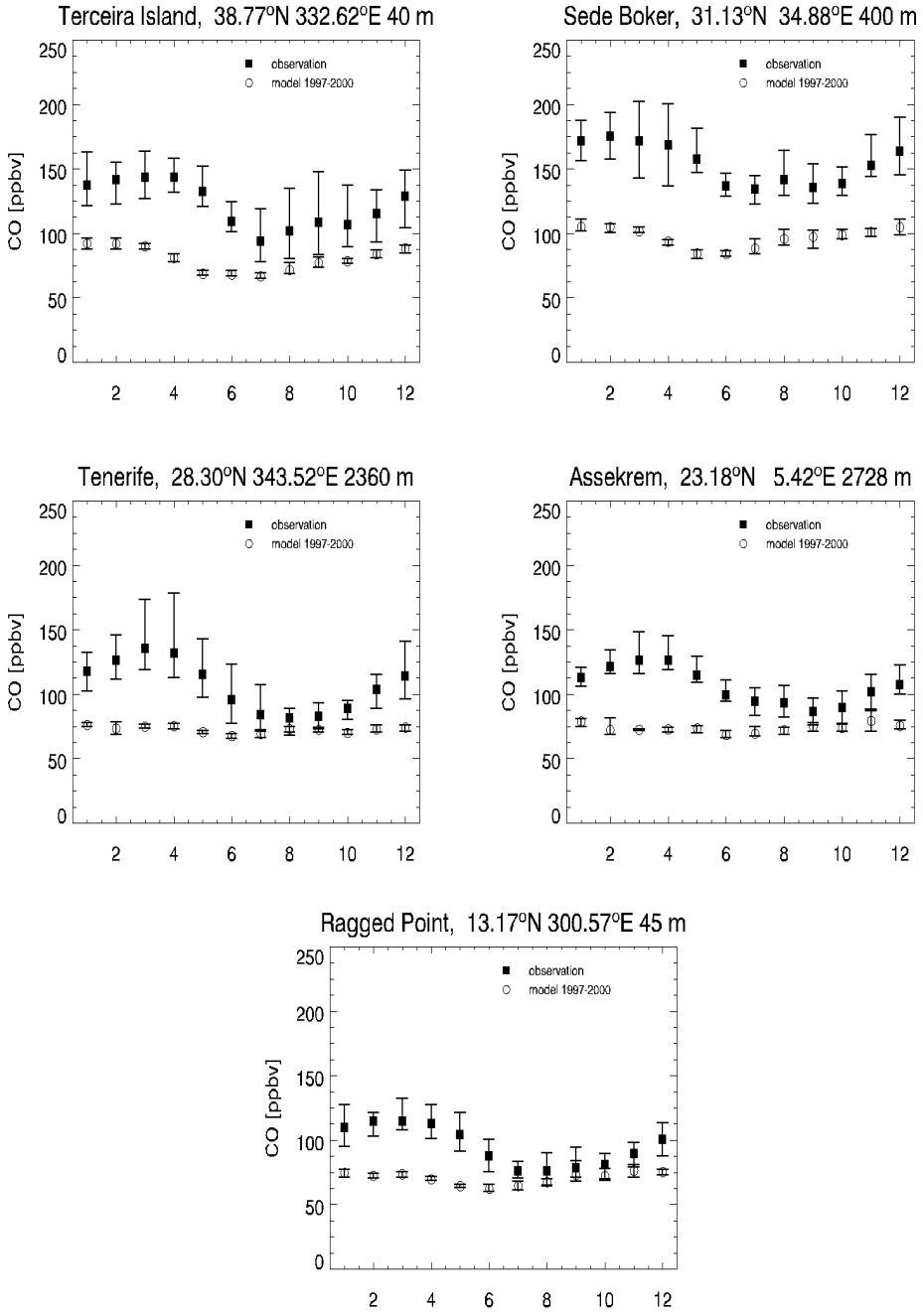

Figure 4.11— Monthly mean surface CO concentrations in ECHAM5-MOZ (open circles) compared to NOAA/ESRL-GMD CO (filled squares) at stations in the northern hemisphere (i.e. Terceira Island (Azores), Sede Boker (Negev desert, Israel), Tenerife (Canary Island), Assekrem (Algeria), Ragged Point (Barbados)). Error bars denote the inter-annual variations in both model and measurements.

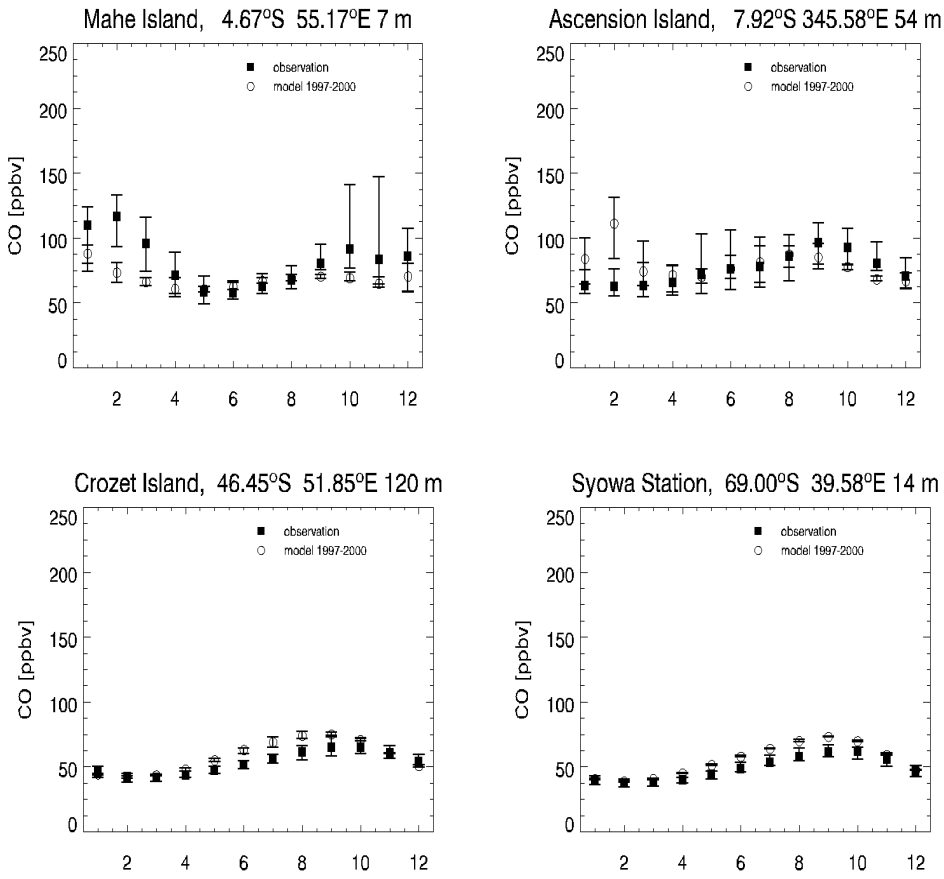

Figure 4.12— Monthly mean surface CO concentrations in ECHAM5-MOZ (open circles) compared to NOAA/ESRL-GMD CO (filled squares) at stations in the southern hemisphere (i.e. Mahe Island (Seychelles), Ascension Island, Crozet Islands and Syowa (Antarctica). Error bars denote the inter-annual variations in both model and measurements.

Chapter 5

Sensitivity of tracers' transport to model resolution, forcing data and chemical lifetime in the general circulation model ECHAM5

Abstract

The transport characteristics of the general circulation model (GCM) ECHAM5 are evaluated using independent idealized tracers with constant lifetimes released in different altitude regions of the atmosphere. The source regions were split into the tropics, northern and southern hemisphere. The experiments were run in the resolutions T21L19, T42L19, T42L31, T63L31 and T106L31 for a minimum period of 4 years each, using prescribed sea surface temperatures and sea ice fields of the 1990s and tracers' chemical lifetime of 5 months. One experiment was performed in the T63L31 resolution by forcing the model to the European Centre for Medium Range Weather Forecast (ECMWF) 40 years re-analysis data (ERA40). To evaluate the influence of lifetimes, two additional experiments were performed with lifetimes of 15 days and 50 months, respectively. In general, the transport pattern of each of the tracers is similar in all model resolutions. Large difference occurs when there is a change in the vertical resolution and tracers' chemical lifetime, and when the model is forced towards ERA40 meteorology. We found a decrease in the meridional transport of surface and tropopause tracers in the coarse resolution models due to an increase in the vertical mixing and recirculation within the source region. However, coarse model resolution leads to enhanced inter-hemispheric transport in the stratosphere. The use of ERA40 data causes a small change of between 1 – 3% in the meridional transport of surface and tropopause tracers. Whereas in the stratosphere, it significantly increases the transport of tracers to northern and southern

hemisphere, causing between 10% – 150% increase. ERA40 meteorology has little effect on the vertical mixing of the surface and tropopause tracers within the troposphere, but it increases their transport to the stratosphere by about a factor of 2.5, while it causes about 30% – 70% increase in the stratosphere tracers transported to the troposphere. It also generates quasi-biennial oscillation at the tropical stratosphere. We calculate the inter-hemispheric transport time of between 7 – 14 months for surface tracers, and 8 – 10 years for the stratosphere tracers.

5.1 Introduction

Horizontal and vertical transports play a crucial role in determining the distribution of gas-phase and particulate atmospheric trace constituents. Time scales of atmospheric transport processes range from minutes to years (Smagorinsky, 1974). Of particular interest for global tropospheric chemistry studies are the exchange between stratosphere and troposphere (e.g., Holton et al., 1995; Appenzeller et al., 1996; Van Noije et al., 2004; Gray, 2003), the inter-hemispheric transport (Prather et al., 1987; Plumb and Mahlman, 1987; Taguchi, 1993; Hartley and Black, 1995; Lintner, 2003; Lintner et al., 2004) and the inter-continental transport of air pollution (cf. Stohl et al., 2002; Schultz and Bey, 2004; Aghedo et al., 2007).

Numerical models of atmospheric chemistry and transport are an essential tool for evaluating the composition of the global atmosphere and for assessing the impact of emissions or changes in other parameters on air quality and climate. For example, atmospheric CO_2 measurements have been used to infer the emissions and sinks of CO_2 using atmospheric transport model (Fung et al., 1983; Enting and Mansbridge, 1989; Heimann and Keeling, 1989; Tans et al., 1990; Ciais et al., 1995; Enting et al., 1995; Kaminski et al., 1999; Law et al., 1996; Law, 1999; Rayner et al., 1999; Bousquet et al., 1999a,b, 2000; Baker, 2001).

However, models ability to simulate observed distributions of atmospheric constituents is largely dependent on their capability to reproduce the transport and mixing of the real atmosphere. Gurney et al. (2002, 2003) show that differences in the models simulated transport is a significant source of uncertainty, while Hall et al. (1999) concluded that transport inaccuracies significantly affect the simulation of important long-lived chemical species in the lower stratosphere. Model resolution also plays an important role. Genthon and Armengaud (1995) hinted that model spatial resolution is an important factor in the simulation of Radon 222 distribution, while Austin et al. (1997) have demonstrated the influence of model vertical resolution on the simulation of ozone distribution in the stratosphere. Moreover, in order for models to make reliable predictions of future changes, the model's ability to reproduce the atmospheric mean state and its variability and trend must also be tested. While this is generally achieved by comparing model results with observational data, there are not always sufficient observations available to reach a meaningful conclusion.

Therefore, idealized tracer experiments can help to investigate specific character-

istics of a model, and by comparing the results from different model configurations, they may also contribute to a better understanding of some discrepancies observed between the tropospheric chemistry simulations of different models (e.g. Genthon and Armengaud, 1995; Jacob et al., 1997; Denning et al., 1999; Stevenson et al., 2006). Gray (2003) used such online passive tracers to study the influence of convection on stratosphere – troposphere transport. Another example of idealized tracer parameterisation is the synthetic ozone (SYNOZ) model by McLinden et al. (2000).

In this study, we evaluate the transport characteristics of the ECHAM5 (Roeckner et al., 2003) general circulation model (GCM), by performing a series of idealized tracer experiments in various model resolutions and with different forcing conditions. We focus on the tracers' inter-hemispheric transport and vertical exchange between the troposphere and the stratosphere, and how they are influenced by model resolutions, ERA40 meteorology and tracers' chemical lifetimes. A brief description of the ECHAM5 model and the details of the model set-up are given in Sect. 5.2. The results are presented in Sect. 5.3 through 5.6. These include the diagnosis of tracers' global mass in Sect. 5.3, and the discussion of the inter-hemispheric and vertical transport of tracers in Sect. 5.4. Sections 5.3 and 5.4 also include concurrent discussion of the influence of model resolution and the use of ERA40 meteorology as boundary condition. We discuss the sensitivity of our findings to the chemical lifetime of the tracers in Sect. 5.5. The inter-hemispheric transport time of surface tracers are presented in Sect. 5.6. Conclusions and the summary of the main findings are given in Sect. 5.7.

5.2 Model Description

5.2.1 The ECHAM5 general circulation model

The atmospheric general circulation model ECHAM5 is the fifth-generation climate model developed at the Max Planck Institute for Meteorology, evolving originally from the model of the ECMWF (Simmons et al., 1989). The dynamical core of ECHAM5 solves prognostic equations for vorticity, divergence, logarithm of surface pressure and temperature, which are expressed in the horizontal by spectral coefficients. The model uses a semi-implicit leapfrog time integration scheme (Robert et al., 1972; Robert, 1981, 1982) and a special time filter (Asselin, 1972). The vertical axis uses a hybrid terrain-following sigma-pressure coordinate system and finite-difference scheme (Simmons and Burridge, 1981). The finite-difference scheme is implemented such that energy and angular momentum are conserved. Water vapour, cloud liquid water, cloud ice and trace components are transported with a flux form semi-Lagrangian transport scheme (Lin and Rood, 1996) on a Gaussian grid (Arakawa C-grid, Mesinger and Arakawa, 1976). ECHAM5 contains a new microphysical cloud scheme (Lohmann and Roeckner, 1996) with prognostic equations for cloud liquid water and ice. Cloud cover is predicted with a prognostic-statistical scheme solving equations for the distribution moments of total water (Tompkins, 2002). Convective clouds and convective transport

are based on the mass-flux scheme of Tiedtke (1989) with modifications based on Nordeng (1994). A detailed model description is given in Roeckner et al. (2003). The model successfully participated in recent scenario experiments for the fourth assessment report of the Intergovernmental Panel on Climate Change (http://www.mpimet.mpg.de/fileadmin/grafik/presse/Klimaprojektionen2006.pdf). The sensitivity of the ECHAM5 simulated climate to various resolutions is investigated in Roeckner et al. (2006).

ECHAM5 can be run as a coupled ocean-atmosphere model, or with forced boundaries from prescribed sea surface temperatures and sea ice cover fields. In addition, a Newtonian relaxation technique , also termed "nudging" (Hoke and Anthes, 1976; Jeuken et al., 1996) can be applied in order to simulate real weather episodes. The atmospheric forcing (surface pressure, temperature, vorticity, and divergence) is then obtained from numerical weather prediction models with data assimilation. Van Aalst et al. (2004) applied the nudging technique to a middle-atmosphere GCM, MAECHAM4 (Manzini and McFarlane, 1998) and showed that the nudging offered a good representation of chemistry and transport processes. The experiments in this study are performed using a set-up similar to the Atmospheric Model Intercomparison Project 2 (AMIP2, Gates et al., 1999) using the AMIP2 sea surface temperature and sea ice climatologies of the 1990s. We contrast these simulations with one experiment which was forced by data from the European Center for Medium range Weather Forecast (ECMWF) 40-years re-analysis data (ERA40, Simmons and Gibson, 2000).

5.2.2 Experiment description

ECHAM5 contains a flexible software structure for defining idealized atmospheric tracers. These tracers are then subjected to advection, convection and diffusion. Additional processes such as emissions, depositions and chemical reactions can also be added through the standard software interface.

For this study, we define 9 independent idealized tracers with constant concentrations at the source region (see Fig. 5.1). The tracers are set to a constant mixing ratio of 1.0 in the source region at each time step. This is equivalent to prescribing a source strength of varying magnitude, which is proportional to the outflow from the region. Once, the simulation has reached a steady state, changes in total tracer mass on the seasonal scale can thus be used to diagnose the transport activity.

Horizontally, we divide the earth surface into three equal-area latitude bands called "north" (N), "tropics" (T) and "south" (S). "North" refers to the region north of 19° N, the region south of 19° S is "south" and the region in the latitude bands in-between 19° N and 19° S is "tropics". These latitudinal divisions are consistent with the findings of (Bowman and Carrie, 2001; Bowman and Erukhimova, 2004; Erukhimova and Bowman, 2006), that the atmosphere can be divided into three parts during an idealized transport study. Vertically we introduce the tracers at three different altitude regimes (i.e. "surface", "tropopause" and "stratosphere"). The "surface" tracers are defined at the lowest model level. The "tropopause" tracers

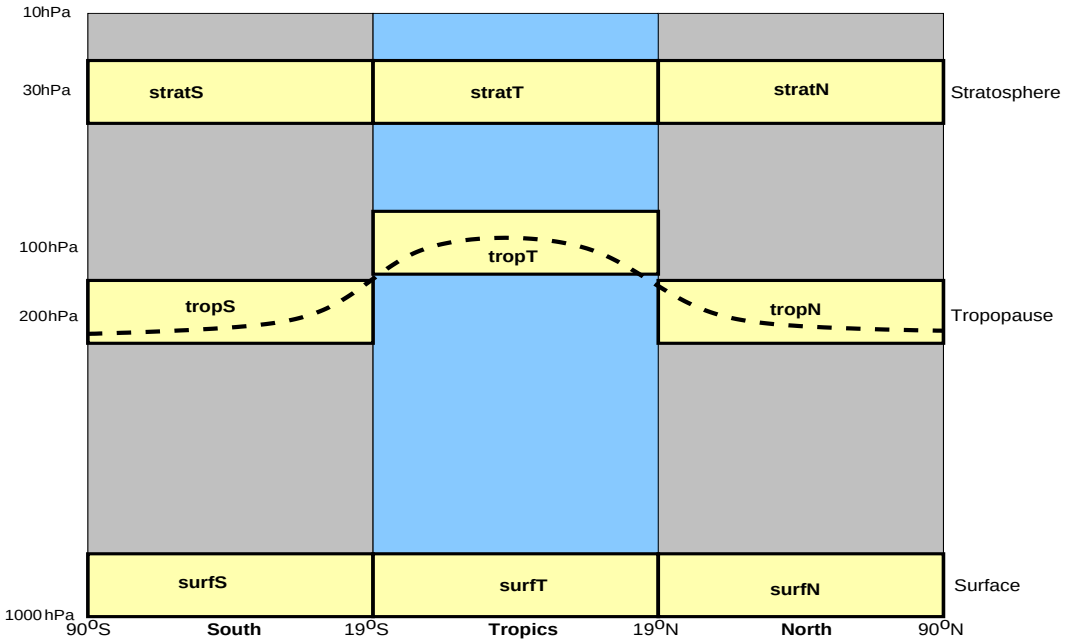

Figure 5.1— The schematic diagram showing the independent idealized tracers source regions. The dashed line is the tropopause, while the grey shaded parts are the "north" (N) and "south" (S) regions. The blue shaded region is the "tropics" (T). The surface tracers (surfN, surfT and surfS) are introduced at the lowest model level, while the stratosphere tracers (stratN, stratT and stratS) are emitted at 30 hPa level. The tropopause tracers are released at 100 hPa and 200 hPa for tropT and tropN (or tropS) respectively. Note that the diagram is not drawn to scale.

are defined at the tropopause, which is assumed to correspond to 100 hPa height in the T region and 200 hPa height in the N and S regions. The "stratosphere" tracers are defined at the model level corresponding to 30 hPa, which is the second level in the vertical resolutions L19 and L31 used in the simulations. Henceforth, we will abbreviate the tracer names by combining their vertical and horizontal source region names; surfT for example will identify the surface tracer with source region at the tropics, while tropN stands for the tracer which is kept at constant concentrations in the northern hemisphere tropopause region (see Fig. 5.1).

Experiments involving the tracers with chemical lifetime of 5 months were performed in the resolutions T21L19, T42L19, T63L31, T106L31 and T42L31. The first four resolutions are the most adequate matches of horizontal and vertical resolution according to Roeckner et al. (2004, 2006). A sensitivity experiment was also performed for testing the impact of ERA40 meteorology in the T63L31 resolution (run T63L31-era40) using the tracers with 5 months lifetime. All simulations involving tracers with 5 months lifetime were run for minimum of 4 years excluding the spin-up time of 1 year.

Additional sensitivity experiments for analysing the changes in the chemical lifetime of the tracers were performed in T63L31 resolution employing tracers with 15

Table 5.1— Source region mass relative to T63L31 source region mass across the resolutions.

	Model resolutions				
Tracers	T21L19	T42L19	T42L31	T63L31	T106L31
surfN,surfS,stratN,stratS	0.92	0.98	0.98	1.0	0.99
surfT, stratT	1.18	1.05	1.05	1.0	1.02
tropN, tropS	1.79	1.91	0.98	1.0	0.99
tropT	1.86	1.65	1.05	1.0	1.02

days and 50 months chemical lifetimes. The T63L31 experiment concerning tracers with 50 months chemical lifetime needed more years to reach a steady state, therefore, the experiment were run for a total period of 13 years. The last three years of the simulation was used in the analysis. Though the experiments to study the influence of ERA40 meteorology and chemical lifetime of tracers on the transport of tracers were performed in the T63L31 resolution, we expect that similar effects would be seen in other model resolutions.

5.3 Global mass of tracers

The global mass of our tracers with chemical lifetime of 5 months, and how they are influenced by different model resolutions and ERA40 meteorology is presented in this section. The discussions are based on the last four years of our simulations.

At steady state, the tracer' global mass is a function of the source strength, volume (or mass) of the source region and the tracer' chemical lifetime. The experiments are designed such that the latter two variables are constant. However, individual grid of each of the resolutions falls at different latitudinal and longitudinal boundaries, leading to a slightly different source region mass. Our calculations of the source region mass of each of the tracers across the resolutions show that the influence of the source region mass is significant for the resolutions with 19 vertical levels (T21L19 and T42L19), most especially in the case of tropical and tropopause tracers (Table 5.1). Figure 5.2 shows the global mass of the tracers measured relative to the average global mass of T63L31 resolution, taking into account the differences in the source region mass across all the resolutions.

The transport of surface and tropopause tracers increases as the model resolution increases. More importantly, transport from the surface and tropopause shows a significant dependence on the number of vertical levels, evident by the clear separation between the 19-level and 31-level models (Fig. 5.2). However, the stratosphere tracers show little difference across the resolutions. While the pattern of the zonal average of each of the tracers is similar across the different model resolutions, major differences occur with respect to the extent and shape of specific isolines (see figures in the Appendix C).

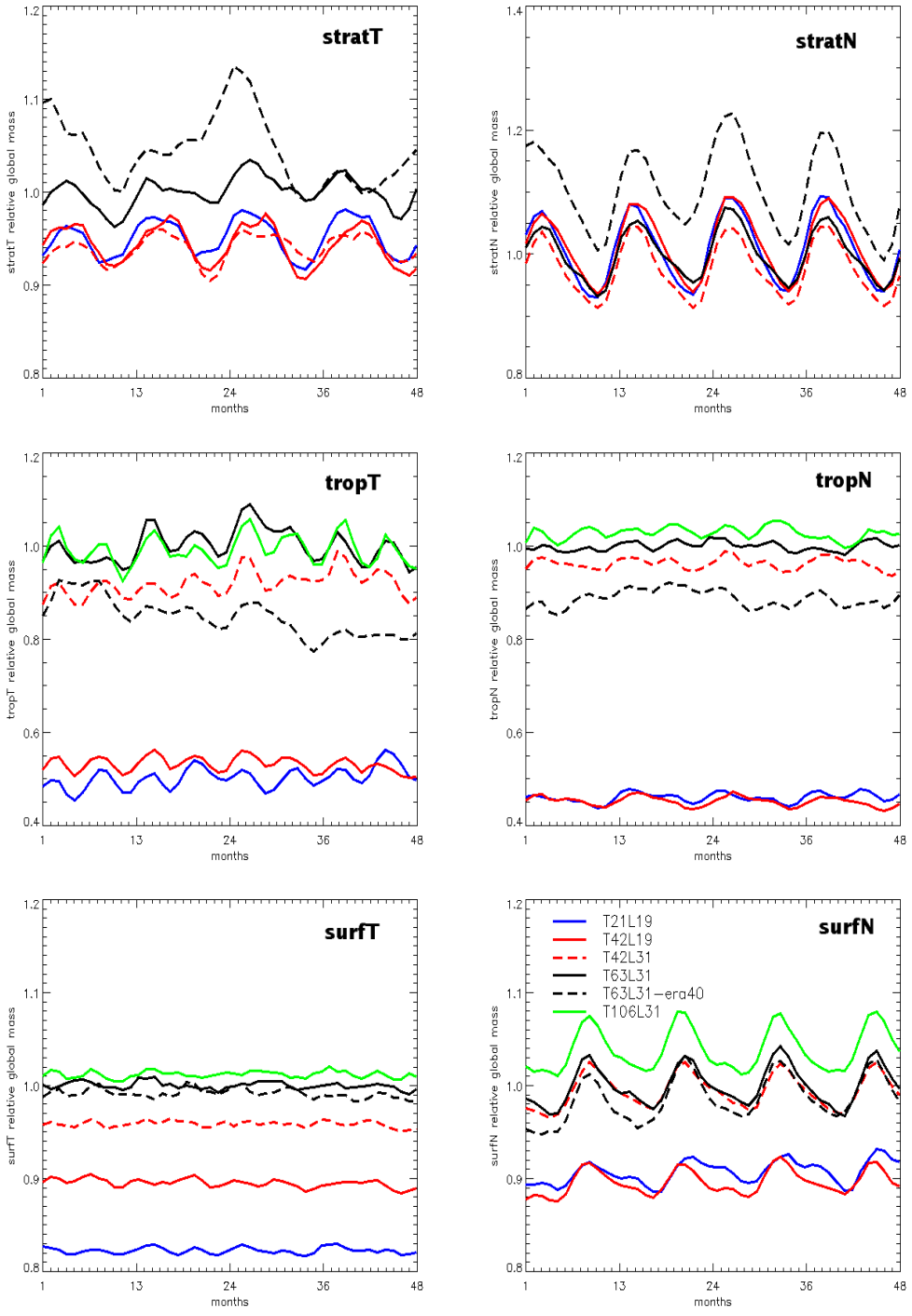

Figure 5.2— Global mass of the tracers relative to the average global mass of T63L31 resolution across T21L19, T42L19, T42L31, T63L31, T63L31-era40 and T106L31 resolutions. The differences in tracers' source region mass have been taken into account. The S tracers are not shown because they are similar to the N tracers.

A striking feature in Fig. 5.2 is the closeness of the T42L31 lines to the other 31-level models. Therefore T42L31 seems to be a good representative of the 31-level resolutions. This shows that when considering transport of chemical species that exhibit strong vertical concentration gradients, it is worth using T42 horizontal resolution with 31 vertical levels. However, Roeckner et al. (2004, 2006) show that using 31 vertical levels instead of 19 does not improve the meteorology in the T42.

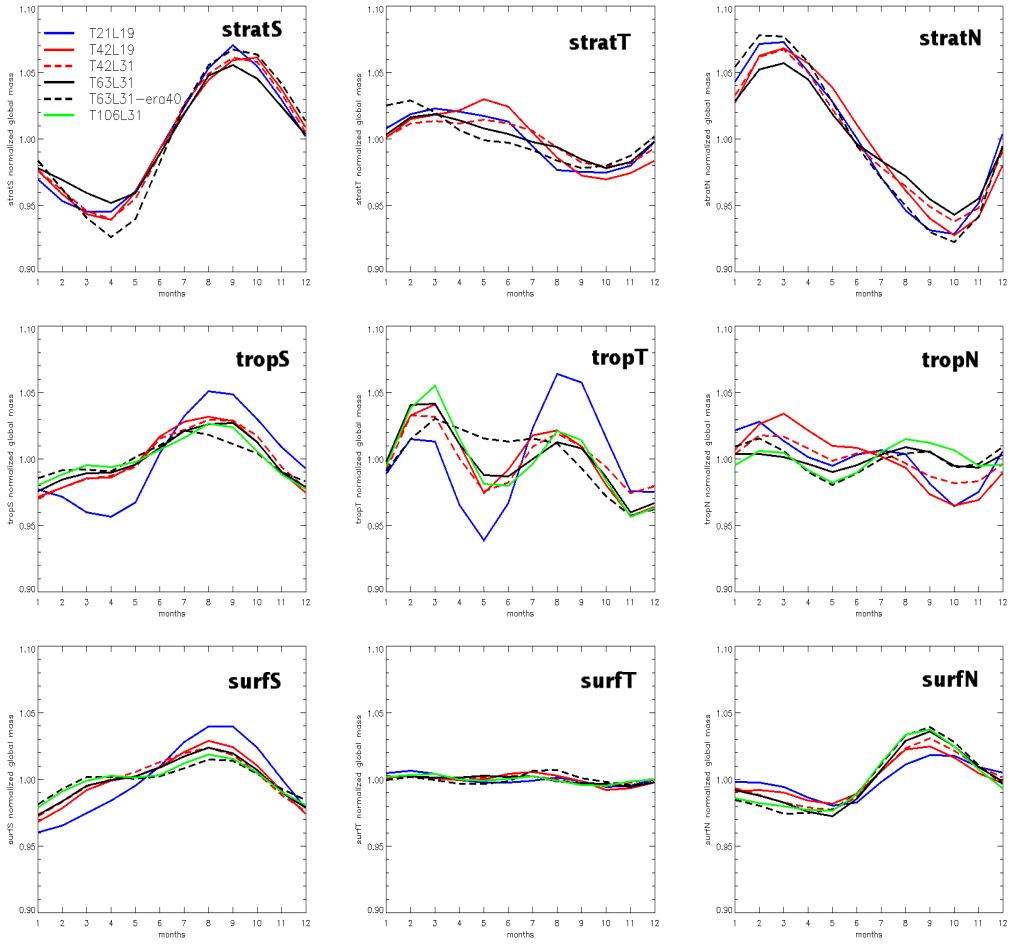

Figure 5.3— The plots showing the seasonal variation of the normalized global mass of each of the tracers across the resolutions. The tracers' 4-year average monthly global mass are normalized with respect to the 4-year mean global mass.

ERA40 data leads to a slight reduction of transport from the surface. It also leads to a reduction of about 10% – 15% in the transport from the tropopause. This difference may be partly explained by the difference in the tropopause height of the T63L31 and T63L31-era40 simulations calculated according to the World Meteorological Organisation (WMO) definition. However, ERA40 data leads to an

increase of up to 10% in the transport of stratosphere tracers (Fig. 5.3). It also generates a quasi-biennial oscillation (QBO) at the tropical stratosphere (see stratT in Fig. 5.2). As demonstrated by (Giorgetta et al., 2002), the ECHAM5 model can generate a QBO signal only when run in the middle-atmosphere configuration with at least 80 vertical levels.

The influence of resolution on the seasonality of each of the tracers is shown in Fig. 5.3. In the figure, 4-year monthly average of the tracers' global mass are normalized by the respective 4-year-average global mass across each of the resolution. The surface and tropopause tracers in the T21L19 resolution generally have larger amplitude when compared to other resolutions. The maximum of surfN and surfS tracers occurs in September and August respectively, while their minimums have a phase shift of about 4 months (minima occur in May and January respectively). The seasonal cycle of surfT is very weak. The tropopause tracers exhibit less coherent seasonality across the resolutions. Interestingly, tropN and tropS tracers have different seasonality, while tropN has two maximums, tropS have only one. The stratN and stratS tracers have a distinct seasonal cycle with a comparable amplitude, however, they are opposite in phase to each other. The maximum and minimum global mass of stratN is found around March and October respectively, while for stratS, they occur in September and April respectively. The seasonal cycle of stratT tracer is in phase with the seasonal cycle of stratN tracer. In conclusion, the seasonal variation of tropopause tracers shows the largest difference across the resolutions.

5.4 Transport of tracers

This section discusses the inter-hemispheric and the vertical exchange of the tracers with the chemical lifetime of 5 months. It also presents the concurrent results of the variation in the transport due to changes in model resolution and meteorology. We report the amount of tracers found in the respective regions under consideration (i.e. the three inter-hemispheric regions N, S, and T) in percent of the global mass. This makes our results independent of the seasonally varying flux out of the source region.

5.4.1 Inter-hemispheric transport

Figure 5.4 shows the percentage amount of each of the tracers found in the three regions at steady state. It shows that about 15%, 18% and 2% of the surface, tropopause and stratosphere tracers, respectively are exchanged between N and S regions. While these fractions are also about 28%, 31% and 26% respectively for the tropical tracers transported to both hemispheres. The N and S region tracers transported to T region is about 31%, 35% and 15% for the surface, tropopause and stratosphere tracers respectively. Generally, about half of the tracer mass remains in the region of origin, except for the stratN and stratS tracers, where this fraction is as large as 80% owing to the much slower meridional circulation in the stratosphere.

Coarse resolution models lead to a decrease in the inter-hemispheric transport at the surface and the tropopause, but the opposite is true in the advection to tropical region (Fig. 5.4a and b) . As will be discussed in Sect. 5.4.2, this is a consequence of increased vertical mixing and recirculation in the coarser resolution models. However, coarser model resolution leads to an increase in the inter-hemispheric transport in the stratosphere (Fig. 5.4c), with the exception of stratT tracer transported to S region.

ERA40 data generally leads to a small reduction of about 1 – 3% in the exchange of surface and tropopause tracers among the three regions, except for surfS transported to T region and tropT transported to both hemispheres. In latter cases, it causes about 2% increase (Fig. 5.4a and b). In contrast to its influence at the surface and the tropopause, ERA40 data increases the inter-hemispheric transport in the stratosphere by about 10 – 15% for transport from tropical region to both hemisphere and about a factor of 2 for exchange between the N and S regions (Fig. 5.4c). The generated QBO in the T63L31-era40 run (Fig. 5.5) must have contributed to the higher inter-hemispheric mass exchange observed in the stratosphere tracers, which would be consistent with the results in O'Sullivan and Chen (1996).

The seasonal cycle of the inter-hemispheric transport of the stratosphere tracers in T63L31 resolution is shown in Fig. 5.6. It shows that the stratosphere tracers have an enhanced exchange of air between the tropical stratosphere and the extra-tropical stratosphere starting from late autumn to spring (October – May in the northern hemisphere and May – October in the southern hemisphere). This seasonal cycle is somewhat consistent with the seasonality of the isentropic mass exchange between the tropics and the extra-tropics at the stratosphere as reported in previous studies (e.g. Chen et al., 1994; Waugh, 1996). Transport from stratosphere tropical region has a larger amplitude than the exchange between other regions. This is a consequence of the Brewer-Dobson circulation (Brewer, 1949; Dobson, 1956), which describes a residual flow from the tropical stratosphere to the poles. Less distinctive and weaker patterns are observed in the seasonal cycle of inter-hemispheric transport of the tropopause and surface tracers. The seasonality of the inter-hemispheric transport of stratosphere tracers in other model resolutions is similar to T63L31 seasonal cycle described here, but with varying amplitudes.

5.4.2 Vertical exchange of tracers

The most important vertical transport is the cross-tropopause transport. Therefore, in this section we consider the transport of the surface and tropopause tracers to the stratosphere (above the 50 hPa level) and the transport of the stratosphere tracers to below 750 hPa. These are shown in Fig. 5.7.

Owing to the long residence time of air in the stratosphere relative to the chosen lifetime of 5 months of our idealized tracers, less than 1.2% and 6% of the surface and tropopause tracers' mass are found at levels above 50 hPa, respectively across all model resolutions. About 1.0% of the stratosphere tracers are transported to below 750 hPa. The amount of surface and tropopause tropical tracers transported

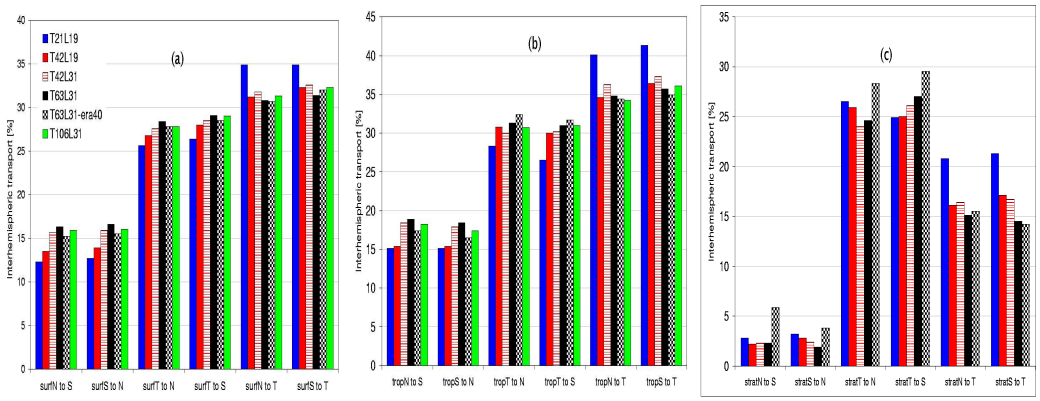

Figure 5.4— Inter-hemispheric transport of (a) surface tracers, (b) tropopause tracers and (c) stratosphere tracers between the N, S and T regions. Figures shows 4 years average, and each of the bars represents the percentage amount of tracers' mass found in the region specified.

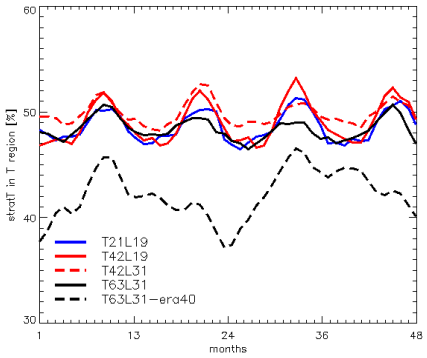

Figure 5.5— The seasonal variation in the percentage of the stratT tracer's mass remaining in the T region across the model resolution and T63L31-era40 runs.

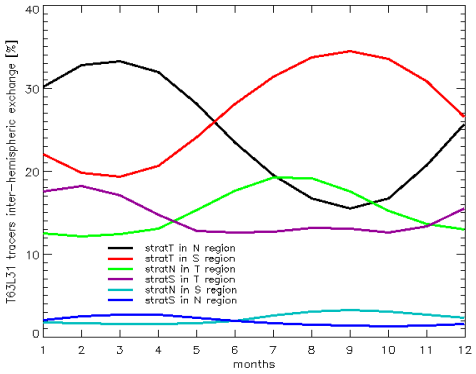

Figure 5.6— The percentage amount of the T63L31 stratosphere tracers' mass found in N, T and S regions. The plot also shows the seasonal variability.

to the stratosphere is larger than that transported from their corresponding N and S tracers. This is due to the influence of convection on the tropical surface tracer and a higher source region altitude on the tropical tropopause tracer.

The vertical uplift of surface and tropopause tracers decreases as the model resolution increases (Fig. 5.7 left and middle). Again, the number of vertical levels plays a significant role. The stratosphere tracers transported to below 750 hPa decreases as the model vertical resolution increases (Fig. 5.7 right).

ERA40 data increases the vertical transport of surface and tropopause tracers to the stratosphere by about a factor of 2.5 (Fig. 5.7 left and middle), while it has little effect on their vertical mixing within the troposphere (figures not shown).

ERA40 data also increases the transport of stratosphere tracers to the troposphere by up to 70% (Fig. 5.7 right). This is consistent with findings from Van Noije et al. (2004), who investigated the sensitivity of STE towards different meteorological forcing conditions in their chemistry transport model.

The seasonal cycle of the stratosphere tracers transported to below 750 hPa across the model resolution is shown in Fig. 5.8. The figure shows that the seasonal cycle varies from one model resolution to another. Again the T42L31 values and seasonality are comparable to that of T63L31.

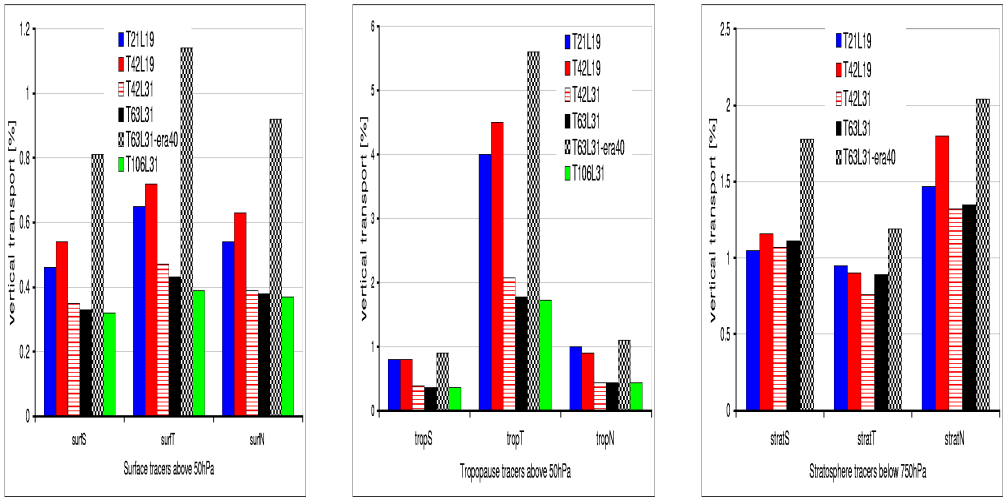

Figure 5.7— The percentage of surface (left) and tropopause (middle) tracers' mass transported to the stratosphere (above 50 hPa), and the stratosphere tracers (right) transported to the surface (below 750 hPa). It shows the differences across the model resolutions and T63L31-era40 run. Value of each bar represents 4-years average.

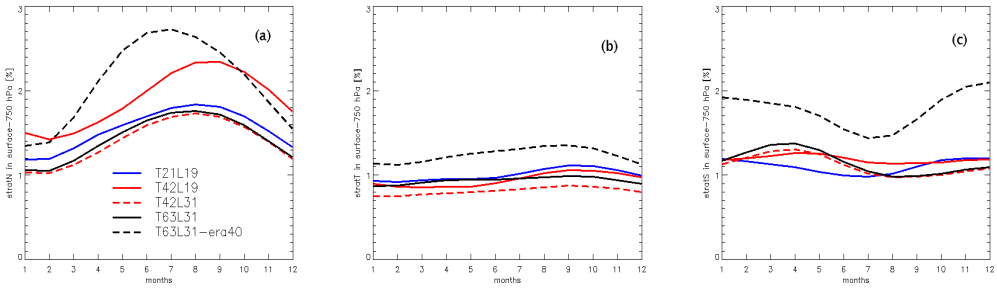

Figure 5.8— The seasonality of the percentage of (a) stratN (b) stratT and (c) stratS tracers' mass transported to below 700 hPa for all the model resolutions and T63L31-era40 run.

5.5 Sensitivity towards chemical lifetime of tracers

In this section, we discuss the influence of the tracers' lifetime on the transport of tracers discussed above. In order to contrast the results discussed so far with model simulations of tracers with different lifetimes, we therefore performed additional model simulations in T63L31 with a tracer lifetime of 15 days and 50 months. The experiments concerning tracers with 50 months chemical lifetime needed a much longer spin-up time (a trend in the stratospheric tracers was detected up to year 10). Therefore the experiments were conducted for a total period of 13 years. In this section, we present the results for the last 3 years of the simulation.

The percentage mass exchanged between the three hemispheric regions (N, S, and T) for each of the tracers across the different chemical lifetimes is shown in Table 5.2. The table reveals that the long-range inter-hemispheric transport between the northern and the southern hemisphere, and the inter-hemispheric transport of the stratosphere tracers are most affected by the tracers' chemical lifetime. The largest differences are however found between the tracers which chemical lifetime of 15 days and 5 months. The 50 months surface and tropopause tracers are well mixed, therefore the distribution within the regions vary by less than 7%, whereas this variation in the stratosphere tracers is up to 30% (see 50 months tracers in column 4 of Table 5.2). The measurement of remote tropospheric methane concentrations also vary by less than 10% across the globe (Dlugokencky et al., 1994).

Table 5.3 shows the vertical transport of the tracers across the different chemical lifetimes. The fraction of the surface and tropopause tracers transported to the stratosphere, and the stratosphere tracers that gets to the surface are almost reduced to 0% when the chemical lifetime is 15 days. This fraction increases to about 0.4% and 1.0% for the surface and tropopause tracers respectively, when the lifetime is increased from 15 days to 5 months. When the lifetime is increased from 5 months to 50 months, these fractions are further increased by about a factor of 10, except for the tropopause T tracer, where the increase is only a factor of 3. Figure 5.9 shows an example of the changes in the seasonality of the stratosphere tracers transported to below 750 hPa due to a change in the chemical lifetime. These changes provide a demonstration of the strong connections between atmospheric chemistry and transport, which may have important implications for atmospheric chemistry data assimilation.

5.6 Estimating tracers' transport time

In this section, we present a box model of tracer transport and calculate the inter-hemispheric and vertical transport time of tracers based on this box model using the results presented in earlier sections.

The entire atmosphere is divided into two boxes as shown in Fig. 5.10. Each of the boxes has a volume, V, mass density, ρ and a rate of chemical extinction $\alpha = 1/\tau$. Where τ is the chemical lifetime of tracer in the box. The subscripts 1

Table 5.2— Comparison of the inter-hemispheric transport of tracers (in %) with chemical lifetime of 15 day, 5 months and 50 months in the T63L31 resolution.

	Chemical lifetime of tracers		
Tracers and receptor region	15 days	5 months	50 months
Exchange of mass between N and S regions			
surfN to S	1.2	16.3	30.8
surfS to N	1.5	16.6	30.7
tropN to S	2.6	18.9	31.3
tropS to N	2.3	18.4	31.1
stratN to S	0.01	2.3	22.3
stratS to N	0.01	1.9	21.5
Transport from N and S to T region			
surfN to T	18.3	30.8	32.6
surfS to T	19.2	31.4	32.8
tropN to T	30.8	34.8	33.1
tropS to T	32.5	35.7	33.2
stratN to T	6.7	15.1	26.4
stratS to T	6.8	14.5	25.9
Transport from T to N and S regions			
surfT to N	14.8	28.4	32.9
surfT to S	15.2	29.1	33.2
tropT to N	20.2	31.3	33.3
tropT to S	20.6	31.0	33.6
stratT to N	8.2	24.6	33.9
stratT to S	8.8	27.0	35.5
Tracers remaining in source region			
surfN in N	80.5	52.9	36.6
surfS in S	79.3	51.9	36.5
surfT in T	70.0	42.5	33.9
tropN in N	66.6	46.3	35.6
tropS in S	65.2	45.9	35.7
tropT in T	59.2	37.7	33.1
stratN in N	93.3	82.7	51.3
stratS in S	93.2	83.6	52.6
stratT in T	83.0	48.4	30.6

and 2 make a distinction between boxes 1 and 2 respectively. Tracer in box 1 is transported into box 2 at a rate $\gamma_- = 1/\tau_-$ while the tracer in box 2 is transported to box 1 at a rate $\gamma_+ = 1/\tau_+$. Tracer has a source, with source strength s. The rate

Table 5.3— The comparison of the percentage mass transported vertically in the T63L31 tracers for the different chemical lifetimes.

	15 days	5 months	50 months
Surface tracers			
surfN above 50 hPa	0.0057	0.38	3.68
surfS above 50 hPa	0.0042	0.33	3.63
surfT above 50 hPa	0.0124	0.43	3.74
Tropopause tracers			
tropN above 50 hPa	0.011	0.43	3.72
tropS above 50 hPa	0.007	0.36	3.67
tropT above 50 hPa	0.196	1.77	5.11
Stratosphere tracers			
stratN below 750 hPa	0.0004	1.35	15.63
stratS below 750 hPa	0.0003	1.11	15.32
stratT below 750 hPa	0.0008	0.89	14.04

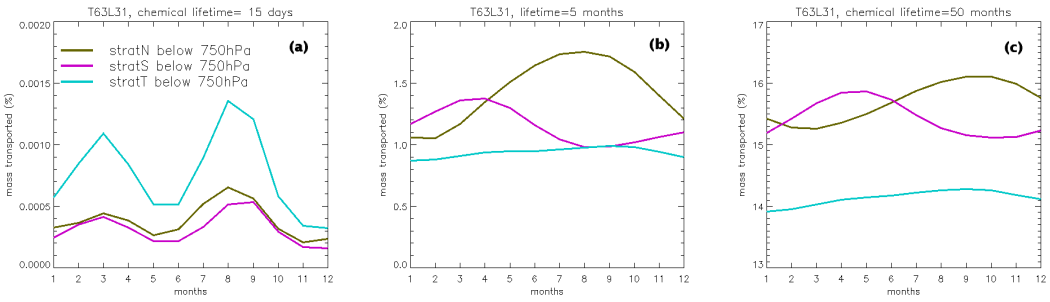

Figure 5.9— The monthly time series of the percentage of the T63L31 stratosphere tracers' transported to below 750 hPa when the lifetime is (a)15 days (b) 5 months and (c) 50 months. Note the difference in the seasonal variation.

of change of ρ in box 1 and 2 due to exchange of tracer between the two boxes are:

$$\dot{\rho_1} = -\alpha_1 \rho_1 - \gamma_- \rho_1 + \gamma_+ \frac{V_2}{V_1} \rho_2 + s \tag{5.1}$$

$$\dot{\rho_2} = -\alpha_2 \rho_2 - \gamma_+ \rho_2 + \gamma_- \frac{V_1}{V_2} \rho_1 \tag{5.2}$$

where the parameters α_1, α_2, γ_+ and γ_- are positive real numbers.

At steady state, the LHS of Equations (5.1) and (5.2) is equal to zero. If we solve the resulting equations simultaneously for steady state $\bar{\rho_1}$ and $\bar{\rho_2}$, assuming s

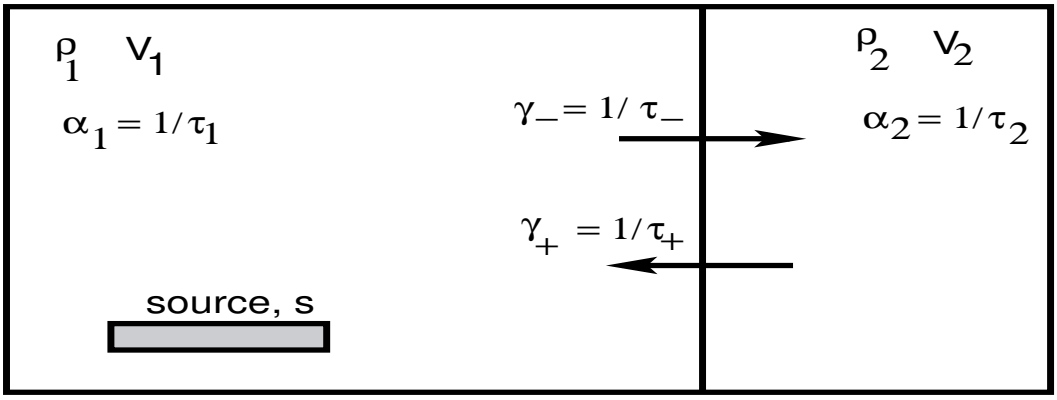

Figure 5.10— The box model of transport of tracer. See text for details description of the parameters.

is known yields:

$$\bar{\rho_1} = \frac{(\alpha_2 + \gamma_+)\, s}{(\alpha_1\, \alpha_2 + \alpha_1\, \gamma_+ + \alpha_2\, \gamma_-)} \tag{5.3}$$

$$\bar{\rho_2} = \frac{\gamma_-\, V_1\, s}{V_2\, (\alpha_1\, \alpha_2 + \alpha_1\, \gamma_+ + \alpha_2\, \gamma_-)} \tag{5.4}$$

Dividing Equation (5.3) by Equation (5.4) and further simplications yield:

$$\frac{V_1\, \bar{\rho_1}}{V_2\, \bar{\rho_2}} = \frac{\bar{m_1}}{\bar{m_2}} = \frac{1}{\gamma_-}\, \alpha_2 + \frac{\gamma_+}{\gamma_-} \tag{5.5}$$

$$Y = \tau_-\, \alpha_2 + \frac{\tau_-}{\tau_+} \tag{5.6}$$

To calculate the inter-hemispheric transport time between both hemispheres, we assume that the boundary between the two boxes is at the equator. This is physically consistent due to the inter-tropical convergence zone (ITCZ) at the equator, which acts as a major resistance to air mass exchange between northern and southern hemispheres. Using Equation (5.6), we calculate that it will take about 7 and 10 – 14 months for the surface tracer with source in southern and northern hemisphere, respectively to be transported to the other hemisphere. These results are at the lower end of the inter-hemispheric exchange time of 1.5 – 1.7 years calculated from ^{85}Kr concentration by Levin and Hesshaimer (1996) with the use of a different two box model. Our calculation shows that the inter-hemispheric transport time of the stratosphere tracers are within the range of 8 – 10 years.

Applying the box model to our vertical transport results, with the assumption that the tropopause is at 155 hPa, shows that it will take about 35 and 56 months for surface tracers with the source region in the northern and southern hemisphere, respectively to get into the stratosphere. Whereas, it will take only 17 days for the

surface tropical tracer to get into the stratosphere. These results are very sensitive though to the assumed height of the tropopause level. We also calculated that the stratosphere tracers cross-tropopause transport time is of the order of 5, 6 and 8 years for stratN, stratS and stratT tracers respectively.

5.7 Summary and Conclusions

The influence of model resolution, ERA40 meteorology and the chemical lifetime on the transport of tracers in ECHAM5 has been examined. These influences are assessed through the changes in the tracers global mass, inter-hemispheric exchange and vertical transport of the 9 independent idealized tracers we introduce into ECHAM5.

Generally transport increases in the finer resolution models and are mostly dependent on the number of vertical levels. The transport of tracers in the T42L31 resolution is similar to the other model resolutions with 31 vertical levels, and it could be their good representative, although the ECHAM5 model climate simulations give better results at higher spatial resolutions (Roeckner et al., 2006). We found a decrease in the meridional transport of surface and tropopause tracers in the coarse resolution models, as a consequence of an increased vertical mixing and recirculation within their source region. Hence percentage amount of surface and tropopause tracers transported vertically is larger in the coarse resolution models. In contrast to this, coarse model resolution leads to an enhanced inter-hemispheric transport in the stratosphere, except for the tropical stratosphere tracer, which shows a decrease in the meridional transport with increasing model resolution.

ERA40 data causes a slight reduction in the transport of surface tracers. About 10 – 15% reduction observed in the transport of tropopause tracers due to ERA40 data may be largely caused by the difference in the height of the tropopause calculated according to the WMO criteria. Whereas, ERA40 data leads to an increase of up to 10% in the transport of the stratosphere tracers. An interesting feature of the ERA40 data is the generation of the QBO at the tropical stratosphere, which can only be generated in the ECHAM5 middle-atmosphere configuration with at least 80 vertical levels according to Giorgetta et al. (2002). ERA40 meteorology also leads to the reduction of about 1 – 3% in the meridional transport of surface and tropopause tracers, except at the tropical tropopause, where transport is increased by about 2%. In contrast to its influence at the surface and the tropopause, ERA40 data increases the inter-hemispheric transport in the stratosphere by about 10 – 15% for transport from tropical region to both hemisphere and by about a factor of 2 for exchange between the N and S regions. ERA40 data increases the vertical transport of surface and tropopause tracers to the stratosphere by about a factor of 2.5. It also leads to an increase of stratosphere tracers transported to the surface by up to 70%. This is in agreement with findings in Van Noije et al. (2004).

The long-range inter-hemispheric transport between the northern and the southern hemisphere, and the inter-hemispheric transport of the stratosphere tracers are

most affected by the tracers' chemical lifetime. The surface and tropopause tracers with chemical lifetime of 50 months are well mixed, therefore the distribution within the three hemispheric regions vary by less than 7%, irrespective of their source regions, however, those emitted at the stratosphere show variations of up to 30%. The chemical lifetime of tracers not only affects the amount of tracers transported, but it also has a strong influence on the seasonal cycle of the tracers.

Using a simple box model, we have calculated the inter-hemispheric and vertical exchange time of our tracers. We found that it will take about 7 and 10 – 14 months for the surface tracer with source in southern and northern hemisphere respectively to be transported to the other hemisphere. These results are at the lower end of the inter-hemispheric exchange time of 1.5 – 1.7 years calculated from ^{85}Kr concentration by Levin and Hesshaimer (1996) with the use of a different two box model. We also calculate that the inter-hemispheric transport time of the stratosphere tracers are within the range of 8 – 10 years. Assuming that the tropopause is at 155 hPa, we calculate the cross-tropopause transport time of 35 and 56 months for surfN and surfS tracers respectively. Whereas, it will take only 17 days for the surface tropical tracer to get into the stratosphere. We also calculate that the stratosphere tracers cross-tropopause transport time is of the order of 5, 6 and 8 years for stratN, stratS and stratT tracers respectively. These results are very sensitive though to the assumed height of the tropopause level.

Chapter 6

The influence of African air pollution on regional and global tropospheric chemistry[1]

Abstract

We investigate the influence of African biomass burning, biogenic, lightning and anthropogenic emissions on the tropospheric ozone over Africa and globally using a coupled global chemistry climate model. Our model studies indicate that surface ozone concentration may rise by up to 50 ppbv in the burning region during the biomass burning seasons. Biogenic emissions yield between 5 ppbv and 30 ppbv increase in the near surface ozone concentration over tropical Africa. The impact of lightning on surface ozone is negligible, while anthropogenic emissions yield a maximum of 7 ppbv increase in the annual-mean surface ozone concentration over Nigeria, South Africa and Egypt. Our results show that biogenic emissions are the most important African emission source affecting total tropospheric ozone. The influence of each of the African emissions on the global tropospheric ozone burden (TOB) of 384Tg yields about 9.5 Tg, 19.6 Tg, 9.0 Tg and 4.7 Tg for biomass burning, biogenic, lightning and anthropogenic emissions emitted in Africa respectively. The impact of each of these emission categories on African TOB of 33 Tg is 2.5 Tg, 4.1 Tg, 1.75 Tg and 0.89 Tg respectively, which together represents about 28% of the total TOB calculated over Africa. Our model calculations also suggest that more than 70% of the tropospheric ozone produced by each of the African emissions is found outside the continent, thus exerting a noticeable influence on a large part of the tropical troposphere. Apart from the Atlantic and Indian Ocean, Latin America experiences the largest impact of African emissions, followed by Oceania, the Middle East, Southeast and south-central Asia, northern North America (i.e. the United States and Canada), Europe and north-central Asia, for all the emission categories.

[1]Published in *Atmos. Chem. Phys.*, **7**, 1193–1212, 2007, with M. G. Schultz and S. Rast as co-authors.

6.1 Introduction

Air pollution emitted in Africa comes from four sources, mainly biomass burning, natural emission from vegetation and soil, lightning NO_x emissions, and other anthropogenic sources – such as emissions related to the combustion of fossil-fuel for energy, industrial, transport and domestic uses. Africa contributes a significant amount to the global emissions from the first three categories, while emissions from fossil fuel combustion are important only on the regional scale. Emissions of trace species (e.g. CO, NOx, volatile organic compounds (VOCs)) significantly affect tropospheric chemistry and lead to the formation of tropospheric ozone, which influences the radiative forcing (e.g. Naik et al., 2005; Dentener et al., 2005).

African biomass burning activities, generally categorised as savanna, forest and agricultural waste burning, are driven by the "slash and burn" agricultural practices that take place during the dry seasons – late November to early March in the northern hemisphere (NH), and July to October in the southern hemispheric (SH) part of Africa (Marenco et al., 1990). African biomass burning contributes about 40% to trace species emitted by global biomass burning activities (Crutzen et al., 1979; Andreae, 1991; Helas et al., 1995a, Schultz et al., in review[2]), and exerts a large influence on tropospheric chemistry (Crutzen and Andreae, 1990; Andreae, 1993; Helas et al., 1992, 1995a; Marufu et al., 2000). Marufu et al. (2000) used a global chemistry transport model to test the sensitivity of tropospheric ozone over Africa to emissions from biomass burning from all over the world and found that about 16% of the 26 Tg tropospheric ozone burden (TOB) over Africa is due to these global biomass burning emissions.

Lightning produces NO_x, mostly in the middle to upper troposphere (Ridley et al., 1996; Pickering et al., 1996; Lamarque et al., 1996; Pickering et al., 1998; DeCaria et al., 2000), where it has a longer lifetime and greater ozone production potential than in the lower troposphere (Liu et al., 1987; Pickering et al., 1990). For example, DeCaria et al. (2005) calculated a photochemical ozone enhancement of about 10 ppbv 24 h after a storm observed during the Stratosphere-Troposphere Experiment: Radiation, Aerosols and Ozone (STERAO-A) using a 3-D cloud-scale chemistry transport model (CTM). The maximum lightning activity occurs in the tropics. However, tropical thunderstorms are the least well characterized, therefore, the uncertainty of tropical lightning NO_x is particularly large. Generally, the total contribution of lightning to the global NO_x budget is highly uncertain. Estimates range from 2–20 Tg (N) per year (Lawrence et al., 1995; Price et al., 1997; Huntrieser et al., 2002; Labrador et al., 2005). However, several studies published after 2000 have suggested an estimate closer to the lower limit. Huntrieser et al. (2002) estimated about 3 Tg (N) yr^{-1} from lightning NO_x based on detailed analysis of airborne NO_x measurements of European thunderstorms. Tie et al. (2001) and Martin et al. (2002) found that using a global lightning emission value of 7 Tg (N) yr^{-1} and

[2]Schultz, M. G., Heil, A., Hoelzemann, J. H., Spessa, A., Thonicke, K., Goldammer, J., Held, A. C., and Pereira, J. M.: Global Emissions from Wildland Fires in 1960 to 2000, Global Biogeochem. Cycles, in review.

$6\,\mathrm{Tg\,(N)\,yr^{-1}}$ respectively, their model simulations show reasonable agreement with airborne observations of reactive nitrogen species.

Vegetation emits a wide range of VOCs (Kesselmeier and Staudt, 1999). Among these biogenic VOCs, isoprene is one of the most important (e.g., Fehsenfeld et al., 1992; Guenther et al., 1995), followed by terpenes and methanol (CH_3OH). Estimates of global isoprene emissions vary between 200 Tg and 600 Tg (Kesselmeier and Staudt, 1999; Guenther et al., 2006, and references therein), of which Africa contributes about a fifth. Biogenic VOCs can have a significant impact on tropospheric chemistry as soon as they are released into the air, because of their high reactivity. They lead to the production (or destruction) of ozone in high (or low) NO_x conditions. Wang and Shallcross (2000) found an increase in surface ozone concentration of about 4 ppbv over the ocean and about 8 – 12 ppbv over the mid-latitude land areas when isoprene emissions were included in their 3-D model simulations. Using biogenic CH_3OH emissions of $117\,\mathrm{Tg\,(C)\,yr^{-1}}$, Tie et al. (2003) calculated an increase of about 3 – 4% in the tropical ozone at 300 hPa.

In this study we performed multi-year sensitivity calculations with a newly developed global chemistry climate model using the biomass burning, biogenic and anthropogenic emissions employed in the recent IPCC-ACCENT simulations in preparation for the fourth assessment report (e.g. see Stevenson et al., 2006; Shindell et al., 2006). The lightning NO_x emissions are calculated interactively within our model. These sensitivity studies are used to investigate the regional and global influence of each of the African emissions on primary and secondary tropospheric trace species concentrations. In particular, we focus on tropospheric ozone produced from the photochemical reactions involving precursors emitted in Africa. Tropospheric ozone is a greenhouse gas (Wang et al., 1980; Hansen et al., 2002), high ozone concentrations in the air affect human health (e.g. Peden, 2001; Desqueyroux et al., 2002; Mortimer et al., 2002) and damage vegetation, including agricultural crops (e.g. Mauzerall and Wang, 2001; Oksanen and Holopainen, 2001).

A description of the model set-up, the simulation experiments and the emissions used are given in Section 6.2. The relative influence of African emissions on the ozone concentrations over six African cities is presented in Section 6.3. The results of the sensitivity experiments are discussed in Sections 6.4 through 6.7, including the discussions on seasonality and inter-annual variability in Sections 6.6 and 6.7 respectively. We present the uncertainties in our results in Section 6.8, while the conclusions and a summary are given in Section 6.9.

6.2 Model set-up

The global chemistry climate model ECHAM5-MOZ, which is described and evaluated in Chapters 2 and 4 respectively, is employed in this study. This section describes the simulations performed in this study and the emission fields.

6.2.1 Model simulations

The model experiments follow the general setup for the IPCC-ACCENT intercomparison experiment (Stevenson et al., 2006). The experiments were run for present-day climate and emissions. The climate conditions (sea surface temperatures and sea ice fields) were taken from six consecutive years of coupled ocean-atmosphere simulations performed at the Max Planck Institute for Meteorology, Hamburg in the framework of the fourth IPCC assessment report (Roeckner et al., 2006). Present-day constant concentrations of 1760 ppbv, 367 ppm and 316 ppbv were maintained for CH_4, CO_2 and N_2O respectively.

ECHAM5 model climate simulations give better results at higher spatial resolutions (Roeckner et al., 2006). Specifically, T42L19 and T63L31 have a particularly good balance between computational costs and quality of the results. However, the sensitivity of tracers' transport in ECHAM5 discussed in Chapter 5 shows that the simulated transport of tracers in T42L31 is significantly different from that in T42L19, but comparable to that in the computationally more expensive T63L31 resolution. Each experiment in this study was therefore performed in the T42L31 resolution for 5 years (1997–2001) after a spin-up of 6 months.

We performed one reference experiment and 4 sensitivity experiments. The reference experiment includes all the emissions, while in each of the sensitivity experiments, we switch off one of the following emission categories over the African continent: biomass burning, biogenic, lightning, or anthropogenic emissions, respectively. The differences between the reference and the sensitivity experiments therefore show the impact of each of the African emissions.

We are aware that setting an emission source to zero affects the lifetime of other trace species in the troposphere. Nevertheless, this approach provides a relatively uncomplicated method in assessing the potential impact of these different emission types. Also, the method has the advantage that the combined effect of different species (e.g CO, NO_x and NMVOC) from the same emission category (e.g biomass burning) on the overall tropospheric chemistry can be assessed. The methane lifetime (average of 7.1 years based on 150 ppbv ozone-threshold tropopause) shows a small increase of about 13, 35 and 50 days in the experiment without anthropogenic, biomass burning and lightning emissions respectively, when compared to the reference experiment, while in the experiment where biogenic emissions are switched off, it decreases by only 32 days.

6.2.2 Emissions

The ECHAM5-MOZ model needs gridded emission data for emissions that are not calculated interactively. The lightning emissions are calculated from the interactive lightning parameterisation in ECHAM5-MOZ as discussed in Sect. 2.2.2. This parameterisation yields global lightning emissions of about 2.7 Tg (N)/yr in ECHAM5-MOZ. Over Africa, total lightning emissions are about 0.7 Tg (N)/yr. Other emissions used for this study are prescribed and identical to those used in the IPCC-

ACCENT experiment (Stevenson et al., 2006).

The prescribed emissions such as biomass burning (this includes all open fires such as savanna, forest, and agricultural burning), aircraft, soil emissions, biogenic and other anthropogenic emissions (such as fossil-fuel combustion by the domestic, transport and industrial sector) are supplied to ECHAM5-MOZ model as monthly-mean globally gridded files. They are injected into the model at various model heights.

These prescribed emissions data sets are a combination of emission inventories of the Institute for Applied System Analysis (IIASA), the Global Emissions Inventory Activity (GEIA), the Global Fire Emissions Database (GFED) version 1 (Randerson et al., 2005) and the Emissions Database for Global Atmospheric Research (EDGAR) version 3.2 (Olivier et al., 1999).

Anthropogenic CO, NO_x and NMHC emissions such as domestic, industrial, road transport, off-road and power-plants fossil-fuel combustion and gas flaring are as calculated by the IIASA global version of the Regional Air Pollution Information and Simulation (RAINS) model (Amann et al., 1999) for the year 2000. The international shipping CO, NO_x and NMHC emissions are based on the EDGAR3.2 global emission inventory (Olivier et al., 1999), while aircraft NO_x emissions are specified according to the IPCC special report on Aviation and the Global Atmosphere (IPCC, 1999).

The biomass burning emissions, which include savanna, forest fires, deforestation fires, and agricultural waste burning are from the GFED version 1 (Randerson et al., 2005) database available at http://daac.ornl.gov/. For the simulations, we use the 1997 – 2002 average data. Ocean CO emissions are from the GEIA database (see Horowitz et al., 2003).

The biogenic VOC emissions from vegetation are based on the global model of natural VOC contributed to the GEIA activity by Guenther et al. (1995). The soil CO, H_2 and NO_x emissions are also from the GEIA database (see Horowitz et al., 2003). The global biogenic emissions are $756\,\mathrm{Tg\,(C)\,yr^{-1}}$, $68\,\mathrm{Tg\,(C)\,yr^{-1}}$, and $8\,\mathrm{Tg\,(N)\,yr^{-1}}$ for non-methane VOCs (NMVOC), CO and NO_x respectively. Isoprene, terpenes and methanol account for about 68%, 17% and 11% of the biogenic NMVOC respectively.

Table 6.1 lists the global CO, NO_x and NMVOC emissions by source used in this study, and the amount contributed by African emissions are included as the percentages of the global emissions. It also contains the comparison of our emissions to those of Marufu et al. (2000). Our biogenic emissions are about twice as high as those of Marufu et al. (2000), while others are comparable.

Table 6.1— Global trace gas emissions by source used in this study and contribution from the African continent in parenthesis.

Source	CO (Tg (C)/yr)	NMHC (Tg (C)/yr)	NO_x (Tg (N)/yr)
Industrial	201 (16%)	66 (14%)	28.0 (5%)
Biomass burning	217 (43%)	19 (42%)	10.0 (46%)
Biogenic	69 (20%)	756 (25%)	8.0 (30%)
Lightning	–	–	2.7 (26%)
Aircraft	–	–	0.7 (4%)
Ocean	9 (–)	4 (–)	–
Total	496 (28%)	845 (24%)	49.4 (18%)
Marufu et al. (2000)	482 (23%)	534 (23%)	40.0 (18 %)

6.3 The influence of African emissions on the ozone concentrations over some African stations

The influence of African emissions on the ozone concentrations over some African cities is presented in this Section. These cities include Cairo (Egypt), Abidjan (Cote d'Ivoire), Lagos (Nigeria), Brazzaville (Congo), Windhoek (Namibia) and Johannesburg (South Africa). The evaluation of the ozone concentrations over these cities has been discussed in Chapter 4.

The red lines in Fig. 6.1 show that the biomass-burning precursors emitted over western Africa lead to an ozone enhancement over central Africa in DJF, as shown by the ozone profile over Brazzaville. Figure 6.1 also shows the reverse influence of central-African biomass burning on west-African ozone in JJA, but at a lesser amount (Abidjan and Lagos). This feature has previously been found by backward trajectories calculated in Sauvage et al. (2005).

Figure 6.1 shows that African emissions have insignificant influence over Cairo. In November – April, lower tropospheric ozone concentrations over Johannesburg are most sensitive to biogenic and anthropogenic emissions. At all stations except Cairo, we see a significant influence of biogenic and lightning emissions on upper tropospheric ozone concentration, especially during the wet seasons.

6.4 The effect of African emissions on surface ozone

We discuss surface ozone concentration due to photochemical reactions involving African emissions in this section. The impact on the surface ozone is important because this provides the quantification of the direct impact on humans and vegetation.

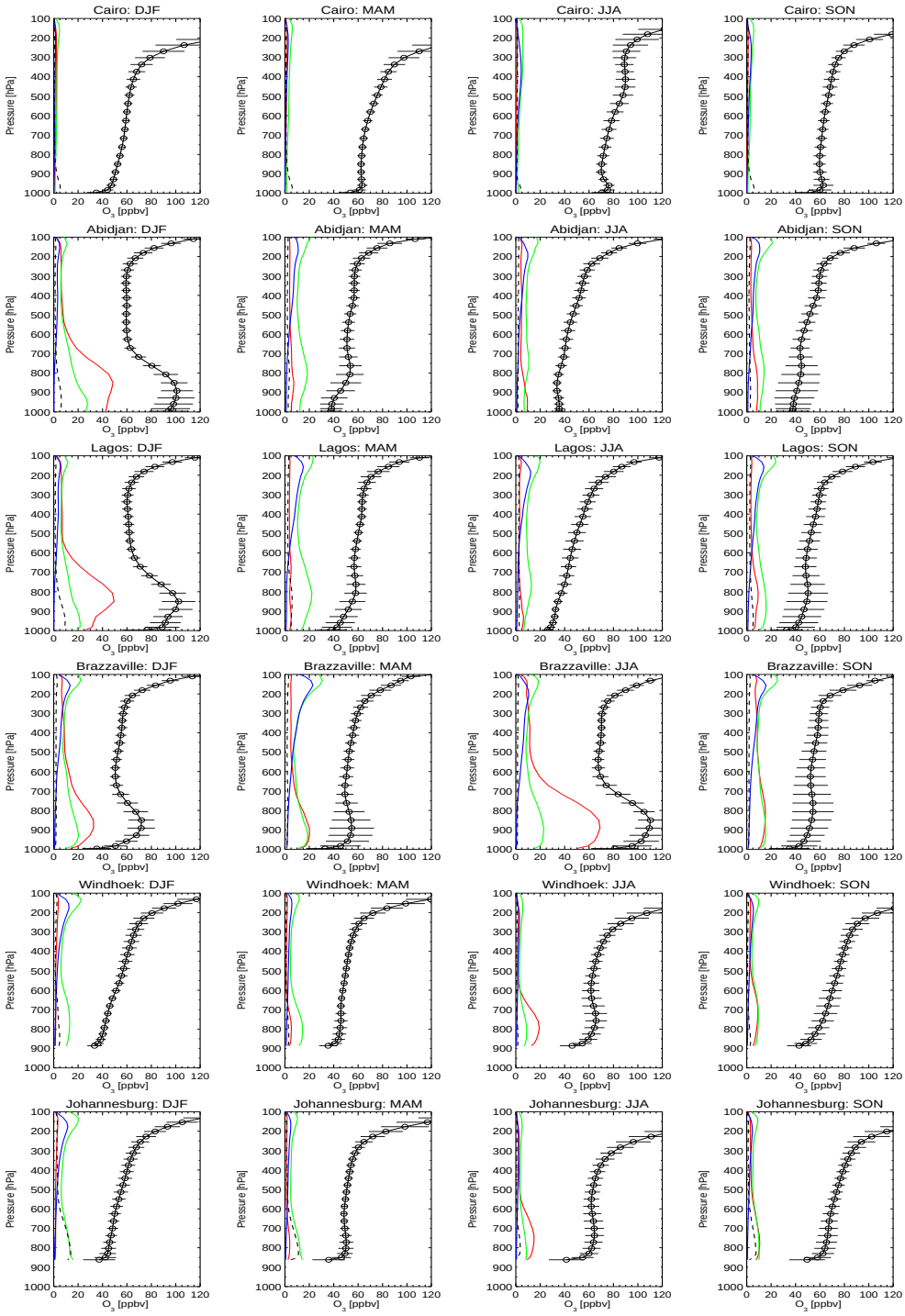

Figure 6.1— The 5-year mean model simulated ozone concentrations (open circles with line) over Cairo (Egypt), Abidjan (Cote d'Ivoire), Lagos (Nigeria), Brazzaville (Congo), Windhoek (Namibia) and Johannesburg (South Africa) in DJF, MAM, JJA, and SON, including the ozone enhancement due to each of the African emissions: biomass burning (red lines), biogenic (green lines), lightning (blue lines) and anthropogenic (dashed-black lines). The red, green, blue and dashed-black lines represent the difference of ozone between the reference and the sensitivity experiments.

The effect of African biomass burning, biogenic and anthropogenic emissions on surface ozone is shown in Figs. 6.2, 6.3 and 6.4 respectively. The figures show the difference in the simulated surface ozone concentrations between the reference experiment and the experiment where each of the emission types was excluded. Lightning has a small impact on surface ozone concentration, and only accounts for a maximum of 1 ppbv over a small area in Africa, and is therefore not presented.

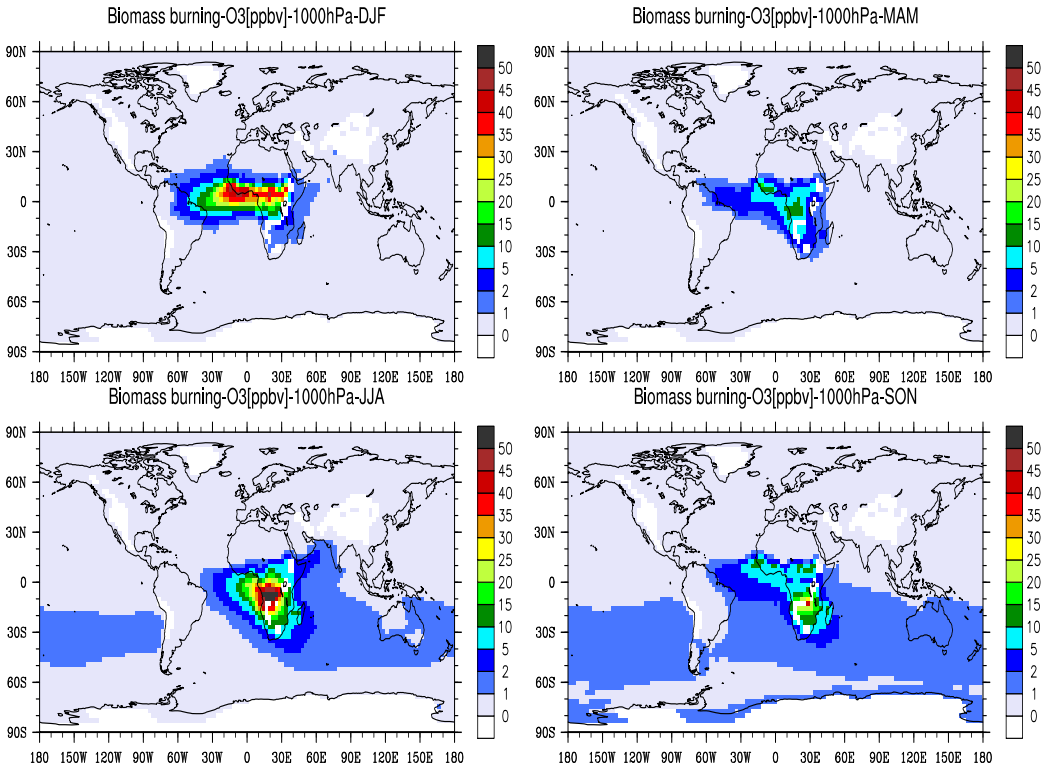

Figure 6.2— The influence of African biomass burning on 5-year of the surface ozone concentrations in DJF, MAM, JJA and SON. The figures show the difference between the reference experiment and the experiment where biomass burning emissions are excluded.

The enhancement of the surface ozone concentrations during the biomass burning seasons (DJF and JJA) generally lies between 10–50 ppbv at the burning region (Fig. 6.2), but can reach 60 ppbv in JJA over large parts of Democratic Republic of Congo and Angola. In DJF, there is a significant enhancement of the surface ozone concentrations over the equatorial Atlantic, reaching farther to the north-eastern part of Brazil. About 1–2 ppbv surface ozone increase due to African biomass burning emissions in JJA as well as September to November (SON), can be found over the southern Atlantic, Indian and Pacific oceans.

The influence of biogenic emissions on surface ozone concentration over Africa is lower than that of biomass burning emissions in DJF and JJA (Fig. 6.3) in the burning regions. The highest enhancement during these 2 seasons is about 30 ppbv.

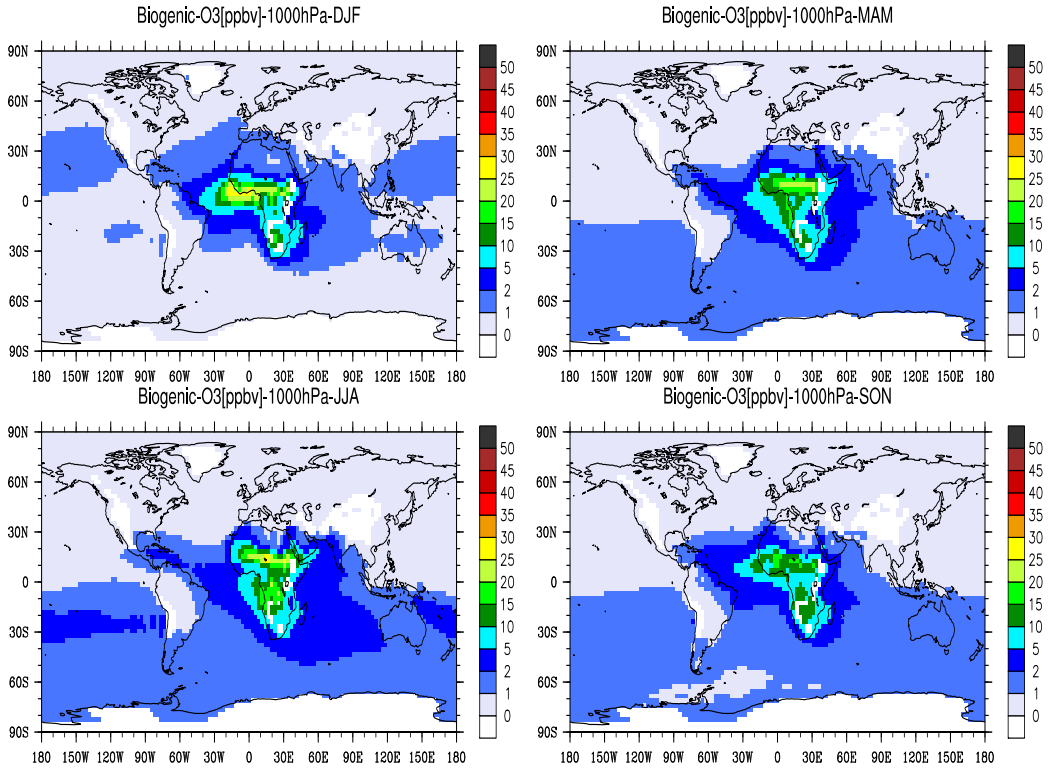

Figure 6.3— The influence of African biogenic emissions on 5-year of the surface ozone concentrations in DJF, MAM, JJA and SON. The figures show the difference between the reference experiment and the experiment where biogenic emissions are excluded.

However, while biomass burning surface ozone enhancement is confined to SH Africa in JJA, the influence of biogenic emissions covers both hemispheres. African biogenic emissions enhance the SH ocean surface ozone concentration by about 1–2 ppbv in all season.

The surface ozone produced by African anthropogenic emissions (Fig. 6.4) shows that Nigeria, South-Africa and Egypt are the countries mainly affected by anthropogenic emissions (up to 10 ppbv). These three countries together account for about 35%, 53% and 37% of the total African anthropogenic CO, NO_x and NMHC emissions respectively. This effect therefore corresponds to the relatively high contribution of these countries to the anthropogenic emissions.

The relative importance of each of the African emission categories to surface ozone concentration over Africa thus depends on the season and the location. For example, biomass burning emissions have the largest influence in the burning regions during the dry season. Whereas, over most of the Saharan desert (i.e. north of Sahel), the surface ozone concentration is enhanced mainly by anthropogenic and biogenic emissions.

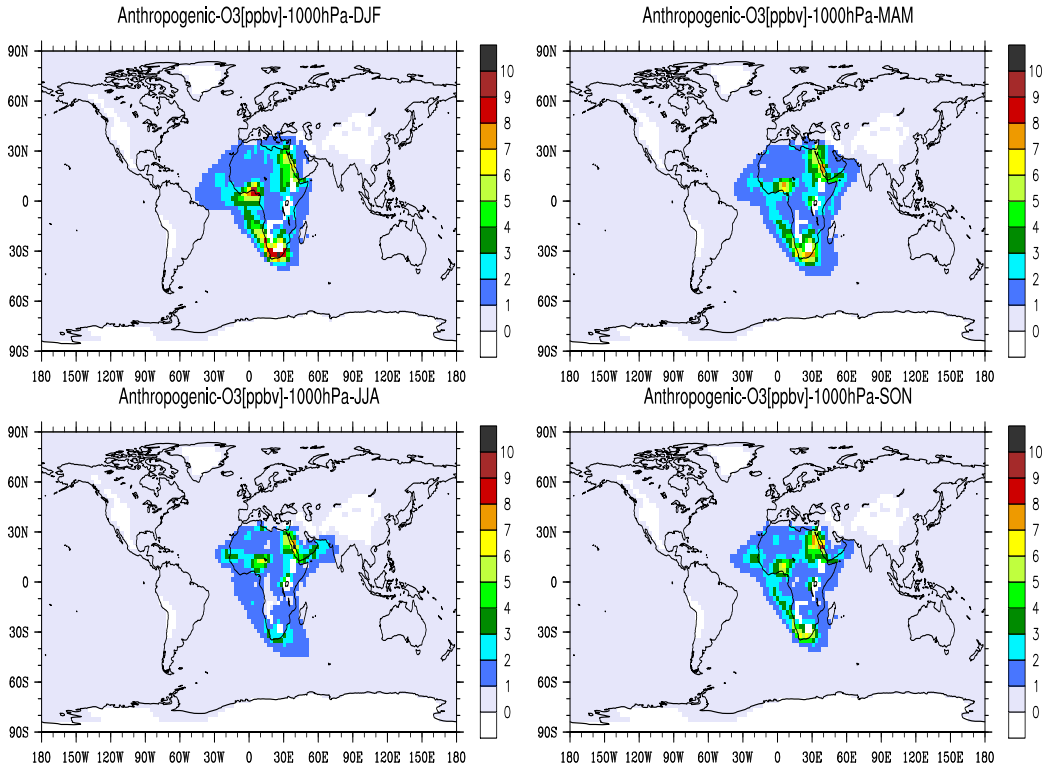

Figure 6.4— The influence of African anthropogenic emissions on 5-year of the surface ozone concentrations in DJF, MAM, JJA and SON. The figures show the difference between the reference experiment and the experiment where anthropogenic emissions are excluded. Note that the scale is reduced from those of Figs. 6.2 and 6.3.

6.5 The influence of African emissions on tropospheric ozone burden

We discuss the influence of African emissions on total tropospheric ozone burden (TOB) over Africa, globally and over other continental regions, in this section. The estimate of the TOB quantifies the impact of each of the African emission on the entire troposphere.

We calculate the burden m_s of a species s in any three-dimensional subdomain $\mathbb{D}$ of the atmosphere describing a particular region, e.g. troposphere over Africa, as:

$$m_s = \sum_j \frac{\Delta P(j)\, A(j)}{g}\, \gamma_s(j)\, \chi_{\mathbb{D}}(j) \tag{6.1}$$

where

$\Delta P(j)$: absolute values of the difference between the pressure at the upper and lower boundary of the grid box j
$A(j)$: area of grid box j
g : earth acceleration
$\gamma_s(j)$: mass mixing ratio of species s in grid box j
$\chi_{\mathbb{D}}(j)$: characteristics function of subdomain $\mathbb{D}$. It is 1 if the grid box j lies in $\mathbb{D}$, otherwise it is 0.

For the purpose of this study, the tropopause is defined as the pressure level at which the ozone concentrations are greater than or equal to 150 ppbv. The TOB discussed in this section and in subsequent sections are calculated using Eqn. (6.1).

The TOB calculated from the reference experiment for various world regions are shown in the last column of Table 6.2. Our estimate of 33 Tg TOB over Africa is higher than the 26 Tg reported by Marufu et al. (2000) using the Tracer Model version 3 (TM3), mostly due to the dry season overestimation of lower tropospheric ozone concentration in ECHAM5-MOZ.

The net influence of each of the African emissions on the regional and global TOB is shown in columns 2 through 5 of Table 6.2. African biomass burning, biogenic, lightning and anthropogenic emissions account for about 9.5 Tg, 19.6 Tg, 8.0 Tg and 4.7 Tg of the global TOB respectively. Over Africa itself, the net influence of each of these emission types is only 2.5 Tg, 4.1 Tg, 1.75 Tg and 0.9 Tg respectively. This indicates that more than 70% of the tropospheric ozone produced by photochemical reactions involving African emissions is found outside the continent due to the transport of precursor species and ozone itself. The largest ozone enhancement is confined to the south Atlantic and Indian oceans. Our calculated value of 9.5 Tg of ozone due to African biomass burning emissions is in good agreement with the 10 Tg suggested in a marked tracer experiment described in Marufu et al. (2000).

Figure 6.5 shows the vertical profiles of the zonal average ozone concentrations produced by African biomass burning, biogenic and lightning emissions as the difference between our reference run and the respective sensitivity simulation. Note that the highest ozone enhancement due to biomass burning occurs in DJF and JJA, while it occurs in MAM and SON for biogenic and lightning emissions. The plots show 5-year averages. The impact of African lightning emission on ozone production is highest at the middle to the upper troposphere (as shown in the right column of Fig. 6.5).

A striking feature in Fig. 6.5 (middle column) is that although biogenic emissions are released into the troposphere at the top of the vegetation canopy (as in the case of biogenic NMVOC) and at the surface (as in the case of soil emissions), relatively large ozone increases are seen in the upper troposphere (between 300 hPa and 100 hPa). This may be due to the combined effect of strong convective activity in the main source region of the emissions (Collins et al., 1999; Lawrence et al., 2003; von Kuhlmann et al., 2004), the transport of biogenic NMVOC with relatively long chemical lifetime, such as methanol (Tie et al., 2003), and the effective storage

Table 6.2— African emissions influence on the tropospheric ozone burden ($Tg\,O_3$) of various geographical land regions. The results are the difference of the 5-year averages from the base run and the sensitivity runs where each of the emission sources were switched off one at a time.

Region	Biomass burning	Biogenic	Lightning	Anthropogenic	Tropospheric O_3 burden
Africa	2.50	4.07	1.75	0.89	33.14
East Asia[a]	0.12	0.31	0.15	0.09	11.33
Europe	0.09	0.24	0.09	0.09	14.25
Latin America[b]	0.43	1.00	0.48	0.20	23.95
Middle East[c]	0.20	0.53	0.24	0.18	11.89
North-central Asia[d]	0.08	0.20	0.08	0.08	14.52
Oceania[e]	0.26	0.57	0.30	0.14	9.99
South-central Asia[f]	0.14	0.33	0.18	0.08	7.25
Southeast Asia[g]	0.18	0.43	0.25	0.08	9.78
United States and Canada	0.14	0.34	0.14	0.10	20.57
Global	9.52	19.59	8.06	4.67	384.32

[a] China, Hong Kong, Japan, Democratic peoples Republic of Korea, Republic of Korea, Macau and Taiwan.
[b] South America, Mexico and the Caribbean Islands.
[c] Middle East countries include the western part of Afghanistan, Bahrain, Cyprus, Gaza strip, Iran, Iraq, Israel, Jordan, Kazakhstan, Kuwait, Kyrgyzstan, Lebanon, Oman, Pakistan, Qatar, Saudi Arabia, Syrian Arab republic, Turkey, Turkmenistan, United Arab Emirates, Uzbekistan, West Bank and Yemen.
[d] Russia Federation and Mongolia.
[e] Australia, New Zealand, Fijis, French Polynesia, Guam, New Caledonia, Niue, Samoa and Vanuatu.
[f] South-central Asia consists of India, Pakistan, Bangladesh, Sri-Lanka, Nepal, Maldives, Kashmir, Bhutan and the eastern Afghanistan.
[g] Southeast Asia consists of Brunei, Cambodia, East timor, Laos, Vietnam, French Indo-China, Indonesia, Malaysia, Myanmar, Papua New Guinea, Philippines, Singapore, Thailand.

of NO_x as peroxy acetyl nitrate (PAN) (Fig. 6.6). Upon sinking of air masses containing these compounds, PAN is thermally decomposed and it releases NO_x and peroxy radicals, which contribute to ozone formation. Figure 6.6 also shows a relatively higher CO concentration enhancement in the middle to upper troposphere from biogenic emissions than biomass burning emissions.

In order to estimate the direct effect of African biogenic CH_3OH, isoprene and terpene emissions on these concentration enhancements, we performed 3 additional sensitivity experiments for 1 year after a spin-up period of 6 months. In each of these experiments, we exclude only one of these emissions, respectively. Together, these emissions account for 96% of the biogenic NMVOC used for this study. The results show that a maximum of 65% and 15% of the upper troposphere (UT) ozone en-

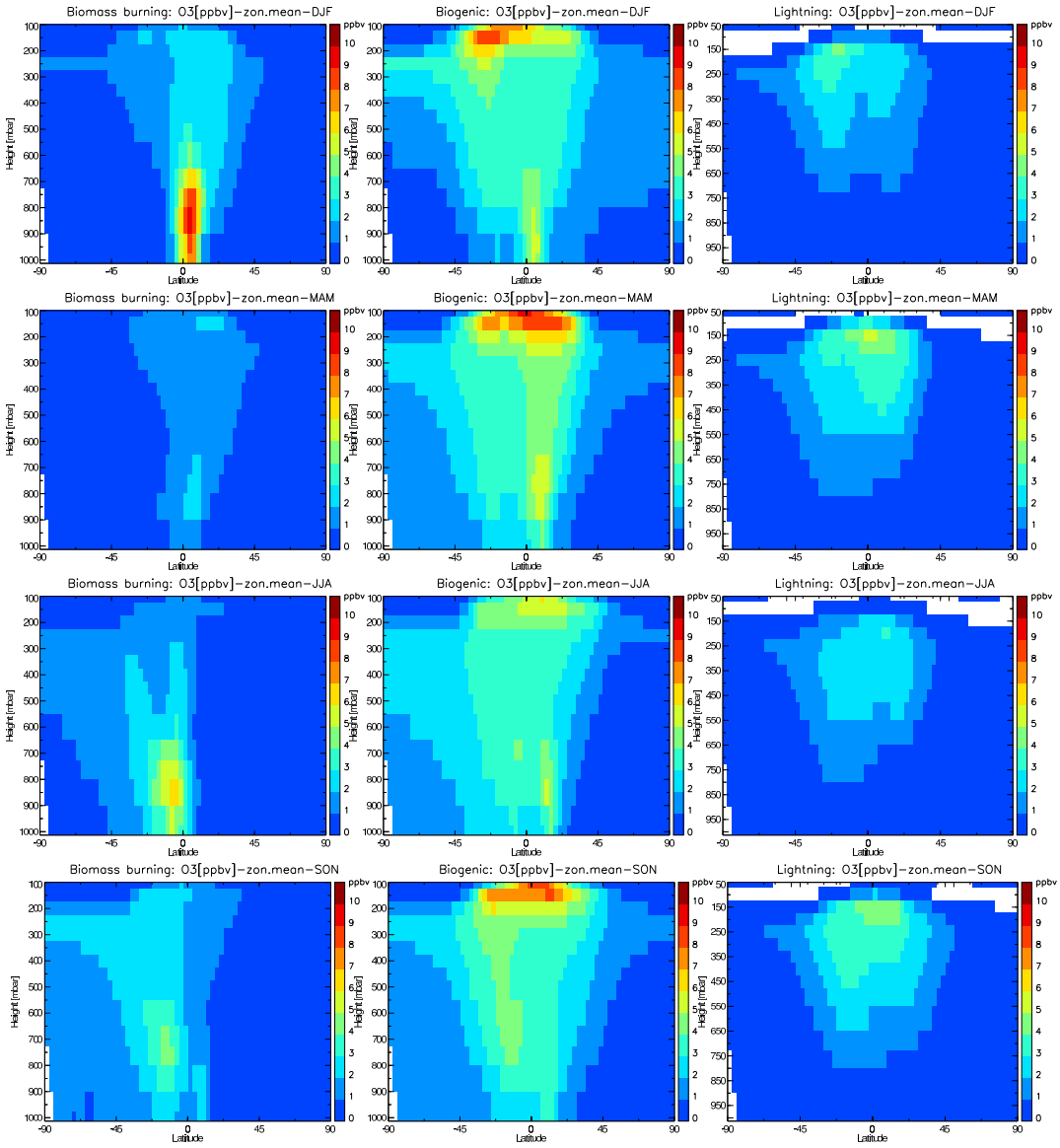

Figure 6.5— 5-year zonal average of the ozone concentration (ppbv) produced by African biomass burning (first column), biogenic (second column) and lightning (third column) emissions in all seasons. Note that the highest ozone enhancement due to biomass burning occurs in DJF and JJA, while it is MAM and SON for biogenic and lightning emissions.

hancement are due to African isoprene and biogenic CH_3OH emissions, whereas the influence of terpenes is negligible. Therefore, the combined effect of the convective transport of biogenic methanol and isoprene, and their reaction products increases the UT ozone (Tie et al., 2003; Doherty et al., 2005).

Globally and over the continental regions outside Africa, the influence of African biogenic emissions on the tropospheric ozone burden is about two times that of biomass burning (as shown in Table 6.2), making them the most important African

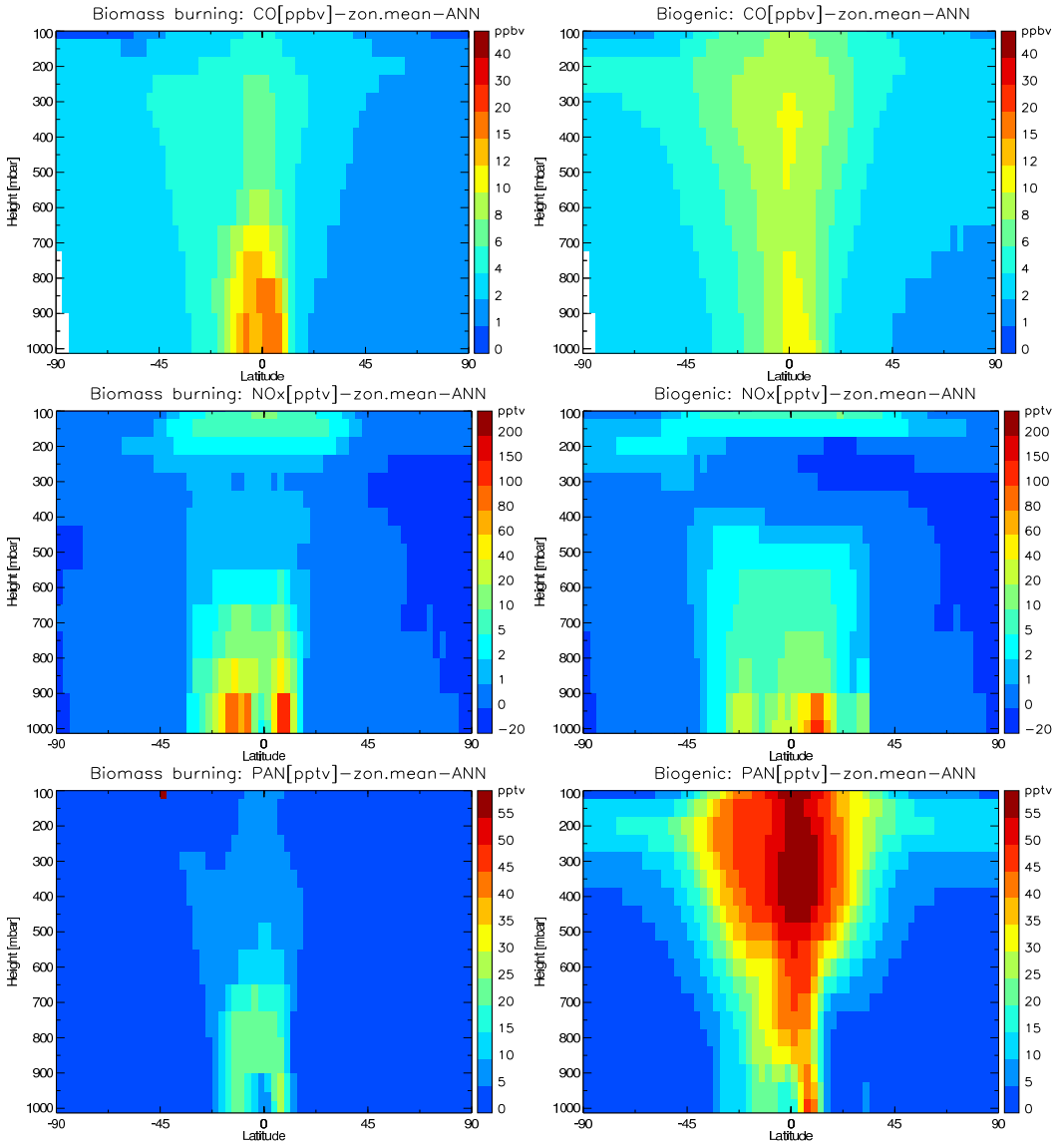

Figure 6.6— 5-year zonal average of the CO (top row), NO_x (middle row) and peroxy acetyl nitrate (PAN, bottom row) concentrations produced by African biomass burning (left column) and biogenic (right column) emissions.

emissions category. This is due to the biogenic emissions enhancement of the ozone concentration in the middle to the upper troposphere (Fig 6.5), where ozone and ozone precursors are easily transported over large distances. The largest influence of each of the African emission categories on TOB of other continental regions occurs in Latin America, followed by Oceania, the Middle East, Southeast and South-central Asia, the United States and Canada, Europe and North-central Asia (Table 6.2).

6.6 Seasonality of the influence of African emissions on regional and global tropospheric ozone burden

6.6.1 Africa

In Fig. 6.7a, we show the seasonal variation of the impact of African emissions on the TOB over Africa. The seasonal variation of the tropospheric ozone burden produced by African biomass burning emissions (red line) shows two peaks. The first peak occurs between December and February, while the second peak occurs in July, with a spread from June to September. This seasonality shows a high correlation with biomass burning emissions (r=0.85, 0.88 and 0.93 for biomass burning NMHC, CO and NO_x respectively), reflecting the DJF and JJA burning seasons in the NH and SH parts of Africa, respectively. During these peaks, the influence of African biomass burning emissions on African TOB is about 3.4 Tg in January and 3.0 Tg in July.

The seasonal variation in African TOB due to African biogenic emissions also show a peak in May (green line in Fig. 6.7a) reaching 4.8 Tg. Lightning emissions over Africa yield the maximum influence on the tropospheric ozone production over the continent in two major seasons: March through May, and September through October; accounting for about 2.1 Tg respectively (blue line in Fig. 6.7a).

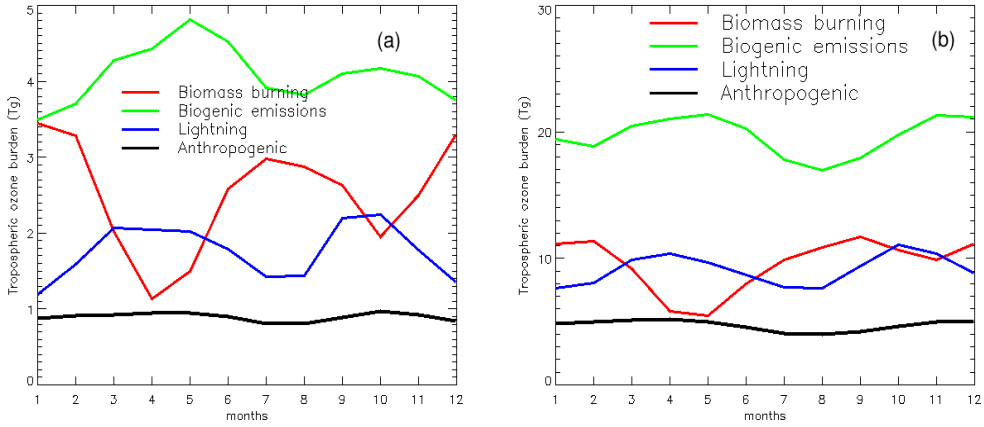

Figure 6.7— The influence of African emissions on (a) African and (b) global tropospheric ozone burden ($Tg\,O_3$). Figure shows 5-year average. Note the difference in the scales.

6.6.2 Global

As shown in Fig. 6.7, African and global TOB is most sensitive to biogenic emissions in all seasons. The two months of maximum influence of biogenic emissions on global TOB are May and November, when they account for a net TOB of 21 Tg. The highest isoprene emissions over Africa occur in April and October, while those of terpenes and biogenic CH_3OH occur in May and October. The seasonal variation

of the global TOB produced by African biomass burning (red line in Fig. 6.7b) shows two peaks in December through February and in September. The maximum values are about 11.5 Tg and 12 Tg, in February and September respectively. African lightning emissions yield their maximum influence on global TOB in April and October. During these months, their impact can be up to 10 Tg and 11 Tg, respectively. As shown by the black lines in Fig. 6.7, the TOB produced by African anthropogenic emissions show a small seasonal variation.

6.6.3 Other continental world regions

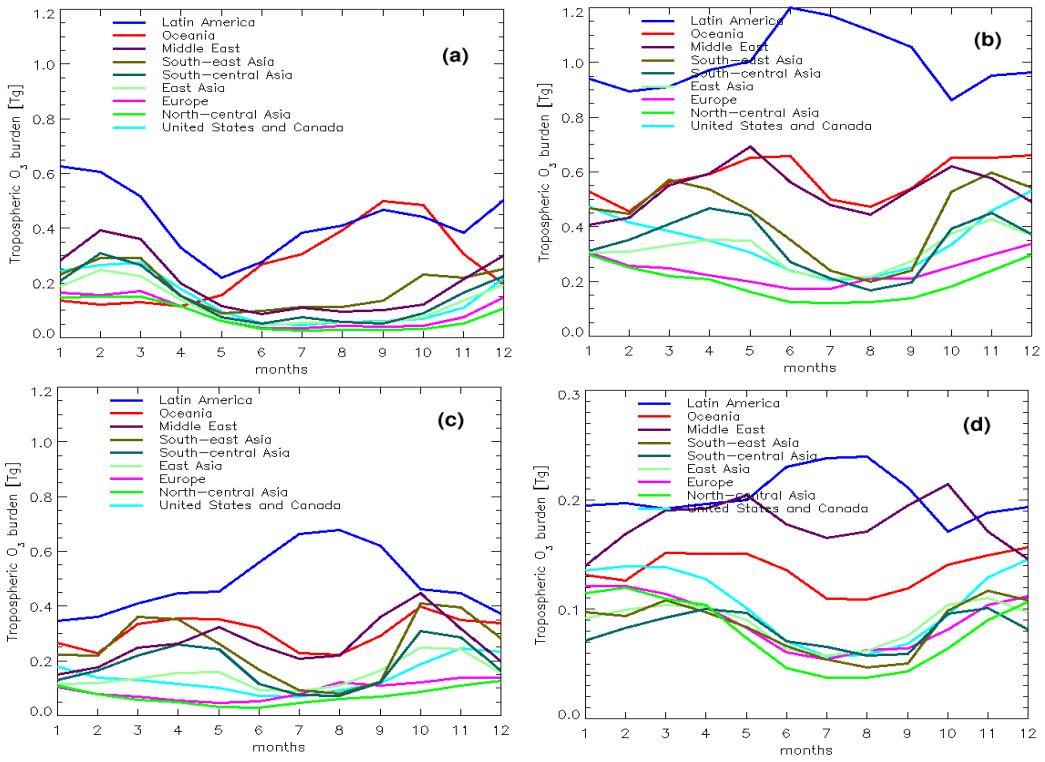

Figure 6.8— Seasonal variation of the influence of African (a) biomass burning, (b) biogenic, (c) lightning and (d) anthropogenic emissions on tropospheric ozone burden ($Tg\,O_3$) of different regions of the world. Note the different scales.

Figure 6.8 shows the seasonal variation of the influence of African biomass burning, biogenic, lightning and anthropogenic emissions on the TOB over various geographical land regions.

Fig. 6.8a reveals that the maximum influence of biomass burning emissions occurs in December – March except over Oceania, where the maximum influence occurs in September – October. The influence of Africa biomass burning experienced in Oceania is due to burning occurring at the southern hemispheric part of Africa.

The figure also shows that only Latin America is influenced by burning from both hemispheres of Africa.

The maximum influence of biogenic, lightning and anthropogenic emissions on TOB over all regions generally occurs in March – June and September – December, except over Latin America, where these emissions have their largest influence on the TOB in June – September (as shown in Fig. 6.8b, c and d respectively). The tropospheric ozone enhancement due to each of the Africa emissions in East Asia, Europe, north-central Asia and north northern America (i.e. United states and Canada) are less than 0.5 Tg in all seasons.

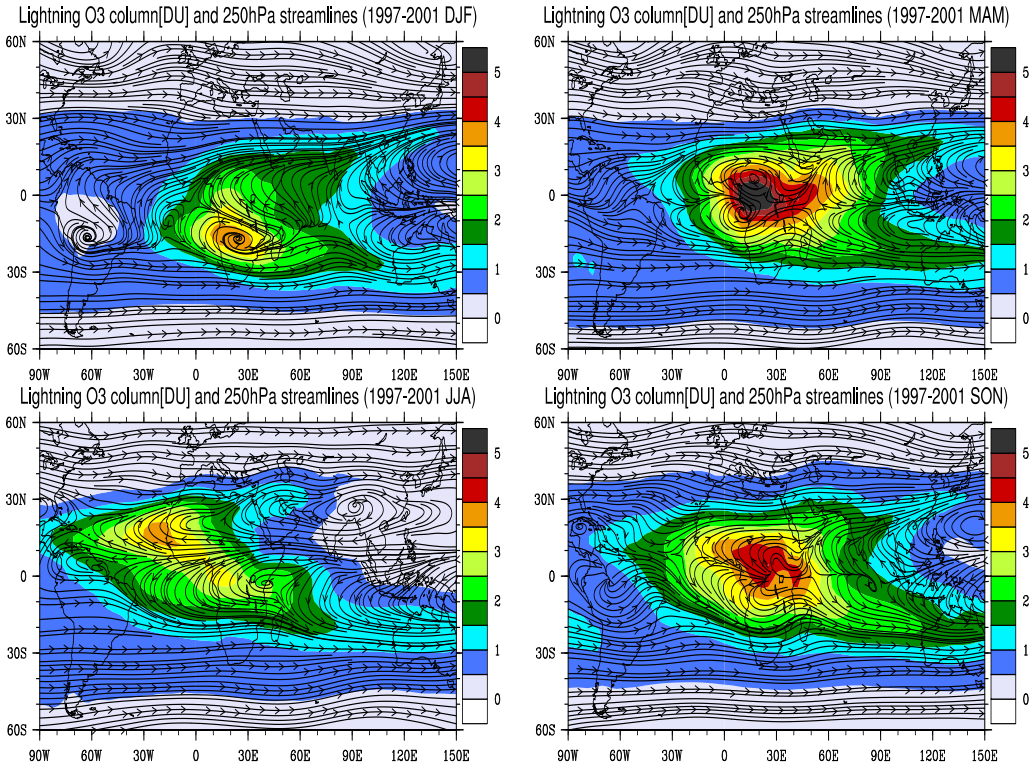

Figure 6.9— 1997 – 2001 average tropospheric ozone column (DU) produced by Africa lightning NO_x emissions in DJF, MAM, JJA and SON; overlaid with streamlines at 250 hPa during the same seasons. The streamlines is generated by the u and v wind vectors of our reference simulations. The tropospheric ozone column is the difference of the ozone column between the reference simulation and the simulation without African lightning emissions.

These seasonalities reveal the combination of seasonal variation in emissions and a seasonal shift in transport pathways out of the emission source regions. This is demonstrated in the example of Fig. 6.9, where the spatial distribution of the total tropospheric ozone column increase due to African lightning emissions corresponds to the transport pathways at 250 hPa in all seasons, as shown by the streamlines. The altitude of 250 hPa for the streamlines was chosen, because this is near the

region of maximum NO_x outflow in thunderstorms.

6.7 Inter-annual variability

Previous studies on the effect of African emissions on tropospheric ozone have always focused on one specific meteorological year. The authors are not aware of any study conducted over several years. Here we investigate the impact of changes in meteorology by analysing the inter-annual variability in our 5-years simulations. All emissions were held constant over the 5-years, but lightning emissions vary according to changes in convective activity.

Table 6.3— Inter-annual variability of the tropospheric ozone burden produced by each of the African emission categories. The entries show the mean absolute bias in percent for various geographical land regions.

Region	Biomass burning	Biogenic	Lightning	Anthropogenic
Africa	2.4	2.3	4.9	2.1
East Asia	6.9	3.4	6.4	3.7
Europe	5.6	3.0	5.5	6.4
Latin America	4.2	3.9	6.8	3.5
Middle East	6.6	4.8	4.9	0.4
North-central Asia	7.5	3.9	5.5	4.9
Oceania	3.9	2.9	6.4	1.9
South-Central Asia	6.1	2.8	4.5	1.3
Southeast Asia	16.2	12.5	18.8	11.2
United States and Canada	7.2	3.5	5.6	4.3
Global	3.0	2.0	5.9	2.0

We give the inter-annual variability calculated as the average deviation relative to the mean results in Table 6.3. Generally, the highest inter-annual variability (more than 11%) is calculated over southeast Asia, while the smallest inter-annual variability (less than 5%) is recorded over Africa for all the emission categories, for all other region, the inter-annual variability of the transport from Africa is less than 10%. Globally, the variability is about 3.0%, 2.0%, 5.9% and 2.0% for global tropospheric ozone burden generated by African biomass burning, biogenic, lightning and anthropogenic emissions respectively.

African emissions influence tropospheric ozone over Southeast Asia throughout the year, with maximum impact in March–April and October–December. This influence is dominated by biogenic and lightning emissions, which together account for about 77% of the TOB related to African emissions over Southeast Asia. The high inter-annual variability recorded over southeast Asia is driven by the particularly low and high transport from Africa to Southeast Asia in the third year and the fifth year

of our simulation period, which causes the TOB over Southeast Asia to be about 18–34% lower and 25–40% higher than the 5-year mean TOB, respectively. This decrease and increase in transport is connected with the cold and warm anomaly in the sea surface temperature in these years, respectively (see Fig. 6.10). This warm (or cold) anomaly has been shown to induce a weakening (or strengthening) of the tropical easterly jet (Palmer et al., 1992; Janicot et al., 2001). The analysis of the streamline anomaly (figures not shown) at 100 to 500 hPa reveals that the transport from Africa to Southeast Asia is enhanced (or reduced) when a warm (or cold) SST anomaly occurs.

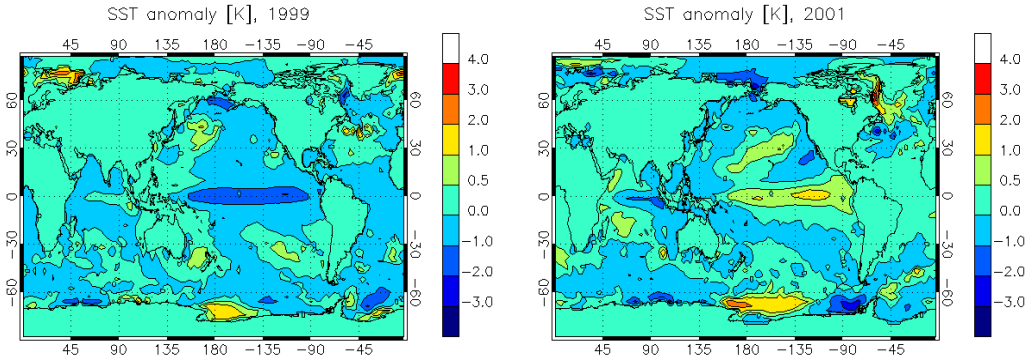

Figure 6.10— The sea surface temperature (SST) anomaly in the third and the fifth year of the simulation period, with respect to the 5-year average SST.

6.8 Uncertainties

Simulations of the global tropospheric ozone budget are still rather uncertain; nevertheless, most models show rather good consistency in simulating the response to emission changes (Stevenson et al., 2006). There are large uncertainties in emission estimates, and these uncertainties will influence our results both in terms of absolute values and with respect to the relative importance of emission source types. While we cannot give a thorough discussion of the uncertainties here, we will at least discuss the potential impact of emission uncertainties on our ozone budget calculations assuming a linear response for simplicity.

African biomass burning emissions are uncertain by about a factor of 2 (Schultz et al., 2006)[2]. Some of this uncertainty may be related to inter-annual variability of these emissions (e.g see, Barbosa et al., 1999), but since we do not take this variability into account in our model simulations, we can regard it as the uncertainty of the mean value here. Thus the influence of African biomass burning emissions on the global tropospheric ozone burden could range from 4.5 Tg (O_3) to 19 Tg (O_3).

The uncertainty of global isoprene emissions reported by Guenther et al. (2006) is about a factor of 3, and about the same uncertainty factor is noted for global methanol emissions in Tie et al. (2003). However, the uncertainty of the biogenic

emissions e.g. isoprene, for a specific location and time in Africa could be up to a factor of 5 (Guenther et al., 1999). Hence the influence of African biogenic emissions on global tropospheric ozone burden could range from 6.5 Tg (O_3) to 59 Tg (O_3).

The uncertainty of global lightning emissions has been briefly discussed in Sect. 6.1. While there is a growing consensus that the upper limit estimate of 20 Tg (N) yr^{-1} is likely too high (Lawrence et al., 1995; Labrador et al., 2005) , there still remains at least an uncertainty of a factor of 3. Our estimate of 2.7 Tg (N) yr^{-1} is closer to the lower limit. We therefore estimate the global tropospheric ozone burden related to African lightning NO_x source as 6 Tg (O_3)–30 Tg (O_3) for global lightning NO_x emissions ranging from 2 Tg (N) yr^{-1}–10 Tg (N) yr^{-1}.

Anthropogenic emissions are also uncertain by at least 30%, but regional uncertainties may be much larger, in particular for domestic burning. We estimate that the impact of African anthropogenic emissions on the global TOB may be between 3 and 6 Tg (O_3) yr^{-1}. All together, the influence of African emissions on the global TOB may range from 20 to 114 Tg (O_3)/yr (representing 5 – 30% of the global TOB).

6.9 Summary and conclusions

We have discussed the effect of African emissions, namely: biomass burning, biogenic, lightning and anthropogenic emissions on the tropospheric ozone over Africa and in other regions of the world, using the new 3-D global atmospheric chemistry model, ECHAM5-MOZ. We gave an overall description of the model and presented a model evaluation for the region around Africa by comparing the ozone and CO concentration calculated by ECHAM5-MOZ to measurements at various stations. Generally ECHAM5-MOZ captures the vertical and seasonal variation of the tropospheric ozone over Africa, except that it has some high biases and overestimates the dry seasons lower tropospheric ozone concentration by more than 30 ppbv. In all other months and at all locations, the ECHAM5-MOZ ozone bias is less than 30 ppbv everywhere in the troposphere up to 300 hPa. Interestingly, the ECHAM5-MOZ model confirms that biomass burning emissions occurring in West Africa in DJF cause lower tropospheric ozone enhancement in central Africa, with a reverse effect on western Africa during the central African burning season in JJA (Sauvage et al., 2005). ECHAM5-MOZ is also able to simulate the seasonal variation and magnitude of the surface CO concentration at all the stations discussed.

We have shown that African biomass burning emissions are responsible for regional surface ozone enhancement of about 10–50 ppbv close to the burning regions. This surface ozone enhancement can even be more than 50 ppbv over parts of central Africa (Democratic republic of Congo, Congo and Angola) during the JJA biomass burning season. Biogenic emissions increase the surface ozone concentration over Africa by about 5–30 ppbv. Lightning is shown to have an insignificant impact on surface ozone, but leads to the second largest impact on the middle to the upper tropospheric ozone concentration, next to biogenic emissions. The relative importance of biomass burning and biogenic emissions on the surface ozone concentration over

Africa is highly dependent on the season and the location. Biomass burning provides the largest impact on surface ozone concentration only during the burning seasons in the vicinity of the burning region. The Sahara desert surface ozone concentration is mainly influenced by anthropogenic and biogenic emissions.

Biogenic, biomass burning, lightning and anthropogenic emissions over Africa account for an increase of the net global tropospheric ozone burden of about 19.6 Tg (6.5 – 60 Tg), 9.5 Tg (4.5 – 19 Tg), 8.0 Tg (6 – 30 Tg), and 4.7 Tg (3 – 6 Tg) respectively. The influence of these emissions on the African tropospheric ozone burden is about 4.1 Tg, 2.5 Tg, 1.8 Tg and 0.9 Tg, respectively. Therefore, this study shows that more than 70% of the tropospheric ozone produced by each of the African emission categories is found outside the continent.

We have also estimated the impact of biogenic, biomass burning, lightning and anthropogenic emissions on the tropospheric ozone burden of various world regions. We found that for all emission categories, Latin America experiences the highest impact of African emissions, followed by Oceania, the Middle East, Southeast and South-central Asia. This is in effect due to the proximity of these regions to Africa. The tropospheric ozone over Canada, the United States, Northern Asia and Europe are only slightly affected by African emissions. This study shows a teleconnection of the sea surface temperature anomaly over the eastern tropical Pacific and the transport from Africa over the central Indian Ocean to Southeast Asia. Specifically, that warm (or cold) SST anomaly increases (or reduces) transport to South-eastern Asia due to the weakening (or strengthening) of the tropical easterly jet (Palmer et al., 1992; Janicot et al., 2001). In all continental regions outside of Africa, African biogenic emissions have the largest influence on the tropospheric ozone burden, followed by African lightning and biomass burning emissions.

This study presents a discussion of the main African emission categories and their influence on regional and global tropospheric ozone. An earlier study by Marufu et al. (2000) focused on the determination of the source of tropospheric ozone over Africa, with a priority given to biomass burning emissions. Interestingly, our estimate of 9.52 Tg due to African biomass burning emissions is comparable to the 10 Tg estimated by Marufu et al. (2000)

Chapter 7

Summary and Outlook

7.1 General summary

This study investigates the regional and global impact of air pollution emitted in Africa. It quantifies the magnitude and characterises the seasonality, the inter-annual variability and the dynamics of transport of primary and secondary air pollutants due to African emissions. Due to the global nature of pollution impact, the study is carried out with a global three-dimensional model (ECHAM5-MOZ), which encompasses a detailed general circulation model of the atmosphere and a chemistry transport model. Based on its combination of the full dynamics of the ECHAM5 GCM and the tropospheric chemistry of MOZART2, ECHAM5-MOZ provides a good model architecture for studying and assessing the global impact of emissions occurring at any given location, and it is one of the few existing models to allow for the assessment of climate-chemistry interactions.

The model have been evaluated with the MOZAIC ozone data over 18 cities and SHADOZ ozonesonde data at 11 stations, and NOAA/ESRL-GMD surface CO data at 9 locations, which provides a quasi-global coverage. The measurement data recorded in all stations were regridded to model vertical resolution in order to ensure a consistent comparison. Generally the ECHAM5-MOZ model captures the vertical profile and the seasonal variation of the tropospheric ozone in all months and over all the locations considered. The magnitude of the ozone concentrations calculated by the model also show good comparison with MOZAIC and SHADOZ data, and the model bias is generally less than 30 ppbv everywhere in the troposphere up to 300 hPa over all the stations considered. The only exceptions occur over Africa during the dry seasons, where the model shows some high biases much higher than 30 ppbv. Other exceptions are recorded at the surface to around 900 hPa over Delhi, India in March through November and over New York in June through August. During these months, the model bias ranges between 35 ppbv and 55 ppbv. The ECHAM5-MOZ model confirms that biomass burning emissions occurring in West Africa in DJF cause lower tropospheric ozone enhancement in central Africa, with a reverse effect on western Africa during the central African burning season in JJA (Sauvage et al., 2005). ECHAM5-MOZ is also able to simulate the seasonal variation

and magnitude of the surface CO concentration at all the stations discussed.

The MEGAN biogenic emissions implementation in the ECHAM5-MOZ model calculates the emission flux of isoprene, terpenes, carbon monoxide, methanol, acetaldehyde, formaldehyde, acetone, propene, ethane and ethene from vegetation. MEGAN estimates in the present-day climate yield a global emissions of 587 Tg(C)/yr for isoprene, 172 Tg(C)/yr for terpenes, 41 Tg(C)/yr for CO, 175 Tg(C)/yr for other non-terpene VOCs. The modification of isoprene emission factor, ε_i, over Australia and western USA resulted in the reduction of isoprene emission flux by 98.82 Tg(C)/yr compared to the present-day simulation. The effect of climate change in the year 2090s, leads to an increase in the global-mean temperature by about 2 K and 3 K in the SRES scenarios B1 and A2 respectively, leading to 131.89 Tg(C)/yr and 245.88 Tg(C)/yr rise in isoprene emissions, 42.46 Tg(C)/yr and 77.99 Tg(C)/yr increase in terpene emissions, and 53.10 Tg(C)/yr and 98.38 Tg(C)/yr increase in CO and other non-terpene VOCs, respectively. The increase of 165 Tg(C)/yr in isoprene emissions calculated by (Sanderson et al., 2003) in a fixed vegetation experiment, which employs the IS92a scenario of future-climate falls within the estimated increase in this study. However, because the experiments performed in this study do not account for the impact of climate change on vegetation types, their geographical distribution and density, they may overestimate the climate-related biogenic emission changes.

The influence of model resolution, ERA40 meteorology and the chemical lifetime on the inter-hemispheric exchange and vertical transport of tracers in ECHAM5 has been examined using 9 idealized tracers. Large differences occur when there is a change in the vertical resolution, or lifetime of the artificial tracers, or when the model is forced towards ERA40 meteorology, otherwise the tracers show rather similar transport pattern across the model resolutions considered (i.e. T21L19, T42L19, T42L31, T63L31 and T106L31). Transport increases in the finer resolution models and are mostly dependent on the number of vertical levels. One interesting result is that T42L31 behaviour is similar to the other 31-level vertical resolutions and could be a good representative of the 31-level models, although the ECHAM5 model climate simulations give better results at higher spatial resolutions (Roeckner et al., 2006). The use of ERA40 data only slightly affect the meridional and vertical transport of tracers at the surface and the tropopause, whereas it increases the inter-hemispheric and vertical transport of tracers in the stratosphere by about 10% – 150% and a factor of 2.5, respectively, in agreement with findings in Van Noije et al. (2004). The surface and tropopause tracers with chemical lifetime of 50 months are well mixed, therefore the distribution within the 3-latitudinal regions vary by less than 7%, irrespective of their source region, however, those emitted at the stratosphere show variations of up to 30%.

The transport time calculations based on a simple two box model show that it will take about 7 and 10 – 14 months for surface tracer in southern and northern hemisphere respectively to be transported to the other hemisphere. These results are at the lower end of the inter-hemispheric exchange time of 1.5 – 1.7 years calculated from ^{85}Kr concentration by Levin and Hesshaimer (1996) with the use of a different

two box model. The inter-hemispheric transport time of the stratosphere tracers are within the range of 8 – 10 years. If it is assumed that the tropopause is at 155 hPa, the cross-tropopause transport time of 35 and 56 months were calculated for surface tracers in the northern and southern hemisphere, respectively, and only 17 days for tropical tracers at the surface to cross the tropopause. The stratosphere tracers cross-tropopause transport time is of the order of 5, 6 and 8 years for the northern, southern and tropical tracers respectively. These results are very sensitive though to the assumed height of the tropopause level.

The sensitivity of the global tropospheric chemistry to biomass burning, biogenic, lightning and anthropogenic emissions emitted in Africa shows that the African biomass burning emissions are responsible for regional surface ozone enhancement of about 10–50 ppbv close to the burning regions in Africa. This surface ozone enhancement can even be more than 50 ppbv over parts of central Africa (Democratic republic of Congo, Congo and Angola) during the JJA biomass burning season. Biogenic emissions increase the surface ozone concentration over Africa by about 5–30 ppbv. Lightning is shown to have an insignificant impact on surface ozone, but leads to the second largest impact on the middle to the upper tropospheric ozone concentration, next to biogenic emissions. The relative importance of biomass burning and biogenic emissions on the surface ozone concentration over Africa is highly dependent on the season and the location. Biomass burning provides the largest impact on surface ozone concentration only during the burning seasons in the vicinity of the burning region. The Sahara desert surface ozone concentration is mainly influenced by anthropogenic and biogenic emissions.

Biogenic, biomass burning, lightning and anthropogenic emissions over Africa account for an increase of the net global tropospheric ozone burden of about 19.6 Tg (6.5 – 60 Tg), 9.5 Tg (4.5 – 19 Tg), 8.0 Tg (6 – 30 Tg), and 4.7 Tg (3 – 6 Tg) respectively. The influence of these emissions on the African tropospheric ozone burden is about 4.1 Tg, 2.5 Tg, 1.8 Tg and 0.9 Tg, respectively. Therefore, this study shows that more than 70% of the tropospheric ozone produced by each of the African emission categories is found outside the continent.

The impact of biogenic, biomass burning, lightning and anthropogenic emissions on the tropospheric ozone burden of various world regions shows that for all emission categories, Latin America experiences the highest impact of African emissions, followed by Oceania, the Middle East, Southeast and South-central Asia. This is in effect due to the proximity of these regions to Africa. The tropospheric ozone over Canada, the United States, Northern Asia and Europe are only slightly affected by African emissions. This study also shows a teleconnection of the sea surface temperature anomaly over the eastern tropical Pacific and the transport from Africa over the central Indian Ocean to Southeast Asia. Specifically, warm (or cold) SST anomaly increases (or reduces) transport to South-eastern Asia due to the weakening (or strengthening) of the tropical easterly jet (Palmer et al., 1992; Janicot et al., 2001). In all continental regions outside of Africa, African biogenic emissions have the largest influence on the tropospheric ozone burden, followed by African lightning and biomass burning emissions.

7.2 Outlook

This study has dealt with the global influence of air pollution emitted in Africa, portrayed by its impact on other geographical land regions, due to long-range inter-hemispheric and inter-continental transport of trace species and their reaction products. It also shows the impact of Africa emissions over the tropospheric ozone concentrations over the continent. Nevertheless, air pollution is both a global and a local phenomenon, and many questions are left unanswered. Some of these issues are discussed below.

7.2.1 MEGAN biogenic emissions

The present implementation of MEGAN provides an interactive calculation of emissions for climate change and impact studies. However, to fully access this impact, the canopy model must be further extended to permit changes in vegetation distribution and leaf area index. It would also be interesting to investigate the radiative effect of aerosols on isoprene emissions.

7.2.2 Tropospheric ozone and human health in Africa

This study has shown high ozone concentrations in the entire troposphere over Africa, partly due to local African emissions. Specifically, biomass burning and biogenic emissions have been shown to have the largest influence on surface and boundary layer ozone concentrations over the tropical Africa region. This does have consequences on health and agricultural crop yields in Africa. A study linking the calculated ozone concentrations in this study to number of hospital admissions and deaths, and trends in agricultural yields and production, will be a valuable extension of this work. It will also be worthwhile to calculate the exceedances of ozone concentrations over Africa based on popular ozone exposure limit.

7.2.3 African megacities

Closely related to the points raised in the last section is the issue of megacities in Africa, e.g. Lagos, Nigeria. In order to aid effective air pollution control policy and mitigation strategy in African megacities, it would be worthwhile to characterise if ozone production is limited by NO_x or VOCs. This study shows that African emissions contributed very little to ozone concentrations over Cairo, Egypt, so, where do the high concentrations of ozone in the whole troposphere over Egypt come from? Furthermore, given the population bloom projected by the UN World Urbanization Prospects (2005) in Lagos and Cairo, will biogenic and biomass burning remain the highest emission categories influencing tropospheric ozone, or will this change to anthropogenic emissions? Some of the questions dealing with the local impact of air pollution in this outlook would definitely require models with higher spatial resolution or even regional models.

Appendix A

Appendix to MEGAN Implementation

A.1 Emission flux of other MEGAN compounds

The remaining 16 non-terpene VOCs, which are not implemented in the current version of MEGAN in the ECHAM5-MOZ model are:

acetic acid:	$E = 0.50 \times \varepsilon_n \times \gamma_2 \times \rho_2$
benzaldehyde:	$E = 0.05 \times \varepsilon_n \times \gamma_2 \times \rho_2$
butanone:	$E = 0.52 \times \varepsilon_n \times \gamma_2 \times \rho_2$
butene:	$E = 0.52 \times \varepsilon_n \times \gamma_2 \times \rho_2$
carbonyl sulfide:	$E = 0.01 \times \varepsilon_n \times \gamma_2 \times \rho_2$
decanal:	$E = 0.01 \times \varepsilon_n \times \gamma_2 \times \rho_2$
dimethyl sulfide:	$E = 0.03 \times \varepsilon_n \times \gamma_2 \times \rho_2$
ethanol:	$E = 2.3 \times \varepsilon_n \times \gamma_2 \times \rho_2$
formic acid:	$E = 1.0 \times \varepsilon_n \times \gamma_2 \times \rho_2$
hexanal:	$E = 0.35 \times \varepsilon_n \times \gamma_2 \times \rho_2$
hexenal:	$E = 0.76 \times \varepsilon_n \times \gamma_2 \times \rho_2$
hexenol:	$E = 0.76 \times \varepsilon_n \times \gamma_2 \times \rho_2$
hexenyl acetate:	$E = 0.65 \times \varepsilon_n \times \gamma_2 \times \rho_2$
nonanal:	$E = 0.01 \times \varepsilon_n \times \gamma_2 \times \rho_2$
octanal:	$E = 0.01 \times \varepsilon_n \times \gamma_2 \times \rho_2$
toluene:	$E = 0.01 \times \varepsilon_n \times \gamma_2 \times \rho_2$

where the emission flux, E of the non-terpene VOCs includes a factor (the first numbers on the right-hand side of equations above), which relate the lumped emission factor, ε_n (in μg(C) m^{-2}h^{-1}) to emission flux, E (in millimoles of compound km^{-2}h^{-1}).

A.2 MEGAN input files

This section shows the MEGAN input files, that is the emission factors, ε_i, ε_t, ε_n, for isoprene, terpenes and other non-terpene VOCs, respectively. It also shows the activity factors γ_1 and γ_2 for all months of the year.

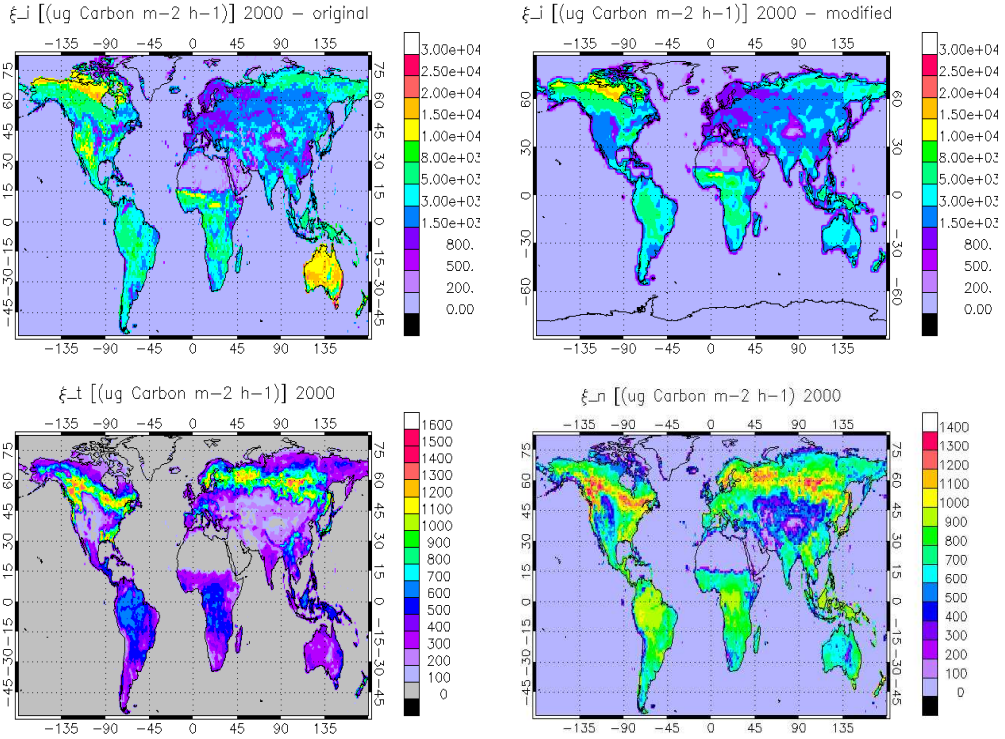

Figure A.1— The MEGAN emission factors for isoprene (ε_i), terpenes (ε_t), and other non-terpene VOCs (ε_n). The top panels show the original and modified isoprene emission factor.

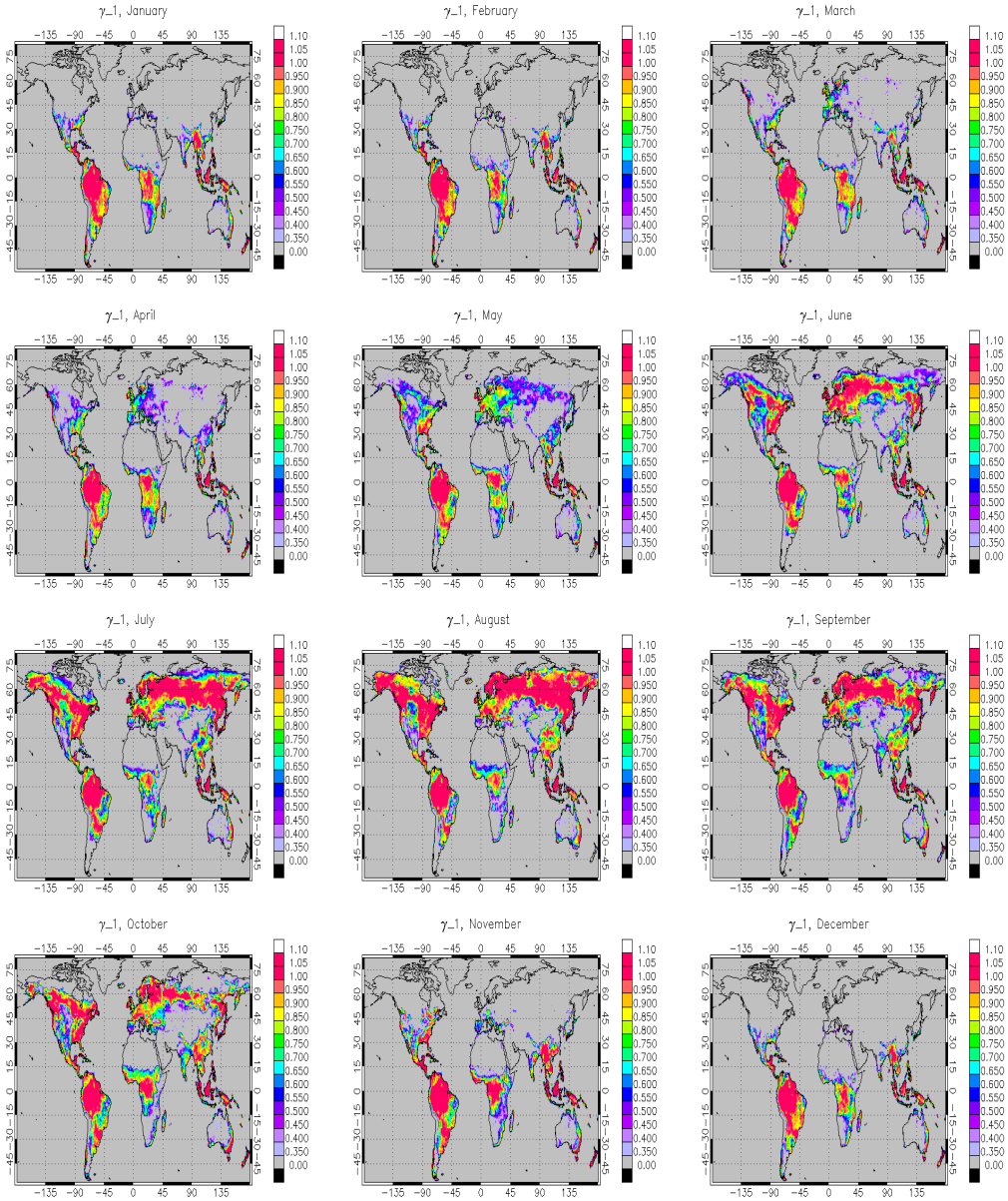

Figure A.2— The MEGAN emission activity for isoprene (γ_1) in all months.

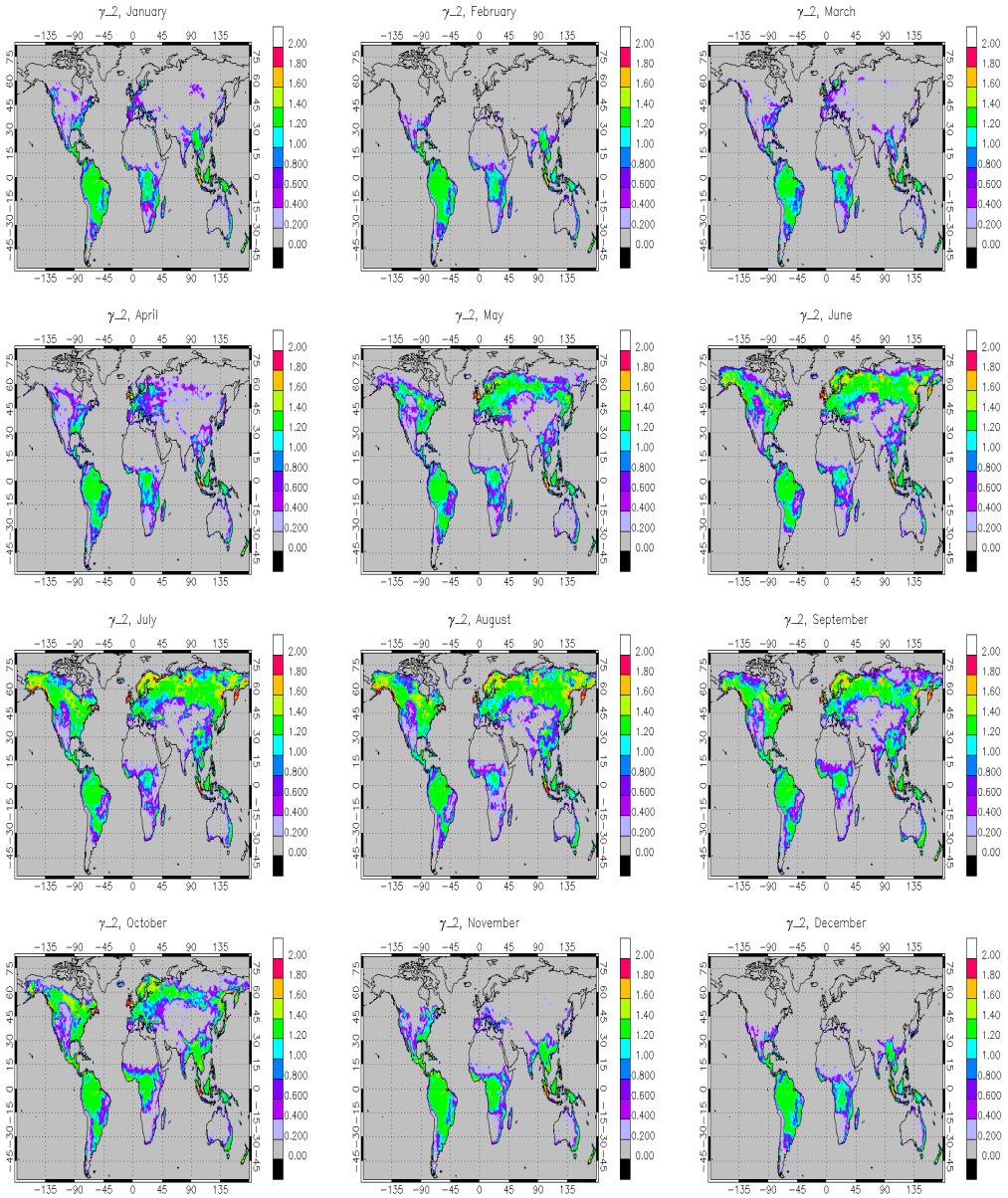

Figure A.3— The MEGAN emission activity for terpenes and other non-terpene VOCs (γ_2) in all months.

Appendix B

ECHAM5-MOZ and SHADOZ vertical profiles

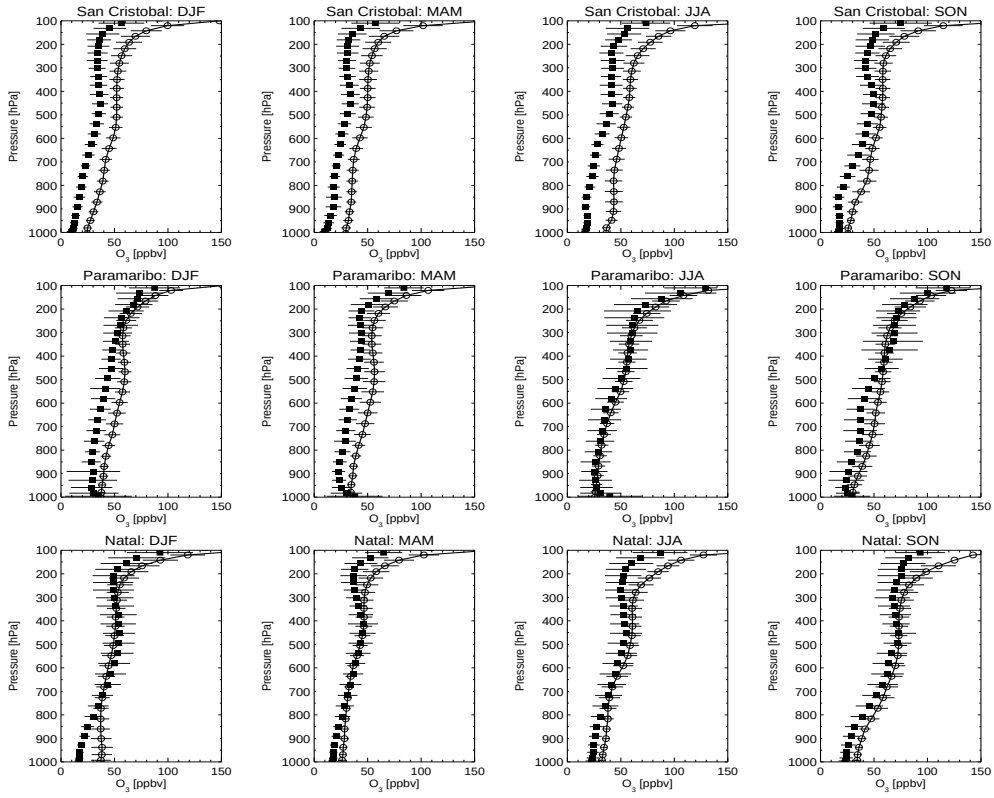

Figure B.1— The comparison of 5-year average (1991–2000) model simulated (open circles with line) with 1997–2000 mean SHADOZ (filled-squares) ozone vertical profiles over San Cristobal (Ecuador), Paramaribo (Suriname), and Natal (Brazil) in December–February (DJF), March–May (MAM), June–August (JJA) and September–November (SON). The horizontal lines indicate $\pm 1\,\sigma$ standard deviation.

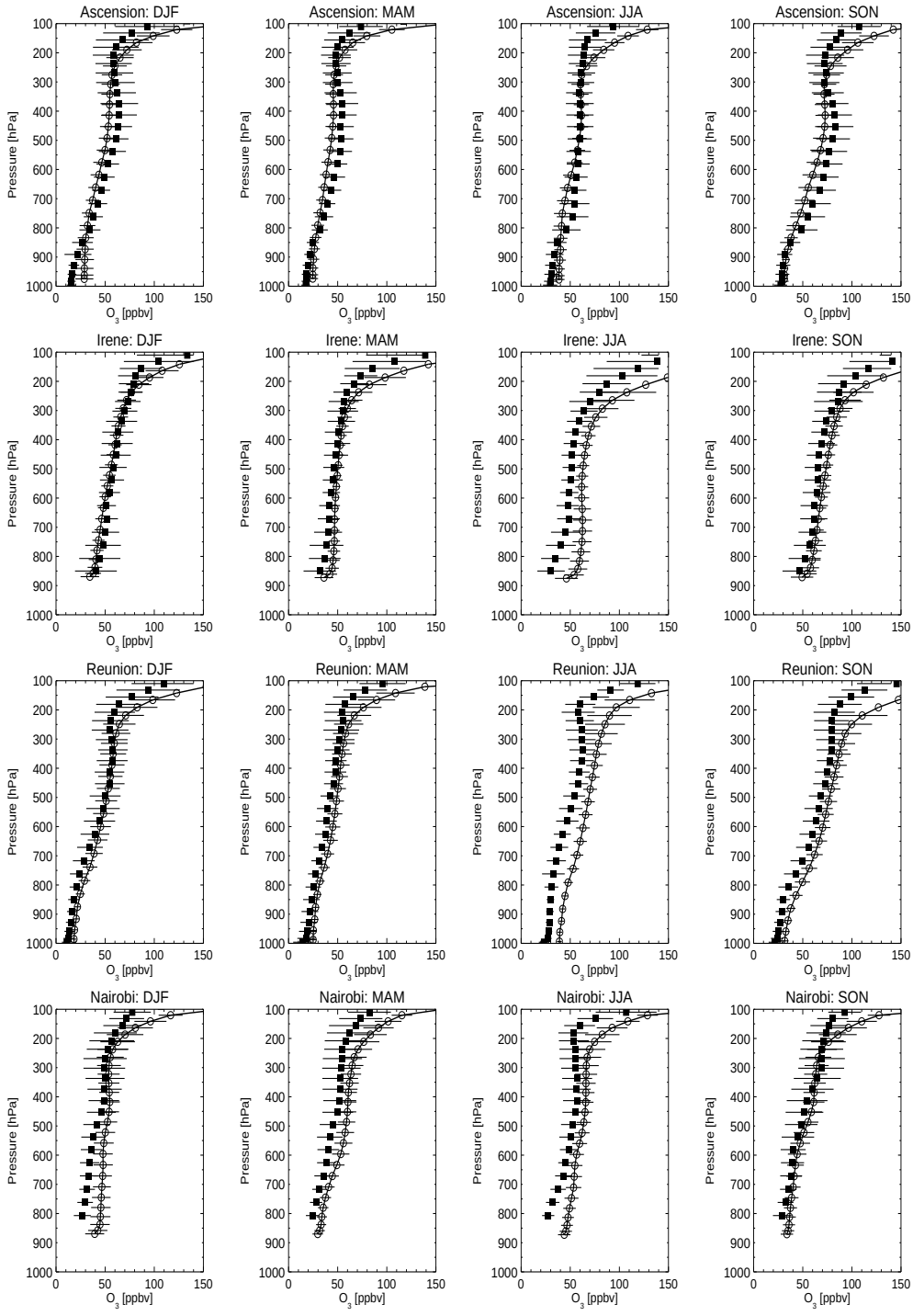

Figure B.2— The comparison of 5-year average (1991–2000) model simulated (open circles with line) with 1998–2004 mean SHADOZ (filled-squares) ozone vertical profiles over Ascension Island, Irene (South Africa), Reunion Island and Nairobi (Kenya) in December–February (DJF), March–May (MAM), June–August (JJA) and September–November (SON). The horizontal lines indicate $\pm 1\,\sigma$ standard deviation.

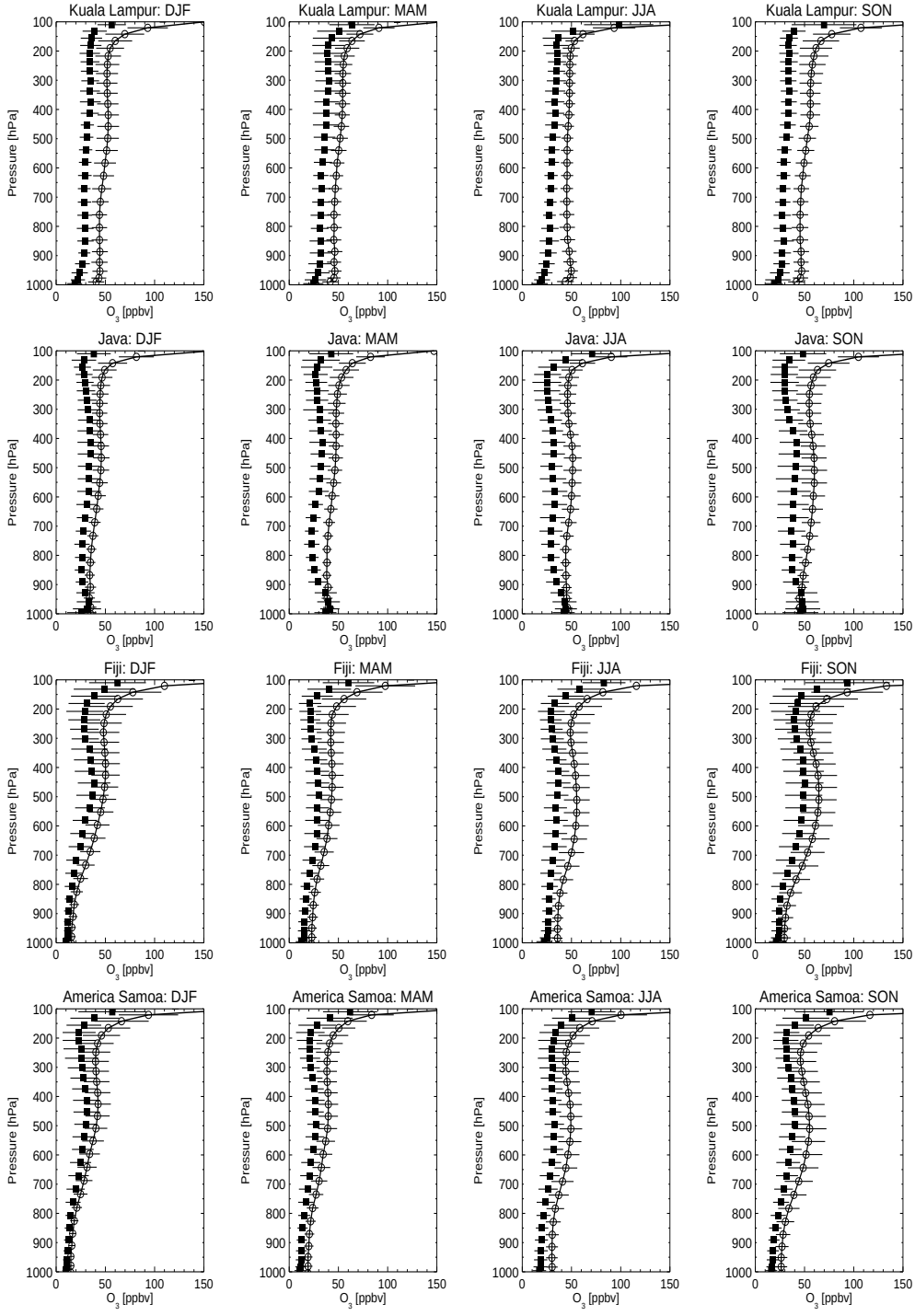

Figure B.3— The comparison of 5-year average (1991–2000) model simulated (open circles with line) with 1997–2000 mean SHADOZ (filled-squares) ozone vertical profiles over Kuala Lumpur (Malaysia), Watukosek, Java (Indonesia), Suva (Fiji), and America Samoa in December–February (DJF), March–May (MAM), June–August (JJA) and September–November (SON). The horizontal lines indicate $\pm 1\,\sigma$ standard deviation.

Appendix C

Transport of idealized tracers in ECHAM5

C.1 Technical description of the tracer module

The three surface tracers (surfN, surfS and surfT) were introduced through the module mo_surface_trspxter, while the three tropopause tracers (tropN, tropS and tropT) and the stratosphere tracers (stratN, stratS and stratT) were also introduced through the modules mo_tropopause_trspxter and mo_stratosphere_trspxter, respectively. The modules are introduced into ECHAM5 through ECHAM5 submodel interface. The switches lbsurf, ltropo and lstra allow for the switching on/off of the surface, tropopause and stratosphere tracers respectively. These switches are defined in the RUNCTL namelist with the default value of .false.

Each of the modules contains three subroutines: call_init, call_request_tracer and call_chem2. The determination of the tracers boundary condition, such as the tropopause and stratosphere level through which the tracers are introduced for different model resolution and the specification of latitude which demarcates the "north", "south" and "tropics" regions are performed in the call_init subroutine. The tracers are created (or requested) with a specific decay time (i.e. lifetime) in the call_request_tracer and the initialisation of the tracers' mass mixing ratio is performed in call_chem2.

The initialisation of tracers to 1.0 is achieved through:

$$\delta c = \frac{c(t) - c(t - \mathrm{d}t)}{\mathrm{d}t} \qquad \text{and} \qquad c(t) = 1.0 \tag{C.1}$$

where δt is the time-step length and δc is the tracer tendency; $c(t)$ and $c(t - \mathrm{d}t)$ are the tracer mass mixing ratio (concentration) at time t and $t - \mathrm{d}t$ respectively. The tracers mass mixing ratio, $c(t)$ cannot be simply set to 1.0 due to the leapfrog time differencing scheme used in ECHAM5.

C.2 Calculating the latitude band at which the earth surface area is divided into three equal parts

For any given sphere shown in Figure C.1, we seek the angle φ such that the surface area, A of the sphere is divided into three equal parts.

$$\mathrm{A} = \int_0^{2\pi}\int_0^{\pi} r^2 \sin\varphi \,\mathrm{d}\varphi \,\mathrm{d}\theta \tag{C.2}$$

where φ and θ are as shown in Figure C.1 and r is the radius of sphere A. Integrated over all angles, Equation (C.2) yields $\mathrm{A} = 4\pi\, r^2$. In order to find the limit angle τ of φ for which the sphere has an area $4\pi r^2/3$ we write:

$$\frac{4\,\pi}{3} = \int_0^{2\pi}\int_0^{\tau} \sin\varphi \,\mathrm{d}\varphi \,\mathrm{d}\theta \tag{C.3}$$

After the first integration over θ and some trivial simplifications, Equation (C.3) reduces to:

$$\frac{2}{3} = \int_0^{\tau} \sin\varphi \,\mathrm{d}\varphi \quad \Longrightarrow \quad \cos\tau = \frac{1}{3} \tag{C.4}$$

hence the latitude angle is the complement angle ψ of angle τ, i.e. $\psi = 90^\circ - \tau$, which yields approximately:

$$\psi = 19.47^\circ \tag{C.5}$$

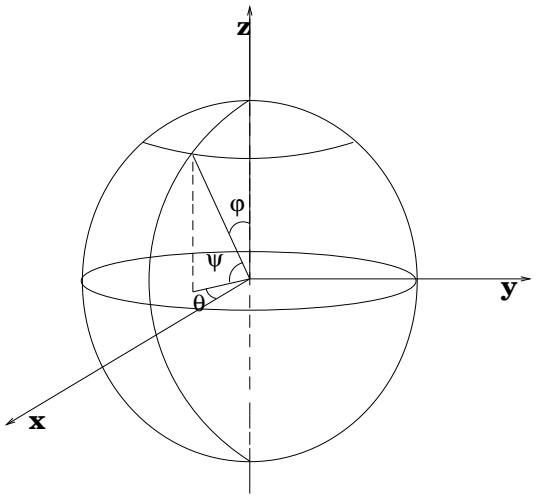

Figure C.1— A spherical coordinate system.

C.3 Tracers zonal mean concentrations at steady state

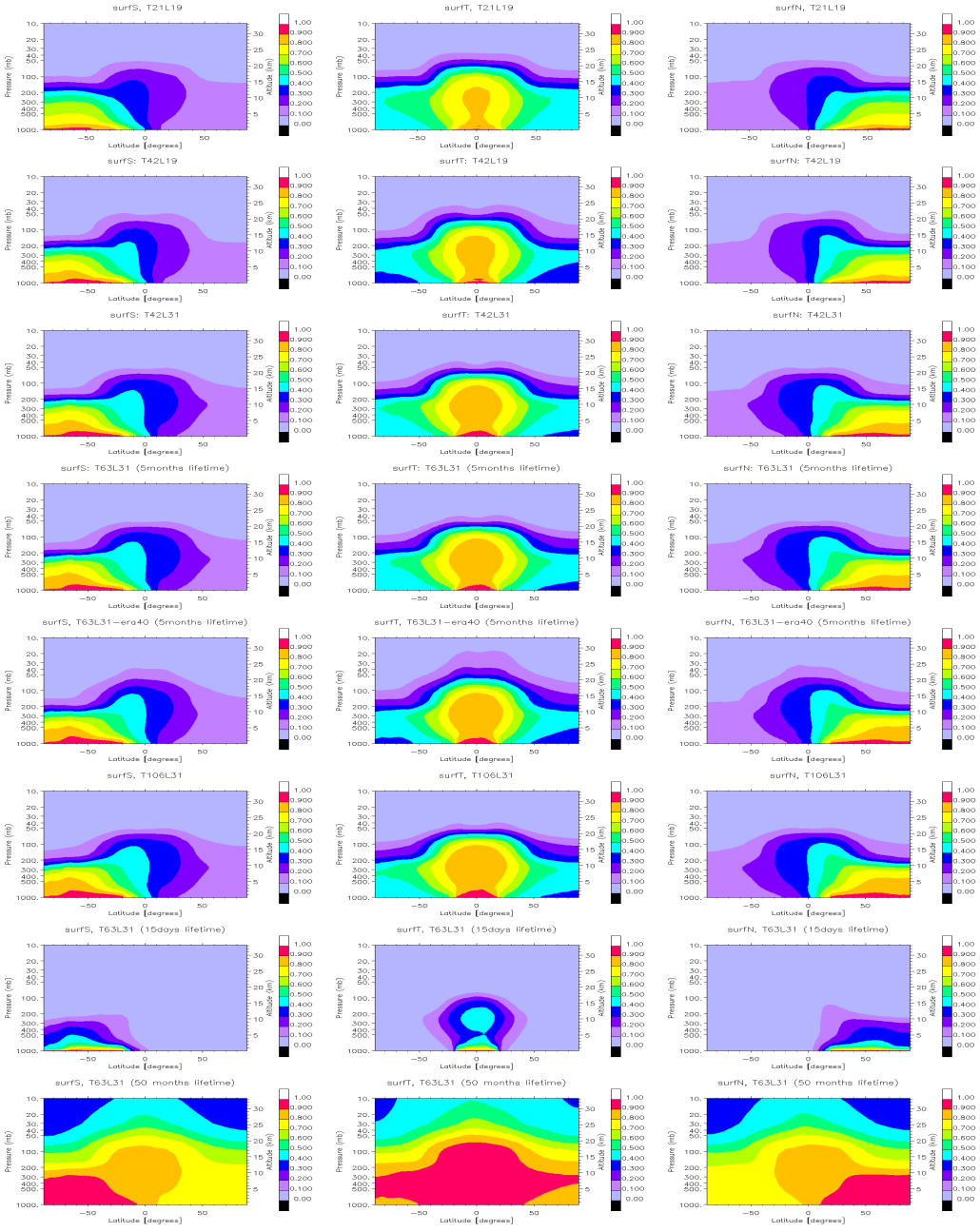

Figure C.2— The climatology zonal mean of surface tracers: surfS (first column), surfT (second column) and surfN (third column) in the resolutions T21L19 (firt row), T42L19 (second row), T42L31 (third row), T63L31 (fourth row), T63L31-ERA40 (fifth row), and the T106L31 (sixth row) with lifetime of 5 months. The seventh and the eight rows show the tracers with lifetime of 15 days and 50 months, respectively in the T63L31 resolution.

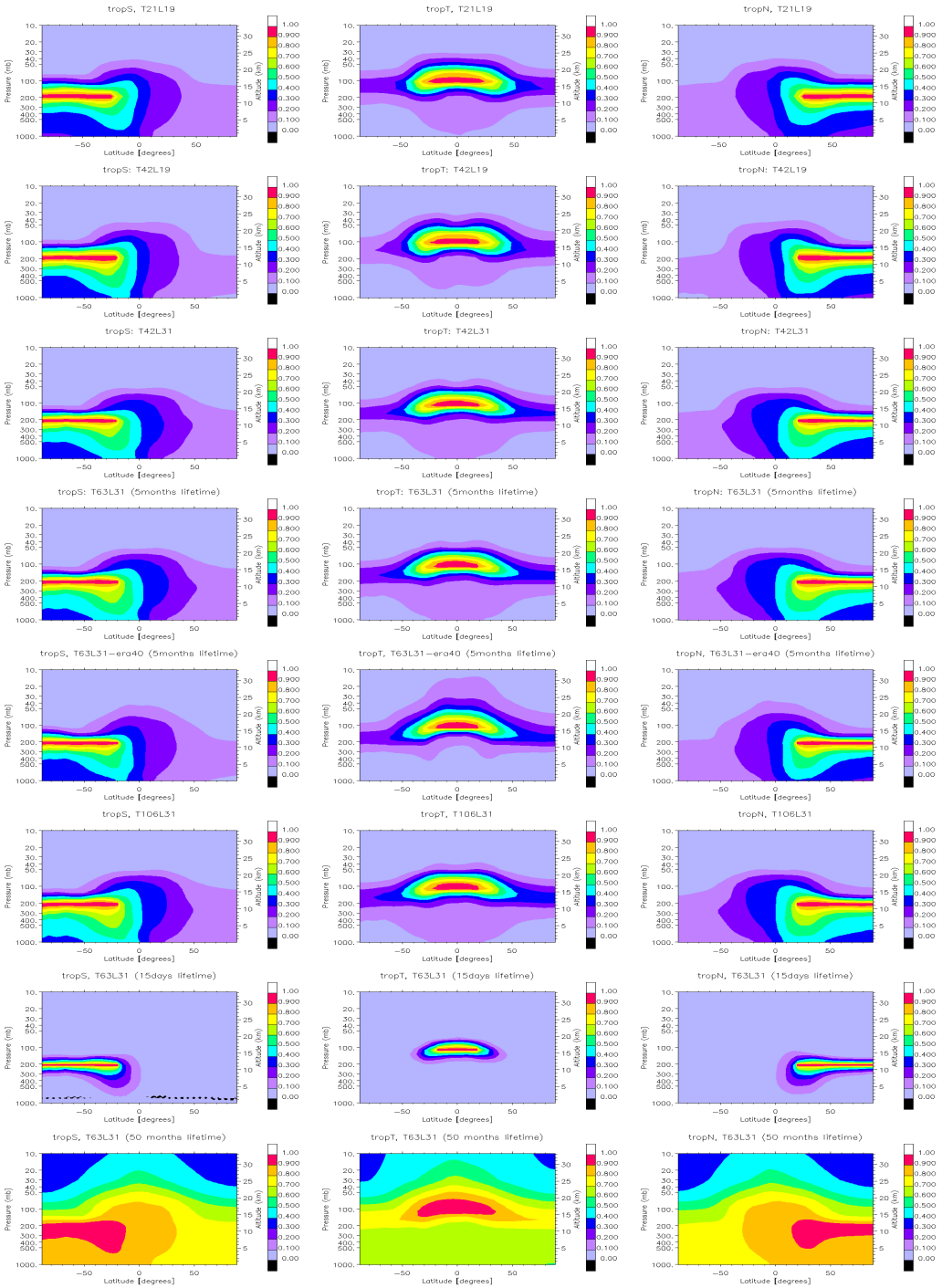

Figure C.3— The climatology zonal mean of tropopause tracers: tropS (first column), tropT (second column) and tropN (third column) in the resolutions T21L19 (firt row), T42L19 (second row), T42L31 (third row), T63L31 (fourth row), T63L31-ERA40 (fifth row), and the T106L31 (sixth row) with lifetime of 5 months. The seventh and the eight rows show the tracers with lifetime of 15 days and 50 months, respectively in the T63L31 resolution.

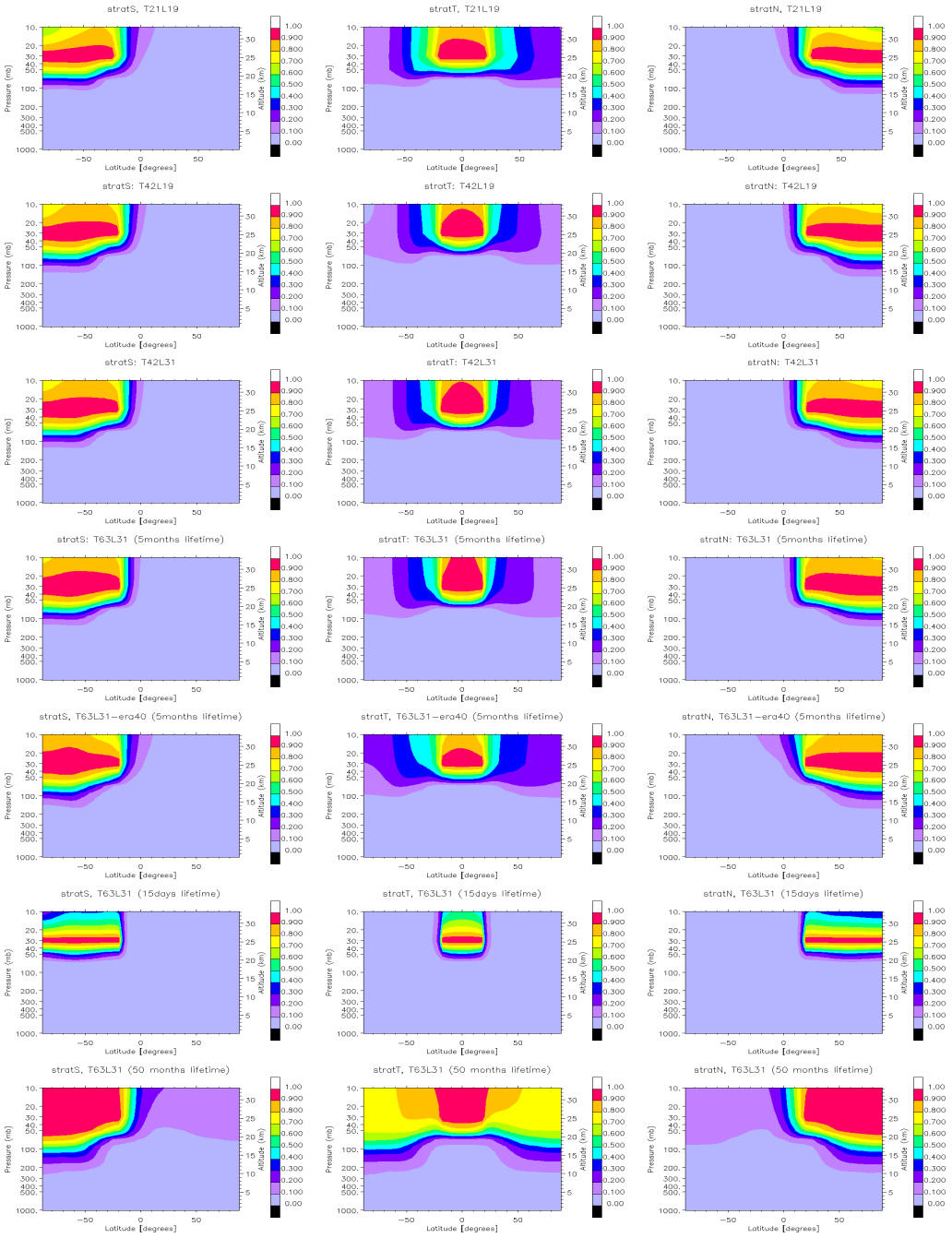

Figure C.4— The climatology zonal mean of stratosphere tracers: stratS (first column), stratT (second column) and stratN (third column) in the resolutions T21L19 (firt row), T42L19 (second row), T42L31 (third row), T63L31 (fourth row) and T63L31-ERA40 (fifth row) with lifetime of 5 months. The sixth and the seventh rows show the tracers with lifetime of 15 days and 50 months, respectively in the T63L31 resolution.

Bibliography

Adams, J. M., J. V. H. Constable, A. Guenther, and P. Zimmerman: An estimate of natural volatile organic compounds emissions from vegetation since the last glacial maximum, Chemosphere, 3, 73–91, 2001.

Adefolalu, D. O.: Monsoon Onset in West Africa, Application of Satellite Imagery, Arch. Met. Geoph. Biocl., Ser. B, 32,219-230, 1983.

Achard, F., H. D. Eva, H.-J. Stibig, P. Mayaux, J. Gallego, T. Richards, and J.-P. Malingreau, Determination of Deforestation Rates of the World's Humid Tropical Forests, Science, 297, 999–1002, DOI: 10.1126/science.1070656, 2002.

Afolayan, A. A.: Is there a Step-wise migration in Nigeria?: A case study of the migrational histories of migrants in Lagos, GeoJournal, 11(2), 183 – 193, 1985.

Aghedo, A. M., Schultz, M. G. and S. Rast: The influence of African air pollution on regional and global tropospheric ozone, Atmos. Chem. Phys., 7, 1193–1212, 2007.

Amann, M., Bertok, I., Cofala, J., Gyarfas, F., Heyes, C., Klimont, Z., Makowski, M., Schöpp, W., and Syri, S.: Cost-effective Control of Acidification and Ground-Level Ozone, Seventh Interim Report, International Institute for Applied Systems Analysis (IIASA), Laxenburg, Austria, 1999.

Andreae, M. O.: Biomass burning: Its history, use, and distribution and its impact on environmental quality and global climate, in J. S. Levine (ed.), Global Biomass Burning, MIT Press, Cambridge, Massachusetts, pp. 121., 1991.

Andreae, M. O.: The influence of tropical biomass burning on climate and the atmospheric environment, in: Biogeochemistry of Global Change: Radiatively Active Trace Gases, edited by: R. S. Oremland, 113–150, Chapman and Hall, New York, 1993.

Anfossi, D., S. Sandroni, and S. Viarengo: Tropospheric ozone in the Nineteenth Century: The Moncalieri series, J. Geophys. Res., 96(D9), 17,349 – 17,352, 1991.

Annegarn, H. J., M. A. Kneen, S. J. Piketh, A. J. Home, H. S. P. Hlapolosa, and G. A. Kirkman: Evidence for large-scale circulation of anthropogenic sulphur over South Africa, paper presented at the National Association for Clean Air Conf., Brits, South Africa, Nov. 11–13, 1993.

Appenzeller C., Holton, J. R. and Rosenlof, K. H.: Seasonal variation of mass transport across the tropopause. J. Geophys. Res., 101(D10), 15071 – 15078, 1996.

Asselin, R.: Frequency filter for time integrations, Mon. Wea. Rev., 100, 487–490, 1972.

Austin, J., Butchart N., and Swinbank, R.: Sensitivity of ozone and temperature to vertical resolution in a GCM with coupled stratospheric chemistry, Q. J. R. Meteorol. Soc., 123, 1405–1431, 1997.

Aviation and the Global Atmosphere: A Special Report of IPCC Working Groups I and III in collaboration with the Scientific Assessment Panel to the Montreal Protocol on Substances that Deplete the Ozone Layer, edited by: Penner, J. E., Lister, D. H., Griggs, D. J., Dokken, D. J., and McFarland, M., Cambridge University Press, UK, pp. 373, 1999.

Avila, L. A., and R. J. Pasch: Atlantic tropical systems of 1991. Mon. Wea. Rev., 120, 2688–2696, 1992.

Baker, D. F.: Sources and Sinks of Atmospheric CO_2 Estimated from Batch Least-Squares Inversions of CO_2 Concentration Measurements. Ph.D. Dissertation, Princeton University, 2001.

Barbosa, P. M., Stroppiana, D., Grégoire, J.-M., and Pereira, J. M. C.: An assessment of vegetation fire in Africa (1981–1991): Burned area, burned biomass, and atmospheric emissions, Global Biogeo. Cycles, 13, 933–950, 1999.

Baumbach, G., Vogta, U., Heina, K. R. G., Oluwole, A. F., Ogunsola, O. J., Olaniyi, H. B., and Akeredolu ,F. A.: Air pollution in a large tropical city with a high traffic density – results of measurements in Lagos, Nigeria, Science of The Total Environment, 169, 25–31, 1995.

Bell, M., Davis, D. L. and Fletcher, T.: A retrospective assessment of mortality from the London smog episode of 1952: the role of influenza and air pollution, Environ. Health Perspect., 112(1), 6–8, 2004.

Benton, J., J. Fuhrer, B. S. Gimeno, L. SkÄrby and G. Sanders: Results from the UN/ECE ICP-Crops indicate the extent of exceedance of the critical levels of ozone in Europe, Water, Air and Soil Pollution, 85 (3),1473–1478, doi: 10.1007/BF00477189, 1995.

Bernard Shaw, A. F.: A histological study of the mummy of Har-mosĕ, the singer of the eighteenth dynasty (circa 1490 B.C.), J. Pathol. and Bacteriol., Vol. 47, Issue 1 , Pages 115 – 123, DOI:10.1002/path.1700470112, July 1938.

Bates, T. S., P. K. Quinn, D. J. Coffman, J. E. Johnson, T. L. Miller, D. S. Covert, A. Wiedensohler, S. Leinert, A. Nowak, and C. Neusüss: Regional physical and chemical properties of the marine boundary layer aerosol across the Atlantic during Aerosols99: An overview, J. Geophys. Res., 106(D18), 20767 –20782, 2001.

Boccippio,D. J.: Lightning scaling laws revisited, J. Atmos. Sci. 59, 1086–1104, 2002.

Bojkov, R. D.: Surface ozone during the second half of the nineteenth century, J. Am. Meteorol. Soc., 25, 343–352, 1986.

Bonan, G. B.: A land surface model (LSM version 1.0) for ecological, hydrological, and atmospheric studies: technical description and user's guide. NCAR Technical Note, NCAR/TN-417+STR, National Center for Atmospheric Research, Boulder, CO, USA, 1996.

Bonan, G. B., Oleson, K. W., Vertenstein, M., Levis, S., Zeng, X., Dai, Y., Dickinson, R. E., and Yang, Z.-L.: The land surface climatology of the Community Land Model coupled to the NCAR Community Climate Model, J. Clim., 15, 3123 – 3149, 2002.

Boucher, O., Pham, M., and Venkataraman, C.: Simulation of the atmosphere sulphur cycle in the Laboiratoire de Meteorologie Dynamique general circulation model: Model description, model evaluation, and global and European budgets, Note scientifique de l'IPSL no. 23, 2002.

Bousquet, P., Ciais, P., Peylin, P., Ramonet, M. and Monfray, P.: Inverse modeling of annual atmospheric CO_2 sources and sinks 1. method and control inversion. J. Geophys. Res., 104, 26161 – 26178, 1999a.

Bousquet, P., Peylin, P., Ciais, P., Ramonet, M. and Monfray, P.: Inverse modeling of annual atmospheric CO_2 sources and sinks 2. sensitivity study. J. Geophys. Res., 104, 26179 – 26193, 1999b.

Bousquet, P., Peylin, P., Ciais, P., Le Quéré, C., Friedlingstein, P. and Tans, P.: Regional changes in carbon dioxide fluxes of land and oceans since 1980. Science, 290, 1342 – 1346, 2000.

Bowman, K. P. and Carrie, G. D.: The mean-meridional transport circulation of the troposphere in an idealized GCM, J. Atmos. Sci., 59, 1502 – 1514, 2001.

Bowman, K. P. and Erukhimova, T.: Comparison of global-scale Lagrangian transport properties of the NCEP Reanalysis and CCM3, J. Climate, 17, 1135 –1145, 2004.

Brasseur, G. P., Orlando, J. J. and Tyndall, G. S.: Atmospheric Chemistry and Physics, Oxford University Press, 654 pages, 1999.

Brewer, A. M.: Evidence for a world circulation provided by the measurement of helium and water vapour distribution in the stratosphere. Q. J. R. Meterol. Soc., 75, 351 – 363, 1949.

Brimblecombe, P.: Industrial air pollution in thirteenth century Britain, Weather, 20, 388 – 396, 1975.

Brimblecombe, P.: Attitudes and responses to air pollution in medieval England, J. Air Poll. Contr. Assoc., 26, 941 – 945, 1976.

Brimblecombe, P.: Interest in Air pollution among early Fellows of the Royal Society, Notes Rec. Roy. Soc. Lond., 32, 123 – 129, 1978a.

Brimblecombe, P.: Air pollution in industrializing England, J. Air Pollution Control Assoc., 28, 115–118, 1978b.

Brimblecombe, P., and Bowler, C.: The history of Air pollution in York, England, J. Air Waste Manage. Assoc. 42, 1562–1566, 1992.

Brothwell, D. R., A. T. Sandison, P. H. K. Gray: Human biological observations on a Guanche mummy with anthracosis, Am. J. Phys. Anthropol., Vol. 30, Issue 3, p. 333 –347, DOI: 10.1002/ajpa.1330300303, 1969.

Burpee, R. W., 1972: The origin and structure of easterly waves in the lower troposphere of North Africa. J. Atmos. Sci., 29, 77–90, 1972.

Carlson, T. N.: Some remarks on African disturbances and their progress over the tropical Atlantic. Mon. Wea. Rev., 97, 716–726, 1969.

Chalita, S., Hauglustaine, D. A., Le Treut, H. and Müller, J.-F.: Radiative forcing due to increased tropospheric ozone concentrations, Atmos. Environ. 30, 1641–1646, 1996.

Chameides, W. L. and Walker, J. C. G.: A photochemistry theory for tropospheric ozone, J. Geophys. Res., 78, 8751 – 8760, 1973.

Chan, C. Y., Chan, L. Y., Harris, J. M.: Urban and Background Ozone Trend in 1984-1999 at Subtropical Hong Kong, South China, 25 (6), 513 – 522, doi: 10.1080/01919510390481829, 2003.

Charter, J. R and Keay, R. W. J.: Assessment of the Olokemeji fire-control experiment (Investigation 254) 28 years after institution, Nigerian For. Info. Bull. (New Series 3, 1–32), 1960.

Chatfield, R. B., J. A. Vastano, L. Li, G. W. Sachse, and V. S. Connors, The Great African plume from biomass burning: A three-dimensional study of TRACE A carbon monoxide, J. Geophys. Res., 103, 28059–28077, 1998.

Chatfield, R. B., Z. Guo, G. W. Sachse, D. R. Blake, and N. J. Blake, The subtropical global plume in the Pacific Exploratory Mission-Tropics A (PEM-Tropics A), PEM-Tropics B, and the Global Atmospheric Sampling Program (GASP): How tropical emissions affect the remote Pacific, J. Geophys. Res., 107(D16), 4278, doi:10.1029/2001JD000497, 2002.

Christian, H.J., Blakeslee, R. J., Boccippio, D. J., Boeck, W. L., Buechler, D. E ., Driscoll, K. T., Goodman, S. J., Hall, J. M., Koshak, W. J., Mach, D. M., and Stewart, M. F.: Globa frequency and distribution of lightning as observed by the Optical Transient Detector, J. Geophys. Res, 108, 4005, doi: 10.1029/2002JD002347, 2003.

Chen, Ping, Holton, James R., O'Neill, Alan, Swinbank, Richard: Isentropic Mass Exchange between the Tropics and Extratropics in the Stratosphere, J. Atmos. Sci., 51, 3006 – 3018, 1994.

Ciais, P., Tans, P. P., Trolier, M., White, J. W. C. and Francey, R. J.: A large northern hemisphere terrestrial CO_2 sink indicated by the $^{13}C\,/\,^{12}C$ ratio of atmospheric CO_2. Science 269, 1098 – 1102, 1995.

Climate change 2001: The scientific basis, the contribution of the working group I to the Third Assessment Report (TAR) of the Intergovernmental Panel on Climate Change (IPCC), Cambridge University Press, The Edinburgh Building, Cambridge CB2 2RU, UK, 2001. Available at http://www.grida.no/climate/ipcc_ tar/.

Climate change 2007: The Physical science basis, the contribution of the working group I to the Fourth Assessment Report (AR4) of Intergovernmental Panel on Climate Change (IPCC), Summary for Policy Markers, released February 2007. Available at http://www.ipcc.ch/SPM2feb07.pdf.

Collins, W. J., Stevenson, D. S., Johnson, C. E., and Derwent, R. G.: Role of convection in determining the budget of odd hydrogen in the upper troposphere, J. Geophys. Res., 104(D21), 26 927–26 942, doi:10.1029/1999JD900143, 1999.

Constable, J. V. H., Guenther, A. B., Schimel, D. S. and Monson, R. K.: Modelling changes in VOC emission in response to climate change in the continental United States, Global Change Biology, 5, 791–806, 1999.

Cook, K. H.: Generation of the African Easterly Jet and Its Role in Determining West African Precipitation, J. of Climate, 1165 – 1184, Vol. 12, Issue 5, May 1999.

Cox, P. M.: Description of the TRIFFID dynamic global vegetation model, Hadley Centre Technical Note No. 24, Met Office, Bracknell, U. K., 2001. http://www.met-office.gov.uk/research/hadleycentre/pubs/HCTN.

Cros, B., D. Nganga, A. Minga, J. Fishman, and V. Brackett, Distribution of tropospheric ozone at Brazzaville, Congo, determined from ozonesonde measurements, J. Geophys. Res., 97, 12869 – 12875, 1992.

Crutzen, P. J.: A discussion of the chemistry of some minor constituents in the stratosphere and troposphere, Pure Appl. Geophys., 106–108, 1385–1399, 1973.

Crutzen, P. J.: Global tropospheric chemistry, in Low-Temperature Chemistry of the Atmosphere, NATO ASI Ser., vol. 121, edited by Moortgat et al., pp. 465–498, Springer-Verlag, New York, 1994.

Crutzen, P. J.: Introductory lecture. Overview of tropospheric chemistry: developments during the past quarter century and a look ahead, Faraday Discuss., 1995, 100, 1 – 21, DOI: 10.1039/FD9950000001, 1995.

Crutzen, P. J., Heidt, L. E., Krasnec, W. H., and Seiler, W.: Biomass burning as a source of atmospheric trace gases CO, H_2, N_2O, NO, CH_3Cl and COS, Nature, 282, 253–256, 1979.

Crutzen, P. J. and Andreae, M. O.: Biomass burning in the tropics: Impact on atmospheric chemistry and biogeochemical cycles, Science, 150, 1669–1678, 1990.

Danielsen, E. F.: Stratosphere-troposphere exchange based on radioactivity, ozone, and potential vorticity, J. Atmos. Sci., 25, 502 – 518, 1968.

DeCaria, A. J., Pickering, K. E., Stenchikov, G. L., Scala, J. R., Stith, J. L., Dye, J. E., Ridley, B. A., and Laroche P.: A cloud-scale model study of lightning-generated NO_x in an individual thunderstorm during STERAO-A, J. Geophys. Res., 105, 11601–11616, 2000.

DeCaria, A. J., Pickering, K. E., Stenchikov, G. L. , and Ott, L. E.: Lightning-generated NO_x and its impact on tropospheric ozone production: A three-dimensional modeling study of a Stratosphere-Troposphere Experiment: Radiation, Aerosols and Ozone (STERAO-A) thunderstorm, J. Geophys. Res., 110, D14303, doi:10.1029/2004JD005556, 2005.

De Leeuw, F., and De Paus, T. A. : Exceedance of EC ozone threshold values in Europe in 1997, Water, Air, and Soil Pollution, 128, 255 – 281, 2001.

Delmas, R. A., Druilhet, A., Cros, B., Durand, P., Delon, C. et al.: Experiment for Regional Sources and Sinks of Oxidants (EXPRESSO): An overview, J. Geophys. Res., 104(D23), 30609 – 30624, 1999.

Denning, A. S., Holzer, M., Gurney, K. R., Heimann, M., Law, R. M. and coauthors.: Three-dimensional transport and concentration of SF_6: A model intercomparison study (TransCom 2). Tellus 51B, 266 – 297, 1999.

Dentener, F; Stevenson, D; Cofala, J; et al.: The impact of air pollutant and methane emission controls on tropospheric ozone and radiative forcing: CTM calculations for the period 1990-2030 Atmos. Chem. Phys., 5: 1731 – 1755, 2005.

Desqueyroux, H., Pujet, J. C., Prosper, M., Squinazi, F., and Momas, I.: Short-term effects of low-level air pollution on respiratory health of adults suffering from moderate to severe asthma, Environ. Res., 89, 29 –37, 2002

Diab, R. D., Jury, M.R., Combrink, J. and Sokolic, F.: A comparison of anticyclone and trough influences on the vertical distribution of ozone and meteorological conditions during SAFARI-92, J. Geophys. Res., 101, 23809–23821, 1996.

Dlugokencky, E. J., Steele, L. P., Lang, P. M., and Masarie, K. A.: The growth rate and distribution of atmospheric methane, J. Geophys. Res., 99(D8), 17021 – 17044, 1994.

Doherty, R. M., Stevenson, D. S., Collins, W. J., and Sanderson, M. G.: Influence of convective transport on tropospheric ozone and its precursors in a chemistry-climate model, Atmos. Chem. Phys., 5, 3205–3318, 2005.

Dobson, G. M. B.: Origin and distribution of polyatomic molecules in the atmosphere. Proc. R. Soc. London A, 236, 187 – 193, 1956.

Ehhalt, D., Prather, M., Dentener F., et al.: Atmospheric chemistry and greenhouse gases, in Climate Change 2001: The Scientific Basis, Contribution of Working Group I to the Third Assessment Report of the Intergovernmental Panel on Climate Change, 239–288, Cambridge University Press, New York.

Enting, I. G., Trudinger, C. M., and Francey, R. J.: A synthesis inversion of the concentration and d13C of atmospheric CO_2. Tellus 47B, 35 – 52, 1995.

Enting, I. G. and Mansbridge, J. V.: Seasonal sources and sinks of atmospheric CO_2: Direct inversion of filtered data. Tellus 41B, 111 – 126, 1989.

Erukhimova, T. and Bowman, K. P.: Role of convection in global-scale transport in the troposphere, J. Geophys. Res., 111, D03105, doi:10.1029/2005JD006006, 2006.

Essery, R., M. Best, and P. Cox: MOSES 2.2 Technical Documentation, Hadley Centre Technical Note No. 30, Met Office, Bracknell, U. K., 2001. http://www.met-office.gov.uk/research/hadleycentre/pubs/HCTN.

Fehsenfeld, F., Calvert, J., Fall, R., Goldan, P., Guenther, A. B., Hewitt, C. N, Lamb, B., Liu, S., Trainer, M., Westberg, H., and Zimmerman, P.: Emissions of volatile organic compounds from vegetation and the implications for atmospheric chemistry, Global Biogeochem. Cycles, 6(4), 389–430, 1992.

Findlater, J. (1969), A major low level aircurrent near the Indian Ocean during the northern summer, Quart. J. Roy. Meteor. Soc. 95, 362–480, 1969.

Findlater, J. (1972), Aerial explorations of the low-level cross-equatorial current over eastern Africa, Quart. J. Roy. Meteor. Soc. 98, 274–289, 1972.

Findlater, J. (1974), The low-level cross-equatorial air current of the western Indian Ocean during the northern summer, Weather 29, 411–416, 1974.

Finlayson-Pitts, B. J. and Pitts Jr., J. N.: Tropospheric air pollution: Ozone, Airborne Toxics, Polycyclic Aromatic Hydrocarbons, and Particles, Science, Vol. 276, 1045 –1052, 16 May 1997.

Fishman, J: Ozone in the troposphere, in Ozone in the free atmosphere, edited by R. C. Whitten and S. S. Prasad, pp. 161–194, Van Nostrand Reinhold, New York, 1985.

J. Fishman and P. J. Crutzen: The origin of ozone in the troposphere, Nature 274, 855 - 858, doi:10.1038/274855a0, 1978.

Fishman, J. and Larsen, J. C.: The distribution of total ozone and stratospheric ozone in the tropics: Implications for the distribution of tropospheric ozone, J. Geophys. Res., 92, 6627–6634, 1987.

Fishman, J., Watson, C. E.,Larsen, J. C. and Logan, J. A.: Distribution of tropospheric ozone determined from satellite data, J. Geophys. Res., 95, 3599 –3617, 1990.

Fishman, J., J. M. Hoell Jr., R. D. Bendura, R. J. McNeal, and V. W. J. H. Kirchhoff, NASA GTE TRACE A Experiment (September – October 1992): Overview, J. Geophys. Res., 101(D19), 23,865 –23,880, 1996.

Flohn, H.: Investigations on the tropical easterly jet. Bonner Meteorol. Abh., 4, 83 pp., 1964.

Foley, J. A., I. C. Prentice, N. Ramankutty, S. Levis, D. Pollard, S. Sitch, and A. Haxeltine: An integrated model of land surface processes, terrestrial carbon balance, and vegetation dynamics, Global Biogeochem. Cycles, 10, 603–628, 1996.

Fontan, J., Druilhet, A., Benech, B., Lyra, R., and Cros, B., The DECAFE experiments: overview and meteorology.J. Geophys. Res. 97, 6123–6136, 1992

Frank N. L.: Atlantic tropical systems of 1969. Mon. Wea. Rev., 98, 307–314, 1970.

Fung, I., Prentice, K., Matthews, E., Lerner, J. and Russell, G.: Three-dimensional tracer model study of atmospheric CO_2: Response to seasonal exchanges with the terrestrial biosphere. J. Geophys. Res., 88, 1281 – 1294, 1983.

Galbally, I. E. and Kirstine, W.: The production of methanol by flowering plants and the global cycle of methanol, J. Atmos. Chem., 43, 195–229, 2002.

Ganzeveld, L.: Surface-Atmosphere Trace Gas and Aerosol Exchanges on the Global Scale, PhD thesis, University of Utrecht, The Netherlands, 2001.

Garstang, M., P. D. Tyson, R. Swap, M. Edwards, P. Kallberg, J. A. Lindesay, Horizontal and vertical transport of air over southern Africa, J. Geophys. Res., 101, 23721–23736, 1996.

Gates W. L., Boyle, J. S., Covey, C., Dease, C. G., Doutriaux, C. M., et al.: An Overview of the Results of the Atmospheric Model Intercomparison Project (AMIP I). Bulletin of the American Meteorological Society, 80(1), pp. 2955, 1999.

Genthon, C. and Armengaud, A.: Radon 222 as a comparative tracer of transport and mixing in two general circulation models of the atmosphere. J. Geophys. Res., 100(D2), 2849 – 2866, 1995.

Giorgetta, M. A., Manzini, E, and Roeckner, E.: Forcing of the quasi-biennial oscillation from a broad spectrum of atmospheric waves, Geophys. Res. Lett., 29, 10.1029/2002GL014756, 2002.

Gordon, C., C. Cooper, C. A. Senior, H. Banks, J. M. Gregory, T. C. Johns, J. F. B. Mitchell, and R. A. Wood: The simulation of SST, sea ice extents and ocean heat transports in a version of the Hadley Centre coupled model without flux adjustments, Clim. Dyn., 16, 147–168, 2000.

Granier, C., Mü ller, J.-F., Madronich, S., and Brasseur, G. P.: Possible causes of the 1990 – 1993 decrease in the global tropospheric CO abundance: A three dimensional sensitivity study, Atmos. Environ., 30, 1673–1682, 1996.

Granier, C., Mü ller, J.-F., Pétron, G., and Brasseur, G.: A three-dimensional study of the global CO budget, Chemosphere Global Change Sci., 1, 255 –261, 1999.

Gray, S. L.: A case study of stratosphere to troposphere transport: The role of convective transport and the sensitivity to model resolution. J. Geophys. Res., 108(D18), 4590, 2003.

Grewe, V., Brunner, D., Dameris, M., Grenfell, J. L., Hein, R., Shindell, D., and Staehelin, J.: Origin and variability of upper tropospheric nitrogen oxides and ozone at northern mid-latitudes, Atmos. Environ. 35, 3421–3433, 2001.

Guenther, A., Hewitt, C. N., Erickson, D., Fall, R., Geron, C., Graedel, T., Harley, P., Klinger, L., Lerdau, M., Mckay, W. A., Pierce, T., Scholes, B., Steinbrecher, R., Tallamraju, R., Taylor, J., and Zimmerman, P.: A global model of natural volatile organic compound emissions, J. Geophys. Res.-Atmos., 100(D5), 8873–8892, 1995.

Guenther, A., Baugh, B., Brasseur, G., Greenberg, J., Harley, P., Klinger, L., Serca, D., and Vierling, L.: Isoprene emission estimates and uncertainties for the Central African EXPRESSO study domain, J. Geophys. Res., 104(30), 625–639, 1999.

Guenther, A., C. Geron, T. Pierce, B. Lamb, P. Harley, and R. Fall: Natural emissions of non-methane volatile organic compounds, carbon monoxide, and oxides of nitrogen from North America, Atmos. Environ., 34, 2205–2230, 2000.

Guenther, A., Karl, T., Harley, P., Wiedinmyer, C., Palmer, P. I, and Geron, C.: Estimates of global terrestrial isoprene emissions using MEGAN (Model of Emissions of Gases and Aerosols from Nature), Atmos. Chem. Phys., 6, 3181–3210, 2006.

Gurney, K. R., Law, R. M., Denning, A. S., Rayner, P. J., Baker, D. and coauthors.: Towards robust regional estimates of CO2 sources and sinks using atmospheric transport models. Nature 415, 626 – 630, 2002.

Gurney, K. R., Law, R. M., Denning, A. S., Rayner, P. J., Baker, D. and coauthors: TransCom 3 CO_2 inversion intercomparison: 1. Annual mean control results and sensitivity to transport and prior flux information, Tellus 55B, 555 – 579, 2003.

Haagen-Smit, A.J.: The control of air pollution, Scientific American, 210, 24–31, 1964.

Hall, T. M., Waugh, D. W., Boering, K. A., and Plumb, R. A.: Evaluation of transport in stratospheric models, J. Geophys. Res., 104(D15), 18815 – 18839, 1999.

Hansen, J., Sato, M., Nazarenko, L., Ruedy, R., et al.: Climate forcings in GISS SI2000 simulations, J. Geophys. Res. 107, 4347, doi:10.1029/2001JD001143, 2002.

Hao, W. M. and Liu, M. H.: Spatial and temporal distribution of tropical biomass burning, Global Biogeochem. Cycles, 8, 495–503, 1994.

Hartley, D. E., and Black, R. X.: A mechanistic analysis of interhemispheric transport, Geophys. Res. Lett., 22, 2945 – 2948, 1995.

Heimann, M. and Keeling, C. D.: A three-dimensional model of atmospheric CO_2 transport based on observed winds: 2. Model description and simulated tracer experiments. In: Aspects of climate variability in the Pacific and Western Americas (ed. Peterson, D. H.). Geophysical Monograph 55, American Geophysical Union, Washington, DC, 237 – 275, 1989.

Helas, G., Lacaux, J. P., Delmas, R., Scharffe, D., Lobert, J., Goldammer, J., and Andreae, M. O.:1992, Ozone as biomass burning product over Africa, Fresenius Environ. Bull. 1, 155 – 160, 1992 .

Helas, G., Lobert, J., Scharffe, D., Schäfer, L., Goldammer, J., Baudet, J., Ahoua, B., Ajavon, A.-L., Lacaux, J.-P., Delmas, R., and Andreae, M. O.: Ozone production due to emissions from vegetation burning, J. Atmos. Chem. 22, 163 – 174, 1995a.

Helas, G., M. O. Andreae, G. Schebeske, and P. LeCanut: SA'ARI-94: A preliminary view on results S. Afr. J. Sci. 91, 360 – 362, 1995b.

Held, G., Scheifinger, H., and Snyman, G.M.: Recirculation of pollutants in the atmosphere of the South African highveld, So. Afr. J. Sci., 90, 91–97, 1994.

Hoell, J. M., D. D. Davis, D. J. Jacob, M. O. Rodgers, R. E. Newell, H. E. Fuelberg, R. J. McNeal, J. L. Raper, and R. J. Bendura, Pacific Exploratory Mission in the tropical Pacific: PEM Tropics A, August – September 1996, J. Geophys. Res., 104, 5567–5584, 1999.

Hoke, J. E. and Anthes, R. A.: The initialization of numerical models by a dynamic-initialization technique, Mon. Wea. Rev., 104(12), 1551–1556, 1976.

Holloway, T., Levy II, H., and Kasibhatla, P.: Global distribution of carbon monoxide, J. Geophys. Res., 105, 12 123–12 147, 2000.

Holton, J. R., Haynes, P. H., McIntyre, E. M., Douglass, A. R., Rood, R. B., and L. Pfister, L.: Stratosphere-troposphere exchange, Rev. Geophys., 33, 403 – 439, 1995.

Hopkins, B.: The role of fire in promoting the sprouting of some savanna species, Journal West. Afr. Sci. Ass. 7, 154 – 162, 1963.

Hopkins, B.: Observations on Savanna Burning in the Olokemeji Forest Reserve, Nigeria The Journal of Applied Ecology, Vol. 2, No. 2., 367–381, 1965.

Horowitz, L. W., Walters, S., Mauzerall, D. L., Emmons, L. K., Rasch, P. J., Granier, C., Tie, X., Lamarque, J.-F., Schultz, M. G., Tyndall, G. S., Orlando, J. J., and Brasseur, G. P.: A global simulation of tropospheric ozone and related tracers: Description and evaluation of MOZART, version 2, J. Geophys. Res., 108(D24), 4784, doi:10.1029/2002JD002853, 2003.

Houghton, R. A.: The Worldwide Extent of Land-Use Change, BioScience, 44, 305–313, 1994.

Hubert, H.: Origine Africaine d'un cyclone tropical Atlantique, Ann. Phys. GIobe France d'Outre-Mer, 6, 97–115, 1939.

Hudman, R. C., D. J. Jacob, O. R. Cooper, M. J. Evans, C. L. Heald, et al.: Ozone production in transpacific Asian pollution plumes and implications for ozone air quality in California, J. Geophys. Res., 109, D23S10, doi:10.1029/2004JD004974, 2004.

Hugh , E. and Lambin, E. F.: Fires and land-cover change in the tropics:a remote sensing analysis at the landscape scale, Journal of Biogeography 27 (3), 765–776, doi: 10.1046/j.1365-2699.2000.00441.x, 2000.

Hulme, M., and N. Tosdevin, The Tropical Easterly Jet and Sudan Rainfall: A Review, Theor. Appl. Climatol. 39, 179–187, 1989.

Hunter, L. M.: The environmental implications of population dynamics, RAND publication MR-1191/WFHF/RF/DLPF, 1700 Main Street, Santa Monica, California, USA, 98 pages, 2000. Available from http://handle.dtic.mil/100.2/ADA387276

Huntrieser, H., Feigl, C., Schlager, H., Schröder, F., Gerbig, C., van Velthoven, P., Flatøy, F., Théry, C., Petzold, A., Höller, H., and Schumann, U.: Airborne measurements of NO_x, tracer species, and small particles during the European Lightning Nitrogen Oxides Experiment, J. Geophys. Res., 107(D11), 4113, doi:10.1029/2000JD000209, 2002.

International Energy Outlook, 2006, report no: DOE/EIA-0484(2006), available at http://www.eia.doe.gov/oiaf/ieo/index.html. Published by the Energy Information Administration Office of Integrated Analysis and Forecasting, U.S. Department of Energy, Washington, DC 20585. 202 pages, June 2006.

Jacob, D. J., et al.: The origin of ozone and NO_x in the tropical troposphere: A photochemical analysis of aircraft observations over the South Atlantic Basin, J. Geophys. Res., 101, 24 235–24 250, 1996.

Jacob, D. J., Prather, M. J., Rasch, P. J., Shia, R.-L., Balkanski, Y. J., Beagley, S. R., et al.: Evaluation and intercomparison of global atmospheric transport models using ^{222}Rn and other short-lived tracers. J. Geophys. Res., 102(D5), 5953 – 5970, doi: 10.1029/96JD02955, 1997.

Janicot, S., Trzaska, S., and Poccard, I.: Summer Sahel-ENSO teleconnection and decadal time scale SST variations, Clim. Dyn., 18, 303–320, 2001.

Jeuken, A. B. M., Siegmund, P. C., Heijboer, L. C., Feichter, J., and Bengtson, L.: On the potential of assimilating meteorological analysis in a climate model for the purpose of model validation, J. Geophys. Res., 101, 16 939–16 950, 1996.

Jonquieres I., Marenco A., Maalej A. and Rohrer F.: Study of ozone formation and trans-atlantic transport from biomass burning emissions over West Africa during the airborne campaigns TROPOZ I and TROPOZ II. J. Geophys. Res., D15, 103, 19059–19073, 1998.

Junge, C. E.: Global ozone budget and exchange between stratosphere and troposphere, Tellus, 14, 363 – 377, 1962.

Kaminski, T., Heimann, M. and Giering, R.: A coarse grid three-dimensional global inverse model of the atmospheric transport, 2. Inversion of the transport of CO2 in the 1980s. J. Geophys. Res., 104, 18555 – 18581, 1999.

Kesselmeier, J. and Staudt, M.: Biogenic volatile organic compounds (VOC): An overview on emission, physiology and ecology, J. Atmos. Chem., 33, 23–88, 1999.

Kley, D.: Tropospheric Chemistry and Transport, Science, Vol. 276, 1043 – 1045, 16 May 1997.

Labrador, L. J., von Kuhlmann, R., and Lawrence, M. G.: The effects of lightning-produced NOx and its vertical distribution on atmospheric chemistry: sensitivity simulations with MATCH-MPIC, Atmos. Chem. Phys., 5, 1815 – 1834, 2005

Kobayashi, N.: Interannual variations of tropical easterly jet stream and rainfall in south Asia. Geophys. Mag.,37, 123–134, 1974.

Koteswaram, P.: Easterly jet stream in the tropics, Tellus, 10, 43–57, 1958.

Krishnamurti, T. N.: Observational study of the tropical upper tropospheric motion field during the Northern Hemisphere summer, J. Appl. Meteor., 10, 1066–1096, 1971a.

Krishnamurti, T. N.: Tropical east-west circulations during the northern summer, J. Atmos. Sci. 28, 1342–1347, 1971b.

Krishnamurti, T. N., Molarinari, J, Pan, H. L.: Numerical Simulations of the Somali Jet. J. Atmos. Sci. 33, 2350-2362 (1976).

Kucharik, C. J., J. A. Foley, D. Delire, V. A. Fisher, M. T. Coe, J. D. Lenters, C. Young-Molling, and N. Ramunkutty: Testing the performance of a dynamic global vegetation model: Water balance, carbon balance and vegetation structure, Global Biogeochem. Cycles, 14, 795–825, 2000.

Lacaux, J. P., J. M. Brustet, R. Delmas, J. C. Menaut, L. Abbadie, B. Bonsang, H. Cachier, J. Baudet, M. O. Andreae and G. Helas, Biomass burning in the tropical savannas of Ivory Coast: An overview of the field experiment Fire of Savannas (FOS/DECAFE 91), J. Atmos. Chem., 22, 195–216, 1995.

Laepple, T., Schultz, M. G., Lamarque, J. F., Madronich, S., Shetter, R. E., Lefer, B. L., and Atlas, E.: Improved albedo formulation for chemistry transport models based on satellite observations and assimilated snow data and its impact on tropospheric photochemistry, J. Geophys. Res., 110, D11308, doi:10.1029/2004JD005463, 2005.

Lamarque, J.-F., Brasseur, G. P, Hess, P. G., and Mueller, J.-F.: Three dimensional study of the relative contributions of the different nitrogen sources in the troposphere, J. Geophys. Res., 101, 22 955–22 968, 1996.

Landsea, C. W.: A climatology of intense (or major) Atlantic hurricanes. Mon. Wea. Rev., 121, 1703–1713, 1993.

Lathiere, J., Hauglustaine, D. A., Friend, A., De Noblet-Ducoudré, N., Viovy, N., and Folberth, G.: Impact of climate variability and land use changes on global biogenic volatile organic compound emissions, Atmos. Chem. Phys., 6, 2199–2146, 2005.

Law, R. M.: CO_2 sources from a mass-balance inversion: Sensitivity to the surface constraint. Tellus 51B, 254 – 265, 1999.

Law, R. M., Rayner, P. J., Denning, A. S., Erickson, D., Heimann, M. and coauthors.: Variations in modelled atmospheric transport of carbon dioxide and the consequences for CO_2 inversions. Global Biogeochem. Cycles 10, 783 – 796, 1996.

Lawrence, M. G., Chameides, W. L., Kasibhatla, P, S., Levy II, H., and Moxim, W.: Lightning and atmospheric chemistry: The rate of atmospheric NO production, in: Handbook of Atmospheric Electrodynamics, edited by: Volland, H., Vol. I, CRC Press, Inc., Boca Raton, 189–202, 1995.

Lawrence, M. G., von Kuhlmann, R., and Salzmann, M.: The balance of effects of deep convective mixing on tropospheric ozone, Geophys. Res. Lett., 30, 18, 1940, doi:10.1029/2003GL017644, 2003.

Levin, I. and Hesshaimer, V.: Refining of atmospheric transport model entries by the globally observed passive tracer distribution of ^{85}Krypton and sulfur hexafluoride (SF_6), J. Geophys. Res., 101(D11), 16745 – 16755, 1996.

Levis, S., Wiedinmyer, C., Bonan, G. B., and Guenther, A.: Simulating biogenic volatile organic compound emissions in the Community Climate System Model, J. Geophys. Res., 108, D21, doi:10.1029/2002JD003203, 2003.

Levy II, H.: Photochemistry of the lower troposphere, Planetary and Space Science Vol. 20, Issue 6, 919 –935, doi:10.1016/0032-0633(72)90177-8, June 1972.

Li, Q., D. J. Jacob, I. Bey, P. I. Palmer, B. N. Duncan, B. D. Field, R. V. Martin, A. M. Fiore, R. M. Yantosca, D. D. Parrish, P. G. Simmonds, and S. J. Oltmans: Transatlantic transport of pollution and its effects on surface ozone in Europe and North America, J. Geophys. Res., 107(D13), 4166, doi:10.1029/2001JD001422, 2002.

Lin, C.-Y. C., D. J. Jacob, and A. M. Fiore : Trends in exceedances of the ozone air quality standard in the continental United States, 1980 – 1998, Atmospheric Environment 35, 3217–3228, 2001.

Lin, S.-J. and Rood, R. B.: Multidimensional Flux-Form Semi-Lagrangian Scheme. Mon. Wea. Rev., 124, 2046–2070, 1996.

Lindesay, J. A., M. O. Andreae, J. G. Goldammer, G. Harris, H. J. Annegarn, M. Garstang, R. J. Scholes, and B. W. van Wilgen: International Geosphere-Biosphere Programme/International Global Atmospheric Chemistry SAFARI-92 field experiment: Background and overview, J. Geophys. Res., 101(D19), 23521–23530, 1996.

Lintner, B. R.: Mechanisms of passive tracer interhemispheric transport: An analysis of model-derived and observational interhemispheric transport climatology and interannual variations, Ph.D. thesis, 264 pp., Univ. of Calif., Berkeley, 2003.

Lintner, B. R., Gilliland, A. B., and Fung, I. Y.: Mechanisms of convection-induced modulation of passive tracer interhemispheric transport interannual variability, J. Geophys. Res., 109, D13102, doi:10.1029/2003JD004306, 2004.

Liu, S. C., Trainer, M., Fehsenfeld, F. C., Parrish, D. D., Williams, E. J. , Fahey, D. W., Huebler, G., and Murphy, P. C.: Ozone production in the rural troposphere and the implications for regional and global ozone distributions, J. Geophys. Res., 92, 4191–4207, 1987.

Lohmann, U. and Roeckner, E.: Design and performance of a new cloud microphysics scheme developed for the ECHAM general circulation model. Climate Dynamics, 12(8), 557 – 572, 1996.

Logan, J. A.: Tropospheric ozone: Seasonal behavior, trends, and anthropogenic influence, J. Geophys. Res., 90, 10463–10482, 1985.

Mahlman, J. D.: Dynamics of Transport Processes in the Upper Troposphere, Science 16, Vol. 276., pp. 1079 - 1083, DOI: 10.1126/science.276.5315.1079, May 1997.

Manzini, E., and McFarlane, N. A.: The effect of varying the source spectrum of a gravity wave parameterization in a middle atmosphere general circulation model. J. Geophys. Res., 103, 31523 – 31539, 1998.

Marenco, A., Medale, J. C., and Prieur, S.: Study of tropospheric ozone in the tropical belt (Africa, America) from STRATOZ and TROPOZ campaigns, Atmos. Environn., Ser. A, 24, 2823–2843, 1990.

Marenco, A., Thouret, V., Nédélec, P., Smit, H., Helten, M., Kley, D., Karcher, F., Simon, P., Law, K., Pyle, J., Poschmann, G., Von Wrede, R., Hume, C., and Cook, T.: Measurement of ozone and water vapor by Airbus in-service aircraft: The MOZAIC airborne program, An overview, J. Geophys. Res.-Atmospheres, 103(D19), 25 631–25 642, 1998.

Martin, R. V., Jacob, D. J., Logan, J. A., Bey, I., Yantosca, R. M., Staudt, A. C., Li, Q., Fiore, A. M., Duncan, B. N., and Liuiu, H., Ginoux, P., and Thouret, V.: Interpretation of TOMS observations of tropical tropospheric ozone with a global model and in situ observations, J. Geophys. Res., 107(D18), 4351, doi:10.1029/2001JD001480, 2002.

Marufu, L., Dentener, F., Lelieveld J., Andreae, M. O., and Helas G.: Photochemistry of the African troposphere: Influence of biomass-burning emissions, J. Geophys. Res., 105, 14 513–14 530, 2000.

Mauzerall, D. L. and Wang, X. P.: Protecting agricultural crops from the effects of tropospheric ozone exposure: Reconciling science and standard setting in the United States, Europe, and Asia, Ann. Rev. Energy Environ., 26, 237–268, 2001.

McLinden, C. A., Olsen, S. C., Hannegan, B., Wild, O., Prather, M. J. and Sundet, J.: Stratospheric ozone in 3-D models: A simple chemistry and the cross-tropopause flux, J. Geophys. Res., 105 (D11) , 14653 – 14665, 2000.

Mesinger, F. and Arakawa, A.: Numerical methods used in atmospheric models, Global Atmospheric Research Programme (GARP) Publication Series 17, World Meteorological Organisation, 1976.

Mortimer, K. M., Neas, L. M., Dockery, D. W., Redline, S., and Tager, I. B.: The effect of air pollution on inner-city children with asthma, Eur Respiratory J., 19, 699–705, 2002.

Müller, J.-F., and Brasseur, G.: IMAGES: A three-dimensional chemical transport model of the global troposphere, J. Geophys. Res., 100, 16445 – 16490, 1995.

Mylona, S.: Sulphur dioxide emissions in Europe 1880-1991 and their effect on sulphur concentrations and depositions, Tellus, 48B, 662–689, 1996.

Naik, V., Delire, C., and Wuebbles, D. J.: Sensitivity of global biogenic isoprenoid emissions to climate variability and atmospheric CO_2, J. Geophys. Res., 109, D06301, doi:10.1029/2003JD004236, 2004.

Naik, V; Mauzerall, D; Horowitz, L; et al.: Net radiative forcing due to changes in regional emissions of tropospheric ozone precursors, J. Geophys. Res., 110(D24), D24306, doi:10:1029/2005jd005908, 2005.

Newell, R. E., J. W. Kidson, D. G. Vincent, and G. J. Boer: The General Circulation of the Tropical Atmosphere and Interactions with Extra-tropical Latitudes, Vol. 1, 258 pp., MIT Press, Cambridge, Massachusetts, 1972.

Nganga, D., A. Minga, B. Cros, C. B. Biona, J. Fishman, and W. B. Grant, The vertical distribution of ozone measured at Brazzaville, Congo, during TRACE A, J. Geophys. Res., 101, 24,095-24,103, 1996.

Nordeng, T. E.: Extended versions of the convective parameterization scheme at ECMWF and their impact on the mean and transient activity of the model in the tropics. Technical memorandum No. 206, European Centre for Medium-range Weather Forecasts (ECMWF), Reading, United Kingdom, 1994.

Novelli, P. C., Steele, L. P., and Tans, P. P.: Mixing ratios of carbon monoxide in the troposphere, J. Geophys. Res., 97, 20,731 –20,750, 1992.

Novelli, P. C., Masarie, K. A., Tans, P. P., and Lang, P. M.: Recent changes in atmospheric carbon monoxide, Science, 263, 1587 – 1590, 1994.

Novelli, P. C., Anderson, B. E., Brenninkmeijer, C. A. M., Brunke, E. G., Doddridge, B. G., et al.: An internally consistent set of globally-distributed atmospheric carbon monoxide mixing ratios developed using results from an intercomparison of measurements, J. Geophys. Res., 103, 19 285 – 19 293, 1998a.

Novelli, P. C., Masarie, K. A., and Lang, P. M.: Distributions and recent changes of carbon monoxide in the lower troposphere, J. Geophys. Res., 103, 19 015 – 19 033, 1998b.

Novelli, P. C., K. A. Masarie, P. M. Lang, B. D. Hall, R. C. Myers, and J. W. Elkins, Reanalysis of tropospheric CO trends: Effects of the 1997– 1998 wildfires, J. Geophys. Res., 108(D15), 4464, doi:10.1029/2002JD003031, 2003.

Ojima, D.S., Galvin, K. A., and Turner, B. L.: The global impact of land-use change, BioScience, 44, 300 – 304, 1994.

Oksanen, E., and T. Holopainen: Responses of two birch (Betula pendula Roth) clones to different ozone profiles with similar AOT40 exposure, Atm. Environ., 35, 5245–5254, 2001.

Olivier, J., Bouwman, A., Berdowski, J., Bloos, J., Visschedijk, A., van der Mass, C., and Zandveld, P.: Sectoral emission inventories of greenhouse gases for 1990 on a per country basis as well as on 1×1 degrees, Environ. Sci. Policy, 2, 241–263, 1999.

O'Sullivan, D. and Chen, P: Modeling the quasi biennial oscillation's influence on isentropic tracer transport in the subtropics, J. Geophys. Res., 101(D3), 6811 – 6821, 1996.

Pabst, M. A. and F. Hofer: Deposits of different origin in the lungs of the 5,300-year-old Tyrolean Iceman, Am. J. Phys. Anthropol., Vol. 107, Issue 1, pages 1–12, Sept. 1998.

Palmer, T. N., Brankovic, C., Viterbo, P., and Miller, M. J.: Modeling inter-annual variations of summer monsoons, J. Clim., 5, 399 –417, 1992.

Peden, D. B.: Air pollution in asthma: effect of pollutants on airway inflammation, Annals Allergy Asthma and Immunology, 87, 12–17, 2001.

Pickering, K. E., Thompson, A. M., Dickerson, R. R., Luke, W. T., McNamara, D. P., Greenberg, J., and Zimmerman, P. R.: Model calculations of tropospheric ozone production potential following observed convective events, J. Geophys. Res., 95, 14 049–14 062, 1990.

Pickering, K. E., Thompson, A. M., McNamara, D. P., and Schoeberl, M. R.: An intercomparison of isentropic trajectories over the south Atlantic, Mon. Weather Rev., 122, 864–879, 1994.

Pickering, K. E., Thompson, A. M., Wang. Y., Tao, W., McNamara, D. P., Kirchhoff, V. W. J. H., Heikes, B. G., Sachse, G. W., Bradshaw, J. D., Gregory, G. L., and Blake, D. R.: Convective transport of biomass burning emissions over Brazil during TRACE-A, J. Geophys. Res., 101, 23 993–24 012, 1996.

Pickering, K. E., Wang, Y., Tao, W., Price, C., and Müller, J.: Vertical distributions of lightning NOx for use in regional and global chemical transport models, J. Geophys. Res., 103(D23), 31 203–31 216 ,1998.

Piersig, W.: Schwankungen von Luftdruck und Luftbewegung sowie ein Beitrag zum Wettergeschehen in Passatgebiet des ostlichen Nordatlantischen Ozeans, Arch. Deut. Seewarte, 54(6), 2–17, 1936. (Part II and III were translated in 1944: The cyclonic disturbances of the sub-tropical eastern North Atlantic. Bull. Amer. Meteor. Soc., 25, 2–17, 1944.

Plumb, R. A., and J. D. Mahlman: The zonally averaged transport characteristics of the GFDL general circulation/transport model, J. Atmos. Sci., 44, 298 – 327, 1987.

Potter, C. S., S. E. Alexander, J. C. Coughlan, and S. A. Klooster: Modeling biogenic emissions of isoprene: Exploration of model drivers, climate control algorithms, and use of global satellite observations, Atmos. Environ., 35, 6151–6165, 2001.

Pozzoli, L.: Chemistry-climate interactions: development and evaluation of a coupled chemistry-aerosol-climate model, PhD thesis, Swiss Federal Institute of Technology, Lausanne, Switzerland, 2007.

Prather, M., McElroy, M., Wofsy, S., Russell, G., and Rind, D.: Chemistry of the global troposphere-fluorocarbons as tracers of air motion, J. Geophys. Res., 92, 6579 – 6613, 1987.

Price, C., Penner, J., and Prather, M.: NO_x from lightning: 1. Global distribution based on lightning physics, J. Geophys. Res., 102, 5929–5941, 1997.

Prinn, R.G., Weiss, R. F., Miller, B. R., Huang, J., Alyea, F. N., Cunnold, D. M., Fraser, P. J., Hartley, D. E., and Simmonds, P. G.: Atmospheric Trends and Lifetime of CH_3CCl_3 and Global OH Concentrations, Science, 269,5221, 187–192, 1995.

Randerson, J. T., Kasibhatla, P. S., Kasischke, E. S., Hyer, E. J., Giglio, L., Collatz, G. J., and van der Werf, G. R.: Global Fire Emissions Database (GFED), Version 1. Data set. Available on-line http://daac.ornl.gov/ from Oak Ridge National Laboratory Distributed Active Archive Center, Oak Ridge, Tennessee, USA, 2005.

Rao, B. R. S., D. V. B. Rao, and V. B. Rao, Decreasing trend in the strength of Tropical Easterly Jet during the Asian summer monsoon season and the number of tropical cyclonic systems over Bay of Bengal, Geophys. Res. Lett., 31, L14103, doi:10.1029/2004GL019817, 2004.

Rayner, P. J., Enting, I. G., Francey, R. J. and Langenfelds, R. L.: Reconstructing the recent carbon cycle from atmospheric CO_2, $\delta^{13}C$ and O_2 / N_2 observations. Tellus 51B, 213 – 232, 1999.

Reed, R. J., Norquist, D. C., Recker, E. E.: The structure and properties of African wave disturbances as observed during Phase III of GATE.Mon. Wea. Rev.,103, 317–333, 1977.

Regula, H., 1936: Druckschwankungen und Tornados an der Westkuste von Afrika. Ann. Hydrogr. Mar. Meteor., 64, 107–111, 1936.

Reichle, H., Jr., Anderson, B. E., Connors, V. S., Denkins, T. C., Forbes, D. A., et al.: Space shuttle based global CO measurements during April and October 1994, MAPS instrument, data reduction, and data validation, J. Geophys. Res., 104, 21 443–21 454, 1999.

Ridley, B. A., Dye, J. E., Walega, J. G., Zheng, J., Grahek, F. E., and Rison, W.: On the production of active nitrogen by thunderstorms over New Mexico, J. Geophys. Res., 101, 20 985–21 005, 1996.

Riehl, H.: Tropical Meteorology. McGraw-Hill, 392 pp., 1954.

Robert, A. J., Henderson, J., and Turnbull, C.: An implicit time integration scheme for baroclinic models in the atmosphere, Mon Wea. Rev., 100, 329–335, 1972.

Robert, A. J.: A stable numerical integration scheme for the primitive meteorological equations, Atmos. Ocean, 19, 35–46, 1981.

Robert, A. J.: A semi-Lagrangian and semi-implicit numerical integration fscheme for the primitive meteorological equations, J. Met. Soc. Japan, 60, 319–325, 1982.

Roeckner, E., Bäuml, G., Bonaventura, L., Brokopf, R., Esch, M., Giorgetta, M., Hagemann, S., Kirchner, I., Kornblueh, L., Manzini, E., Rhodin, A., Schlese, U., Schulzweida, U., and Tompkins, A.: The atmospheric general circulation model ECHAM5, part I: Model description, Max Planck Institute for Meteorology, Report No. 349, 2003.

Roeckner, E, Brokopf, R., Esch, M., Giorgetta, M., Hagemann, S., Kornblueh, L., Manzini, E., Schlese, U., Schulzweida, U.: The atmospheric general circulation model ECHAM5 Part II: Sensitivity of simulated climate to horizontal and vertical resolution. Max-Planck Institute for Meteorology report No. 354, Hamburg, Germany, 63pp, 2004.

Roeckner, E., Brokopf, R., Esch, M., Giorgetta, M., Hagemann, S., Kornblueh, L., Manzini, E., Schlese, U., and Schulzweida, U.: Sensitivity of simulated climate to horizontal and vertical resolution in the ECHAM5 atmosphere model, J. Climate, Vol. 19, Issue 16, 3771 – 3791, doi: 10.1175/JCLI3824.11, 2006.

Roelofs, G.-J. and Lelieveld, J.: Distribution and budget of O_3 in the troposphere calculated with a chemistry general circulation model, J. Geophys. Res., 100, 20983 – 20998, 1995.

Roelofs, G., J. Lelieveld, H. G. J. Smit, and D. Kley, Ozone production and transports in the tropical Atlantic region during the biomass burning season, J. Geophys. Res., 102(D9), 10637–10652, 1997.

Sanderson, M. G., Jones, C. D., Collins, W. J., Johnson, C.E. and Derwent, R. G.: Effect of climate change on isoprene emissions and surface ozone levels, Geophys. Res. Lett., 30(18), 1936, doi:10.1029/2003GL017642, 2003.

Sathiyamoorthy, V.: Large scale reduction in the size of the Tropical Easterly Jet, Geophys. Res. Lett., 32, L14802, doi:10.1029/2005GL022956, 2005.

Sauvage B., Thouret, V., Cammas, J- P., Gheusi, F., G. Athier, G. and Nédélec, P.: Tropospheric ozone over Equatorial Africa: regional aspects from the MOZAIC data. Atmos. Chem. Phys., 5, 311 –335, 2005.

Schultz, M. G., D. J. Jacob, Y. Wang, J. A. Logan, E. L. Atlas, et al., On the origin of tropospheric ozone and NOx over the tropical South Pacific, J. Geophys. Res., 104(D5), 58295844.

Schultz, M. G. and Bey, I.: Numerical modeling of long-range pollution transport, Chp. 8, in: Intercontinental Transport of Air Pollution, edited by: Stohl, A., Springer, New York, 2004.

Schultz, M. G., Heil, A., Hoelzemann, J. H., Spessa, A., Thonicke, K., Goldammer, J., Held, A. C., and Pereira, J. M.: Global Emissions from Wildland Fires in 1960 to 2000, Global Biogeochem. Cycles, in review.

Seinfeld, J. H. and Pandis, S. N.: Atmospheric Chemistry and Physics: From Air pollution to Climate change, John Wiley, United States of America, 1998.

Shindell, D. T., Faluvegi, G., Stevenson, D. S. et al.: Multimodel simulations of carbon monoxide: Comparison with observations and projected near-future changes J. Geophys. Res., 111 (D19), D19306, doi:10:1029/2006JD007100, 2006.

Simmons, A. J and Burridge, D. M.: An energy and angular-momentum conserving vertical finite difference scheme and hybrid vertical coordinates, Mon. Wea. Rev., 109, 758–766, 1981.

Simmons, A. J., Burridge, D. M., Jarraud, M., Girard, C., Wergen, W.: The ECMWF medium-range prediction models development of the numerical formulations and the impact of increased resolution, Met. Atmos. Phys., 40, 28 – 60, doi: 10.1007/BF01027467, 1989.

Simmons, A. J. and Gibson, J. K.: ERA-40 Project plan. ERA40 project report series No 1, 63pp, 2000.

Solberg, S., Derwent, R. G., Hov, O., Langner, J., and Lindskog, A.: European Abatement of Surface Ozone in a Global Perspective, AMBIO: A Journal of the Human Environment: Vol. 34(1), pp. 47 –53, 2005.

Smagorinsky, J.: Global atmospheric modeling and numerical simulation of climate. In Weather and Climate Modifications. W. N. Hess, ed. Wiley, New York, 633 – 686, 1974.

Staehelin, J., Thudium, J., Buehler, R., Thomas, A. V., Graber, W.: Trends in surface ozone concentrations at Arosa (Switzerland), Atmospheric Environment, 28 (1), 75–87. 1994.

Staudt, A. C., D. J. Jacob, J. A. Logan, D. Bachiochi, T. N. Krishnamurti, and N. Poisson, Global chemical model analysis of biomass burning and lightning influences over the South Pacific in austral spring, J. Geophys. Res., 107(D14), 4200, doi:10.1029/2000JD000296, 2002.

Stevenson, D. S., Dentener, F. J., Schultz, M. G., Ellingsen, K., van Noije, T. P. C., et al.: Multi-model ensemble simulations of present-day and near-future tropospheric ozone, J. Geophys. Res., 111(D8), D08301, doi:10.1029/2005JD006338, 2006.

Stier, P., Feichter, J., Kinne, S., Kloster, S., Vignati, E., Wilson, J., Ganzeveld, L., Tegen, I., Werner, M., Balkanski, Y., Schulz, M., Boucher, O., Minikin, A., and Petzold, A.: The aerosol-climate model ECHAM5-HAM, Atmos. Chem. Phys., 5, 1125–1156, 2005.

Stohl, A., Eckhardt, S., Forster, C., James P., and Spichtinger, N.: On the pathways and timescales of intercontinental air pollution transport, J. Geophys. Res., 107(D23), 4684, doi: 10.1029/2001JD001396, 2002.

Swap, R. J. H. J. Annegarn and L. Otter: Southern African Regional Science Initiative (SAFARI 2000): summary of science plan, South African Journal of Science 98, 119–124, 2002.

Swap, R. J., H. J. Annegarn, J. T. Suttles, M. D. King, S. Platnick, J. L. Privette, and R. J. Scholes, Africa burning: A thematic analysis of the Southern African Regional Science Initiative (SAFARI 2000), J. Geophys. Res., 108(D13), 8465, doi:10.1029/2003JD003747, 2003.

Taguchi, S.: Interhemispheric exchange in the troposphere by an atmospheric transport model based on observed winds, J. Met. Soc. Jap., 71, 123 – 134, 1993.

Tanaka, M.: Interannual fluctuations of the tropical easterly jet and the summer monsoon in the Asian region, J. Meteor. Soc. Japan, 60, 865–875, 1982.

Tans, P. P., Fung, I. Y. and Takahashi, T.: Observational constraints on the global atmospheric CO_2 budget, Science 247, 1431 – 1438, 1990.

Tao, Z., and Jain, A. K.: Modeling of global biogenic emissions for key indirect greenhouse gases and their response to atmospheric CO2 increases and changes in land cover and climate, J. Geophys. Res., 110, D21309, doi:10.1029/2005JD005874, 2005.

Thompson, A. M.: The oxidizing capacity of the earth's atmosphere: probable past and future changes, Science, 256(5060), 1157–1165, May 22, 1992.

Thompson, A. M., Witte, J. C., McPeters, R. D., Oltmans, S. J., Schmidlin, F. J., Logan,J. A.,et al.: Southern Hemisphere Additional Ozonesondes (SHADOZ) 1998-2000 tropical ozone climatology 1: Comparison with Total Ozone Mapping

Spectrometer (TOMS) and ground-based measurements, J. Geophys. Res., Vol. 108 No. D2, 8238, doi: 10.1029/2001JD000967, 2003.

Thompson, A.M., Witte, J. C., Oltmans, S. J., Schmidlin, F. J., Logan,J. A.,et al.: Southern Hemisphere Additional Ozonesondes (SHADOZ) 1998-2000 tropical ozone climatology 2: Tropospheric variability and the zonal wave-one, J. Geophys. Res., Vol. 108 No. D2, 8241, doi: 10.1029/2002JD002241, 2003.

Thouret, V., Marenco, A., Logan, J. A., Nédélec, P., and Grouhel, C.: Comparison of ozone measurements from the MOZAIC airborne program and the ozone sounding network at eight locations, J. Geophys. Res., 103(D19), 25 695–25 720, 1998a.

Thouret, V., Marenco, A., Nédélec, P., and Grouhel, C.: Ozone climatologies at 9–12 km altitude as seen by the MOZAIC airborne program between September 1994 and August 1996, J. Geophys. Res., 103(D19), 25 653–25 680, doi:10.1029/98JD01807, 1998b.

Thouret, V. , Cammas, J.-P., Sauvage, B., Athier, G., Zbinden, R., Nédélec, P., Simon, P. and Karcher, F.: Tropopause referenced ozone climatology and inter-annual variability (1994–2003) from the MOZAIC programme, Atmos. Chem. Phys., 6, 1033–1051, 2006.

Tie, X., Zhang, R. , Brasseur, G., Emmons, L., and Lei, W.: Effects of lightning on reactive nitrogen and nitrogen reservoir species in the atmosphere, J. Geophys. Res., 106, 3167–3178, 2001.

Tie, X., Guenther, A., and Holland, E.: Biogenic methanol and its impact on tropospheric oxidants, Geophys. Res. Lett., 30(17), 1881, doi:10.1029/2003GL017167, 2003.

Tiedtke, M.: A comprehensive mass flux scheme for cumulus parameterization in large-scale models, Mon. Wea. Rev., 117, 1779–1800, 1989.

Tompkins, A. M.: A prognostic parameterization for the subgrid-scale variability of water vapour and clouds in large-scale models and its use to diagnose cloud cover. J. Atmos. Sci. 59, 1917 – 1942, 2002.

Industrial development report 2004: Industrialization, Environment and the Millennium Development Goals in Sub-Saharan Africa: The new frontier in the fight against poverty, published by United Nations Industrial Development Organisation (UNIDO), pp. 242, ISBN 92-1-106428-7, available at http://www.unido.org/file-storage/download/?file%5fid=24423.

Industrial development report 2005: Capability building for catching-up: Historical, empirical and policy dimensions, published by United Nations Industrial Development Organisation (UNIDO), pp 204, ISBN 92-1-106431-7, 2005. Available at http://www.unido.org/file-storage/download/?file_id=44688.

World Population Prospects: the 2004 Revision and World Urbanization Prospects: the 2005 Revision, by the Population Division of the Department of Economic and Social Affairs of the United Nations Secretariat, available at http://esa.un.org/unup.

van Aalst, M. K, van den Broek, M. M. P., Bregman, A., Brühl, C., Steil, B., Toon, G. C., Garcelon, S., Hansford, G. M., Jones, R. L., Gardiner, T. D., Roelofs, G. J., Lelieveld, J., and Crutzen, P. J.: Trace gas transport in the 1999/2000 Arctic winter: comparison of nudged GCM runs with observations. Atmos. Chem. Phys., 4, 81 – 93, 2004.

van Noije, T.P.C., Eskes, H. J., van Weele, M., and van Velthoven, P. F. J.: Implications of the enhanced Brewer-Dobson circulation in European Centre for Medium Range Weather Forecasts reanalysis ERA-40 for the stratosphere troposphere exchange of ozone in global chemistry transport models, J. Geophys. Res., 109, D19308, doi:10:1029/2004JD004586, 2004.

Volz, A., and Kley, D.: Evaluation of the Montsouris series of ozone measurements made in the nineteenth century, Nature 332, 240 – 242, doi:10.1038/332240a0, 1988.

von Kuhlmann, R., Lawrence, M. G., Pöschl, U., and Crutzen, P. J.: Sensitivities in global scale 25 modeling of isoprene, Atmos. Chem. Phys., 4, 1–17, 2004.

Walker R., F. Parsche, M. Bierbrier, J. H. McKerrow: Tissue identification and histologic study of six lung specimens from Egyptian mummies, Am. J. Phys. Anthropol., V. 72, Issue 1, 43 – 48, DOI:10.1002/ajpa.1330720106, August 1986.

Wang, W. C., Pinto, J. P., and Yung, Y. L.: Climatic effect due to halogenated compounds in the Earth's atmosphere, J. Atmos. Sci., 37, 333–338, 1980.

Wang, K.-Y. and Shallcross, D. E: Modelling terrestrial biogenic isoprene fluxes and their potential impact on global chemical species using a coupled LSM-CTM model, Atmos. Environ., 34, 2909–2925, 2000.

Wang, Y., Logan, J. A., and Jacob, D. J.: Global simulation of tropospheric O_3 -NO_x-gydrocarbon chemistry, 2, Model evaluation and global ozone budget, J. Geophys. Res., 103(D9), 10727–10756, DOI: 10.1029/98JD00157, 1998a.

Wang, Y., Logan, J. A., and Jacob, D. J.: Global simulation of tropospheric O_3 -NO_x-gydrocarbon chemistry, 3, Origin of tropospheric ozone and effects of nonmethane hydrocarbons, J. Geophys. Res., 103(D9), 10757–10768, DOI: 10.1029/98JD00156, 1998b.

Waugh, D. W. (1996), Seasonal variation of isentropic transport out of the tropical stratosphere, J. Geophys. Res., 101(D2), 40074024.

Webster, P. J.: The elementary monsoons, in Monsoons, edited by J. F. Fein and P. L. Stephens, pp. 3 – 32, John Wiley, New York, 1987.

Wiedinmyer, C., Guenther, A., Harley, P., Hewitt, C., Geron, C., Artaxo, P., Steinbrecher, R., and Rasmussen, R.: Global Organic Emissions from Vegetation, in: Emissions of Atmospheric Trace Compounds, edited by: Granier C., Kluwer Publishing, Dordrecht, 121–182, 2004.

Wilkins E. T.: Air pollution and the London fog of December, 1952, J. R. Sanitary Inst., 74(1), 1–21, 1954.

The World Bank World Development Indicators, 2007, Published by the Development Data Center, 1818 H Street NW, Room MC2-812, Washington, D.C. 20433 USA. Available at http://devdata.worldbank.org/wdi2006/contents/cover.htm

Xue, Y., H.-M. H. Juang, W.-P. Li, S. Prince, R. DeFries, Y. Jiao, and R. Vasic: Role of land surface processes in monsoon development: East Asia and West Africa, J. Geophys. Res., 109, D03105, doi:10.1029/2003JD003556, 2004.

Zbinden, R. M. , Cammas, J.-P., Thouret, V., Nédélec, P., Karcher, F. and Simon, P.: Mid-latitude tropospheric ozone columns from the MOZAIC program: climatology and interannual variability Atmospheric Chemistry and Physics, 6, 1053–1073, 2006.

Publikationsreihe des MPI-M
„Berichte zur Erdsystemforschung“ , „*Reports on Earth System Science*“, ISSN 1614-1199
Sie enthält wissenschaftliche und technische Beiträge, inklusive Dissertationen.

Berichte zur Erdsystemforschung Nr.1 Juli 2004	**Simulation of Low-Frequency Climate Variability in the North Atlantic Ocean and the Arctic** Helmuth Haak
Berichte zur Erdsystemforschung Nr.2 Juli 2004	**Satellitenfernerkundung des Emissionsvermögens von Landoberflächen im Mikrowellenbereich** Claudia Wunram
Berichte zur Erdsystemforschung Nr.3 Juli 2004	**A Multi-Actor Dynamic Integrated Assessment Model (MADIAM)** Michael Weber
Berichte zur Erdsystemforschung Nr.4 November 2004	**The Impact of International Greenhouse Gas Emissions Reduction on Indonesia** Armi Susandi
Berichte zur Erdsystemforschung Nr.5 Januar 2005	**Proceedings of the first HyCARE meeting, Hamburg, 16-17 December 2004** Edited by Martin G. Schultz
Berichte zur Erdsystemforschung Nr.6 Januar 2005	**Mechanisms and Predictability of North Atlantic - European Climate** Holger Pohlmann
Berichte zur Erdsystemforschung Nr.7 November 2004	**Interannual and Decadal Variability in the Air-Sea Exchange of CO2 - a Model Study** Patrick Wetzel
Berichte zur Erdsystemforschung Nr.8 Dezember 2004	**Interannual Climate Variability in the Tropical Indian Ocean: A Study with a Hierarchy of Coupled General Circulation Models** Astrid Baquero Bernal
Berichte zur Erdsystemforschung Nr9 Februar 2005	**Towards the Assessment of the Aerosol Radiative Effects, A Global Modelling Approach** Philip Stier
Berichte zur Erdsystemforschung Nr.10 März 2005	**Validation of the hydrological cycle of ERA40** Stefan Hagemann, Klaus Arpe and Lennart Bengtsson
Berichte zur Erdsystemforschung Nr.11 Februar 2005	**Tropical Pacific/Atlantic Climate Variability and the Subtropical-Tropical Cells** Katja Lohmann
Berichte zur Erdsystemforschung Nr.12 Juli 2005	**Sea Ice Export through Fram Strait: Variability and Interactions with Climate**- Torben Königk
Berichte zur Erdsystemforschung Nr.13 August 2005	**Global oceanic heat and fresh water forcing datasets based on ERA-40 and ERA-15** Frank Röske
Berichte zur Erdsystemforschung Nr.14 August 2005	**The** HAM**burg** O**cean** C**arbon** C**ycle Model HAMOCC5.1 - Technical Description Release 1.1** Ernst Maier-Reimer, Iris Kriest, Joachim Segschneider, Patrick Wetzel
Berichte zur Erdsystemforschung Nr.15 Juli 2005	**Long-range Atmospheric Transport and Total Environmental Fate of Persistent Organic Pollutants - A Study using a General Circulation Model** Semeena Valiyaveetil Shamsudheen

Publikationsreihe des MPI-M
„Berichte zur Erdsystemforschung“ , „*Reports on Earth System Science*“, ISSN 1614-1199
Sie enthält wissenschaftliche und technische Beiträge, inklusive Dissertationen.

Publikationsreihe des MPI-M
„Berichte zur Erdsystemforschung“ , „*Reports on Earth System Science*“, ISSN 1614-1199
Sie enthält wissenschaftliche und technische Beiträge, inklusive Dissertationen.

Berichte zur Erdsystemforschung Nr.30 November 2006	**Long-term interactions between ice sheets and climate under anthropogenic greenhouse forcing Simulations with two complex Earth System Models** Miren Vizcaino
Berichte zur Erdsystemforschung Nr.31 November 2006	**Effect of Daily Surface Flux Anomalies on the Time-Mean Oceanic Circulation** Balan Sarojini Beena
Berichte zur Erdsystemforschung Nr.32 November 2006	**Managing the Transition to Hydrogen and Fuel Cell Vehicles – Insights from Agent-based and Evolutionary Models –** Malte Schwoon
Berichte zur Erdsystemforschung Nr.33 November 2006	**Modeling the economic impacts of changes in thermohaline circulation with an emphasis on the Barents Sea fisheries** Peter Michael Link
Berichte zur Erdsystemforschung Nr.34 November 2006	**Indirect Aerosol Effects Observed from Space** Olaf Krüger
Berichte zur Erdsystemforschung Nr.35 Dezember 2006	**Climatological analysis of planetary wave propagation in Northern Hemisphere winter** Qian Li
Berichte zur Erdsystemforschung Nr.36 Dezember 2006	**Ocean Tides and the Earth’s Rotation - Results of a High-Resolving Ocean Model forced by the Lunisolar Tidal Potential** Philipp Weis
Berichte zur Erdsystemforschung Nr.37 Dezember 2006	**Modelling the Global Dynamics of Rain-fed and Irrigated Croplands** Maik Heistermann
Berichte zur Erdsystemforschung Nr.38 Dezember 2006	**Monitoring and detecting changes in the meridional overturning circulation at 26°N in the Atlantic Ocean- The simulation of an observing array in numerical models** Johanna Baehr
Berichte zur Erdsystemforschung Nr.39 Februar 2007	**Low Frequency Variability of the Meridional Overturning Circulation** Xiuhua Zhu
Berichte zur Erdsystemforschung Nr.40 März 2007	**Aggregated Carbon Cycle, Atmospheric Chemistry, and Climate Model (ACC2) – Description of the forward and inverse modes –** Katsumasa Tanaka, Elmar Kriegler
Berichte zur Erdsystemforschung Nr.41 März 2007	**Climate Change and Global Land-Use Patterns — Quantifying the Human Impact on the Terrestrial Biosphere** Christoph Müller
Berichte zur Erdsystemforschung Nr.42 April 2007	**A Subgrid Glacier Parameterisation for Use in Regional Climate Modelling** Sven Kotlarski

Publikationsreihe des MPI-M
„Berichte zur Erdsystemforschung“ , „*Reports on Earth System Science*“, ISSN 1614-1199
Sie enthält wissenschaftliche und technische Beiträge, inklusive Dissertationen.



ISSN 1614-1199